Development of Electrochemical Sensing Platforms: Detection of Therapeutic Drugs and Heavy Metal Ions

A dissertation submitted to the Department of Chemistry,

Quaid-i-Azam University, Islamabad, in partial fulfillment of the requirements for the degree of

Doctor of Philosophy

In

Physical Chemistry

by

Sundas Sultan

Department of Chemistry

Quaid-i-Azam University Islamabad

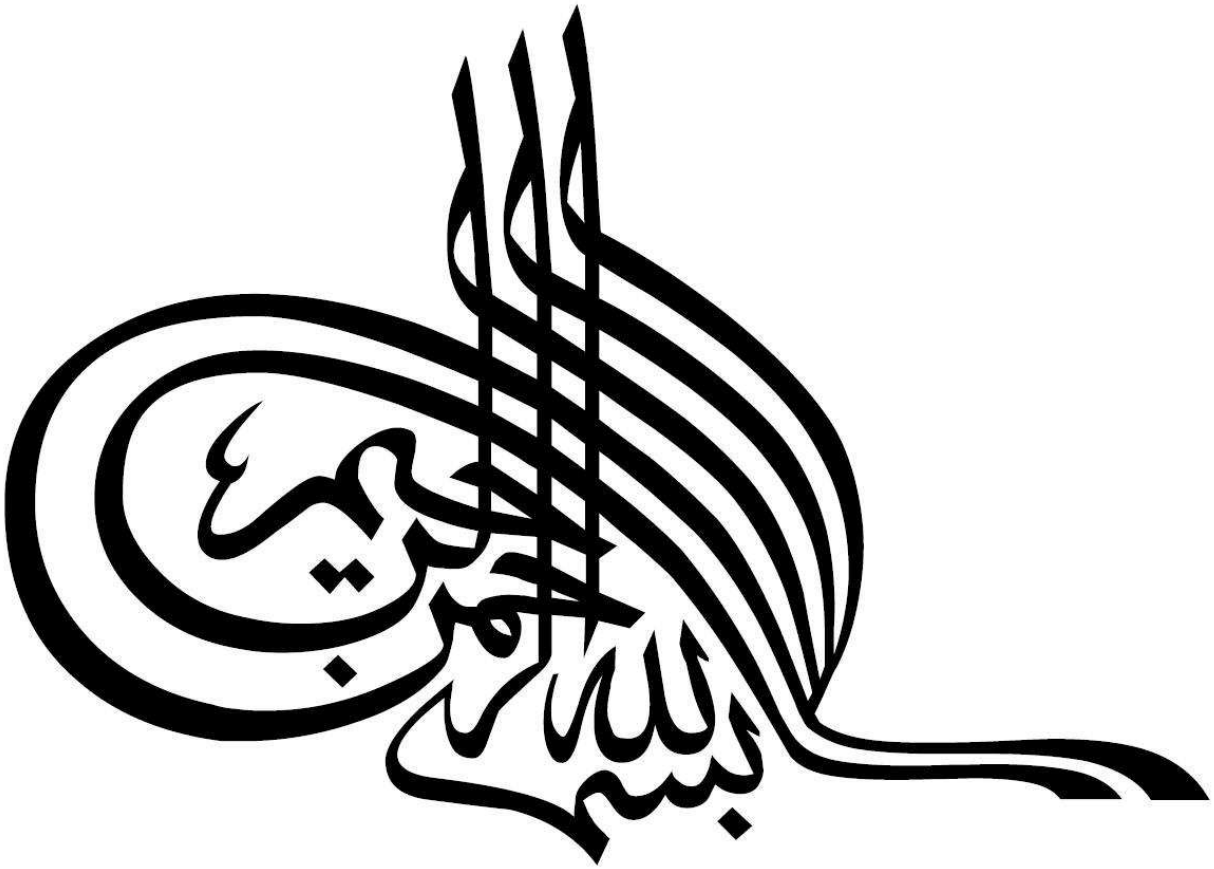

In the name of Allah,
the Most Beneficent,
the Most Merciful

I would like to dedicate this thesis to the Allah Almighty, who has been my constant source of strength and guidance. It is through the Allah's blessings and guidance that I have been able to find the right path towards success.

To my beloved parents and family, whose unwavering support and inspiration has helped me realize my dreams, and to my teachers, whose guidance has shown me the right path.

Declaration

This is to certify that this dissertation submitted by **Sundas Sultan** is accepted in its present form by the Department of Chemistry, Quaid-i-Azam University, Islamabad, Pakistan, as satisfying the dissertation requirements for the degree of **"Doctor of Philosophy in Physical Chemistry".**

Supervisor

_____

Prof. Dr. Afzal Shah
(Department of Chemistry,
Quaid-i-Azam
University,Islamabad,
Pakistan)

Head of the Section

_____

Prof. Dr. Hazrat Hussain
(Department of Chemistry,
Quaid-i-Azam University,
Islamabad, Pakistan)

External Examiner: _____

Chairman: _____

Prof. Dr. Aamer Saeed Bhatti
(Department of Chemistry,
Quaid-i-Azam University,
Islamabad, Pakistan

Acknowledgements

Firstly, I owe my success in this scientific assignment to the mercy and guidance of Allah (SWT), Who guided us through His Beloved Prophet Hazrat Muhammad (P.B.U.H).

I want to express my gratitude and extend my warmest thanks to Prof. Dr. Afzal Shah (my supervisor), whose guidance and support made this work possible. I would like to express my gratitude to Prof. Dr. Aamer Saeed Bhatti, the Chairman of the Department of Chemistry at Quaid-i-Azam University, and Prof. Dr. Hazrat Hussain, the Head the Physical Section for their support. Additionally, I would like to extend my thanks to all the teachers and lab members who generously shared their expertise and provided valuable assistance throughout my studies. Without their help, I would not have been able to achieve my goals.

I would like to convey my sincerest appreciation to my parents, Sultan Mehmood and Zulekha Jan, for their unwavering love, support, and encouragement throughout my life. I am incredibly grateful for all that they have done for me and could not have achieved my successes without their guidance and sacrifices. I would like to extend special thanks to my beloved husband, Eng. Rameez Shahzad, and my dear sons, Hashir bin Rameez and Hashim bin Rameez. I would also like to acknowledge the support of my brother, Squadron Leader Aamir bin Sultan, my sister-in-law, Dr. Naveeda Firdous, and my entire family. Your prayers and encouragement have been highly valuable for me, especially while balancing the demands of a PhD and raising a family. I am truly blessed to have such a wonderful and incredible family, and I thank you all for your love and support.

Abstract

The sensitivity characteristics of the electrode can be enhanced by modifying its surface with suitable modifiers. The surface assisted electron transfer platforms are particularly useful for pharmaceutical analysis and detection of water toxins. The primary objective of the current work is to modify the electrode surface in a way that could significantly boost its sensitivity for medical and environmental applications. Four electrode modifiers including bis-triazole appended calix[4] arene (BTC), Bis (imidazo [4, 5-f][1, 10] phenanthroline) appended bis-triazolo calix[4] arene (BPTC), $FeCoSe_2$ and $CoPd@Al_2O_3$ were synthesized and characterized by various electrochemical, structural, and morphological techniques. The synthesized materials were immobilized individually onto the electrode surface and modification was ensured by electrochemical impedance spectroscopy (EIS), cyclic voltammetry (CV) and square wave anodic stripping voltammetry (SWASV). In the designed nanosensors, $FeCoSe_2$ nano-rods and $CoPd@Al_2O_3$ were used as receptors for the sensing of Isoniazid (INZ) and Venlafaxine (VEN) drugs in biological fluids. For real sample analysis the labelled claims of INZ and VEN in tablets were validated and the detection limits of 0.12 nM and 1.86 pM were evaluated by square wave anodic stripping voltammetry. It was observed that the signals of the drugs remained intense even in the presence of interfering agents such as citric acid, uric acid, ascorbic acid, glucose, sucrose, Ca^{2+}, Mg^{2+} and NH^{4+} ions with concentration higher than INZ and VEN. For the sensing of heavy metal ions, Zn (II), Pb (II), Cd (II), As (III), and Hg (II), BTC and BPBTC were used as receptors on the transducer's surface. The platforms were then used for the detection of metal ions. The selected metal ions were found to interact with the electron rich functionalities of the recognition layers and the resulting host guest complexation led to increase in the oxidation signals, about 5 times at the fabricated electrode as compare to bare GCE. To check the performance of the sensing platforms, EIS, CV, and SWASV were utilized. Conditions were optimized to achieve the highest possible current response of the target analytes. The validity of the modified electrodes for practical applications was verified by testing them with real samples. Results indicated that the designed electrochemical platforms possess the qualities of sensitivity, selectivity, reproducibility, and stability.

Contents

List of Figures

List of tables

List of schemes

List of Abbreviations

HMDE	Hanging mercury drop electrodes
$[Ru(bpy)_3]_2^+$-GO /GE	Graphene oxide (GO) textured with redox active ruthenium(II) bipyridine complex
Graphene/CeO_2 /GCE	Cerium dioxide nanoparticle-decorated graphene hybrid
HAP-Nafion /GCE	Hydroxyapatite-nafion composite
BiFEs	Bismuth film electrode
Y-AlOOH@SiO_2/Fe_3O_4 /GCE	Functionalized Gamma Phase Aluminum Oxyhydroxide Supported on Silicon Dioxide/Iron(II,III) Oxide Composite modified glassy carbon electrode
AuNPs/CNFs /GCE	Gold nanoparticle grown on carbon nanofibers modified glassy carbon electrode
SnO_2-reduced graphene oxide nanocomposite-GCE	Tin(IV) oxide-reduced graphene oxide nanocomposite modified glassy carbon electrode.
NG-GCE	Nitrogen-doped graphene modified glassy carbon electrode.
Bi-ERNGO-GCE	Electrochemically reduced nanoporous graphene oxide/Bismuth film.
NH_2-CMS-GCE	Modified-GCE with amino-functionalized carbon microspheres modified glassy carbon electrode.
Mn_3O_4-GCE	Manganese (III) oxide graphitic-carbon-electrode.
F-MWCNT-Fe_3O_4-0.5% Nafion-GCE	Fluorinated multi- walled carbon nanotubes and magnetite nano-particles modified glassy carbon electrode.
ERGO-GCE	Electrochemically reduced graphene oxide modified glassy carbon electrode.
Ag-P(MMA-co-AMPS)ESP	Silver nanoparticles incorporated copolymer of methyl methacrylate and 2-acrylamido-2-methylpropane sulfonic acid - efficient electrochemical sensing platforms.

GO-PAG-GCE	Graphene oxide/ poly-L-arginine modified glassy carbon electrode.
Cu-GO-GCE	Copper micro particles over graphene oxide nanosheets modified glassy carbon electrode.
SPCE-PH-electrode	Screen-printed carbon electrode- poly-l-histidine- electrode.
MWCPE	Multi-Walled Carbon Paste Electrode
PdNPs-CILE	Palladium nanoparticles electrodeposited carbon ionic liquid electrode.
ERGO-GCE	Electrochemically reduced graphene oxide modified glassy carbon electrode.
RGO–Au/GCE	Reduced graphene oxide and gold nanocomposite supported modified glassy carbon electrode.
CoTRP(dcbpy)$_2$]-Ni-GO	Tetraruthenated cobalt porphyrin-Nikle coordination polymer deposited graphene oxide.
NAF-CNT-GCE	Nafion-carbon nanotube modified glassy carbon electrode.
Fe_3O_4@CNC-Cu-GSPE	Magnetite functionalized cellulose nanocrystals and copper nanocomposite modified graphite screen-printed electrode.
La^{3+}/Co_3O_4-nanocubes-SPE	Lanthanum/ cobalt oxide nanocubes, modified screen-printed electrode.
MWCNT-RTIL-GCE	Multiwall carbon nanotubes- room temperature ionic liquid modified glassy carbon electrode.
Eu^{3+} doped NiO-CPE	Europium-doped nickel oxide incorporated carbon paste electrode.
SD	Standard Deviation
Gd_2O_3-SPE	Gadolinium oxide supported screen-printed electrode.

Chapter 1

INTRODUCTION

Rapid increase in industrialization to meet the needs of ever-growing population also led to environmental pollution, stemming from unchecked and unregulated discharge of harmful substances into the environment, especially water bodies. The United Nations established a series of objectives known as sustainable development goals (SDGs) to address this issue. Two of these SDGs are related with water cleanliness. Therefore, exploring efficient environmentally friendly approaches for the detection of water contaminants would be a useful addition to the existing knowledge economy on this topic. In this regard the current chapter provides an overview of electrochemical sensors and their potential for rapid sensing of analytes with high sensitivity and selectivity.

1.1 Sensors

These are the devices that utilize active substances for transducer modification to sense certain analytes by transmitting and magnifying their signals. The signal could be optical, electrochemical, thermal, or electrical. These instruments are utilized for detecting a targeted analyte directly in the sampling matrix [1]. Artificial sensing systems operate on the same principles as natural sensors, such as those found in the nose and tongue, which enable us to detect changes in physiology and chemistry. These systems typically consist of three key components: a receptor (input device), a transducer, and a data processor unit.

The receptor is responsible for receiving the input signals and sending them to the transducer, which converts the signals into an output signal that can be interpreted by the data processor or intelligence unit. Receptors are made up of recognition elements that receive the stimulus and interact with the target analyte. In sensors, transduction elements play a vital role in converting a recognition event into an output signal. The output signal

could be of different types such as electrical, optical, or thermal, based on the sensor being utilized [2]. The subsequent sections present a brief introduction of the sensor types.

1.2 Electrochemical sensors

Since Max Cremer invented pH electrodes in 1906, electrochemical sensors emerged as promising techniques for chemical sensing [3]. These sensors are used in hospitals, chemical factories, and a variety of other fields after the invention of glucose enzyme amperometric electrodes by L. Clark [4]. Owing to their high accuracy, speed, as well as reliability, these sensors are utilized in several areas of life such as biomedical, agricultural, food and environmental, as well as industrial sectors. To meet the evolving detection needs in various fields, electrochemical sensors require multidisciplinary research that integrates material science, electrochemical engineering, and electronics. Electrochemical sensors consist of three key components: a transducer, a receptor, and an electrochemical cell arranged with counter and reference electrodes. Due to their discrimination ability of species based on their redox potentials, they are currently the predominant probes for simultaneous sensing of several analytes. Fig. 1.1 depicts schematics of an electrochemical sensor.

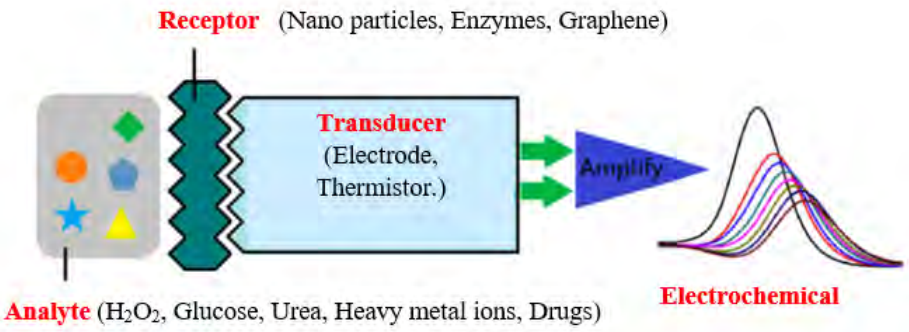

Fig. 1.1. *A simplified representation of an electrochemical sensor, highlighting the essential components that enable it to detect and quantify various analytes. Adapted from reference [5].*

1.3 Classification of electrochemical sensors

There are three distinct categories into which electrochemical sensors can be classified, depending on their operating principles and design: potentiometric sensors, conductometric sensors, and voltammetric /amperometric sensors.

1.3.1 Potentiometric sensors

A potentiometric sensor measures the voltage or potential difference between the WE and the reference electrode. This potential difference changes in response to variations in the concentration of the analytes being measured, allowing for the detection and quantification of the analyte. They have a distinct ion selective membrane at the working electrode, which is made of a crystal, glass, or polymer depending on the ions of interest that bind at the membrane-electrolyte interface. They are extremely selective but are slower and less sensitive than their amperometric counterparts. Because of their simplicity and ease of use, potentiometric sensors are commonly used [6]. Three major categories of potentiometric devices are field effect transistors, coated wire electrode, and ion selective electrodes [7].

1.3.2 Voltammetric sensors

These sensors generate current signal as a function of potential applied across the working electrode. For voltammetric analysis, analytes get reduced or oxidized at the working electrode in a definite potential window where electrolyte/solvent/modifiers decomposition could not occur. Voltammetric sensors are commonly characterized through square wave, differential pulse, and cyclic voltammetry [8].

1.3.3 Amperometric sensors

Through chronoamperometry, the current produced over time is measured at a constant potential resulting from redox reactions of the electroactive species. Amperometric sensors are capable of detecting the presence of analytes. These sensors quantify and detect analytes through electron-transfer process between the analyte and the WE, providing signals that directly correspond to the concentration of electroactive species. A typical amperometric sensor consists a potentiostat along with a three electrodes containing electrochemical cell, the counter, reference, and working electrodes. These electrodes are immersed in an appropriate electrolyte that makes the electron-transfer process faster between the WE and the analyte species. Inert conducting materials serve as the auxiliary or counter electrode. In potentiometric sensors, the reference electrode have a critical part in establishing the reference potential for both the working and counter electrodes. The reaction involving the electron-transfer i.e., desired reaction, happens at the surface of the WE [9]. Fig. 1.2 depicts a standard amperometric sensing device and its operation.

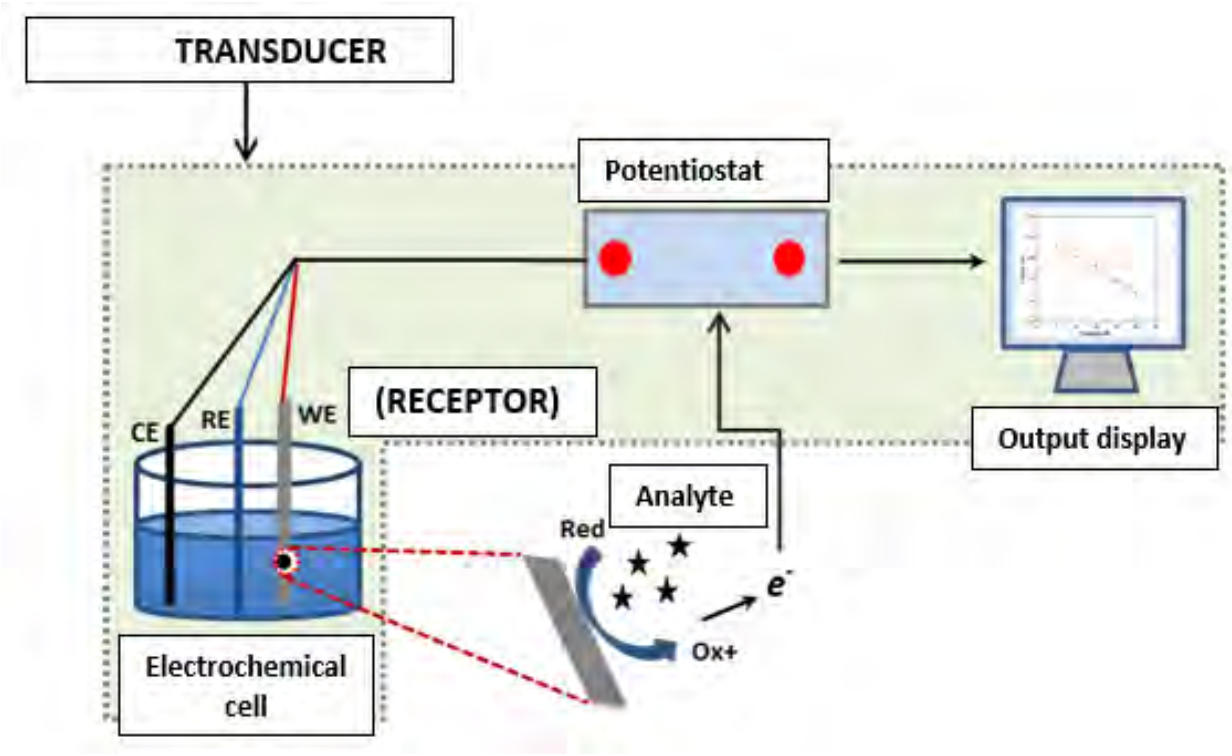

Fig. 1.2. *The key constituents of amperometric sensors: potentiostat, electrolyte solution, and three electrodes. Adapted from reference [10].*

1.4 Working Electrodes (WE)

The WE is a fundamental component in electroanalytical systems as it serves as the site where the electrochemical reaction of interest occurs. To be suitable for electrochemical research, a working electrode should meet certain criteria such as being inert, having low background current, being affordable, and having a high level of reproducibility. The electrochemical reaction in an amperometric sensor can be influenced by the structure as well as geometry of the WE. These factors affect the area and roughness of the WE's surface, which, in turn, can influence the reaction. The quantity of available electrode material for electrochemical reactions is largely determined by the active surface area of the electrode. Moreover, roughness of the electrode's surface can affect the adsorption of reaction intermediates as well as the diffusion of analytes and reaction products to and from

the electrode surface. Therefore, selecting an appropriate working electrode with optimal geometry and structure is important to achieve accurate and precise electro-analytical measurements. The precision and accuracy of electroanalytical analysis can be influenced by the distribution of the electric-field and the diffusion process of reacting species and products produced, which can be affected by the shape as well as size of the WE. Hence, it is crucial to thoroughly analyze and evaluate the structure and geometry of the working electrode, when designing electroanalytical experiments and interpreting electrochemical data. Working electrodes are available in different sizes and shapes, and new types are being developed based on their size and working potential window, and for different applications.

1.4.1 Mercury electrodes

Mercury electrodes, such as dropping-mercury, mercury-film, and hanging mercury drop electrodes, were historically valued in polarography for electroanalytical purposes due to their exceptional selectivity, low detection limits, and reproducibility. However, their usage declined because of mercury's toxicity and limitations in on-site analysis of organic compound oxidation, leading to a shift towards alternative materials in electrochemical analysis [11].

1.4.2 Metal and metal oxide electrodes

Metal and metal-oxide based electrodes, including platinum, gold, silver, titanium, and their oxides, are widely employed in electroanalytical applications due to high conductivity and stability. Platinum electrodes offer a broad working potential window and resistance to corrosion but can be costly. Gold electrodes, preferred for biomolecule studies, exhibit low background currents but are prone to oxidation. Silver electrodes, though less common, have lower background currents and are cost-effective, particularly valuable for redox-active compounds. Metal oxide-based electrodes like TiO_2 or ITO offer high sensitivity

and low cost, suitable for sensors and solar cells, with their choice dependent on application-specific needs, cost, and stability [12].

1.4.3 Carbon-based electrodes

Carbon-based electrodes, renowned for their large surface area, stability, and low background current, find broad application in electroanalytical chemistry, spanning sensing, energy storage, and electrocatalysis. These versatile electrodes, either homogeneous (e.g., carbon nanotubes, graphite) or heterogeneous (e.g., screen-printed electrodes), offer unique categories like glassy carbon (GCEs), carbon paste (CPEs), and carbon fiber electrodes (CFEs). GCEs demonstrate excellent electrochemical properties but are costly and fragile, while CPEs offer flexibility and low cost but may lack sensitivity. CFEs, with high sensitivity and mechanical strength, are costlier and more complex to handle. The diverse range of carbon-based electrodes offers distinct advantages and limitations, with the choice depending on specific electroanalytical needs and applications. Glassy carbon electrodes, chosen for their inert nature and suitability for sensing, were further enhanced through appropriate modifications [13].

1.4.4 Chemically Modified Electrodes (CMEs)

Chemical modification of electrodes, achieved via chemisorption, covalent bonding, composites, and polymer films, offers improved control over electrode surface activity in various electrochemical applications [14]. These modifications notably enhance stability, precision, selectivity, and repeatability in electroanalytical sensing. Adjusting modifier characteristics and concentrations significantly impacts the relationship with target analytes, resulting in enhanced selectivity and sensitivity. Electrode modifications aim to achieve quick electron transfer, improved electrochemical response, and selective permeation, with modifiers such as zeolites, ligands, clays, and silica derivatives being utilized to enhance electrochemical properties [15]. Morphology, modifier structure, and film coverage are critical factors influencing sensitivity and selectivity in electrode

adjustments, particularly crucial in robust and responsive voltammetric sensing. Overall, the choice of modifiers and their characteristics play a pivotal role in enhancing the electrode's recognition abilities for target analytes.

1.5 Modified electrodes for the sensing of toxic HM ions

Wastewater mainly from industries contains a variety of pollutants including heavy metal ions, hydrophobic wastes from pharmaceutical and toiletries. It is a public obligation to develop methods for treating wastewater, so that water dwelling species and human life could be safeguarded [16]. Water contamination is one of the most serious environmental issues. It is the result of inappropriate, unregulated industrials wastewater, agricultural and irrigation drainage schemes that dump sewage directly into water bodies. This has led to crossing the safety limit of water pollutants. The coke plant, for example, emits enormous amounts of manganese ions loaded wastewater, whereas the steel sector emits lead and zinc ions. Lead also comes in the environment from acid batteries, leaded gasoline’s combustion, illegal use of tetraethyl lead as a knocking inhibiting agent in gasoline Volcanic eruptions, natural weathering of rocks, and mining activities are some of the main Cadmium exposure pathways in the environment. Coal combustion also releases cadmium. Excessive use of chemical fertilizers is another source of Cd. Eruption of volcanoes and weathering of rocks are natural sources causing introduction of heavy metals into the environment. Anthropogenic sources include industrial wastes, combustion, mining, casting, and use of pesticides and fertilizers. Fig. 1.3 depicts major environmental pollutants and their sources. Water contamination has serious consequences for marine life, public health, and food quality [17]. If proper pretreatment approaches are not adopted, then scarcity of clean water and toxicity of seafood will be a global challenge in the near future.

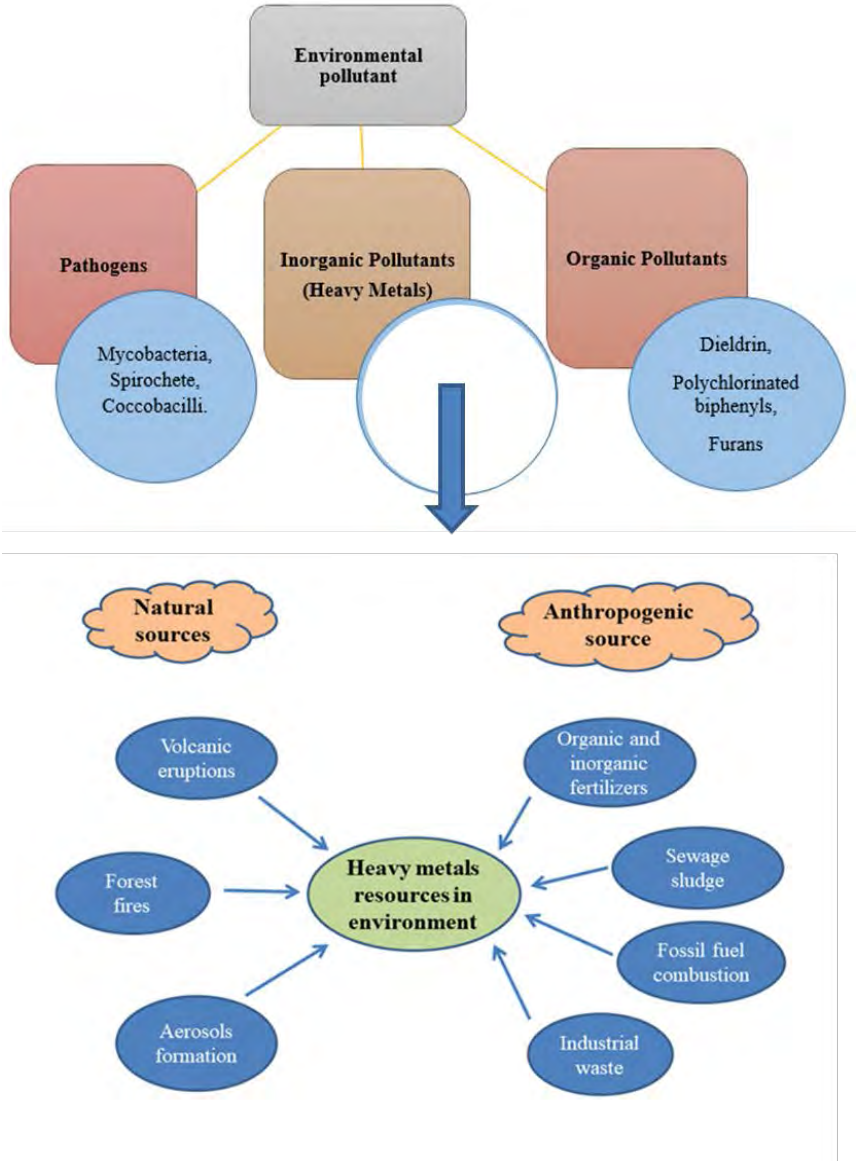

Fig. 1.3. *Classification and sources of common water contaminants Adapted from reference [18].*

The Agency for Toxic Substances and Disease Registry (ATSDR) prioritizes hazardous substances based on their potential impact on public health. Heavy metals are among the most potent environmental health hazards listed. These metals pose serious health threats to humans. They can also have negative impacts on the environment and climate [19].

Many metals are biologically essential to obtain in trace amounts in the diet to keep biological processes like respiration, enzymatic reactions, growth, cell proliferation, gene transcription, and body immune function. With regards to this, these metals like Ca and Fe ions are only toxic when their levels in the body reach a certain threshold. Other metals, on the other hand, are hazardous even at trace levels. As, Hg, and Cd ions for example, have manifested potent toxicity across living cells at all concentrations. Heavy metal toxicity is mostly based on the degradation of the oxidative processes they induce in living cells and occurs as a result of enzyme inhibition. As a consequence, there is an elevation in the levels of reactive oxygen species (ROS), which can cause irreversible damage to the DNA, proteins, and lipid systems. As seen in Fig. 1.4 redundant oxidation of certain important cell constituents causes cell instability and eventually total biological collapse.

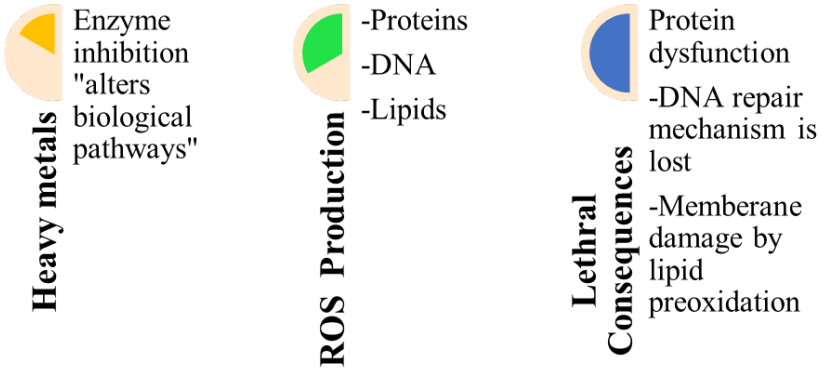

Fig. 1.4. *Diagram showing interaction of heavy metals with biological systems and their lethal effects. Adapted from reference [20].*

The presence of HMs in water has increased over the last few decades largely due to anthropogenic activities such as urbanization, industrialization and agricultural activities. This has resulted in 40% of the world population to face challenging issues with relation to access to clean water and sustainable environment [20]. Metal loaded effluents are a critical environmental and social issue that has been met with global concern due to difficulty in

assessing the safe limits in biotic systems. The term HMs refers to metals and metalloids with an atomic number higher than 20 and an elemental density greater than 5000 kg/m . Though copper, iron, and zinc are essential for biochemical processes in trace amounts, yet many other HMs (lead, cadmium, mercury and arsenic) are highly toxic even in small amounts and are thus a health hazard [21]. Heavy metals like lead, mercury, cadmium, and arsenic can accumulate in the soil over time, posing a risk to human health through ingestion, inhalation, or dermal contact that can leach into groundwater and surface water, contaminating rivers, lakes, and streams. They enter the food chain via contamination through soil and water. As much as they are persistent in environment, they are bio-accumulative and create health issues owing to their acute toxicity [22]. The optimum level of metals is very important even in plants for their normal functioning which when disturbed, affects their water transpiration rate. It can also damage chloroplasts reducing the rate of photosynthesis. Furthermore, metals concentrations beyond the threshold levels disrupt soil microbial equilibrium that affects the fertility of soil. These metal ions can further contaminate waterways through soil erosion, where rainwater can wash away contaminated soil, carrying metal ions into nearby water bodies. The conventional methods that are used for the complete removal of toxic metal are not cost effective and environment friendly. Therefore, concrete steps must be taken for the eradication of toxic metal ions by employing ultrasensitive detection tools and development of efficient removal protocols which are greener, sustainable and renewable.

Once in waterways, metal ions can accumulate in sediments and enter the food chain through bioaccumulation, where aquatic organisms absorb and retain these metals in their tissues. This can lead to the biomagnification of heavy metals in the food chain, where predators at the top of the food chain accumulate higher concentrations of heavy metals than their prey. Accumulation of HMs in the biota of aquatic ecosystem has serious consequences for humans and animals [23]. HMs are considered to be responsible for fish abnormalities having detrimental impact on populations of fishes in terms of their effect on the survival, growth rates, wellbeing, and outward appearance of fishes [24]. Fish are considered a main source of dietary protein and therefore, continuous HMs induction into aquatic habitats results in their increased environmental mobilization that eventually culminates in their entry into the food chain [25]. The toxic effects of HMs on aquatic ecosystems can include

reduced biodiversity, reproductive failure, and death of aquatic organisms. Understanding the bioaccumulation of heavy metals in aquatic organisms is critical for determining the risk of their usage by humans and for devising pollutant control techniques. Therefore, it is essential to develop a detection method that can rapidly and accurately detect metal ions. Atomic absorption spectroscopy (AAS) is a commonly used to measure metals. Currently electrochemical methods such as potentiometry, voltammetry, and chronoamperometry are used to detect metal ions [26]. This technology has the potential to fill the gap between detection and the remedial technologies. In the current work electrochemical methods were used for HM ions detection using calix[4]arene based modified glassy carbon electrode. The amphipathic structure of calix[4]arene derivatives make them suitable as electrode modifier. Their insolubility in aqueous solutions, is might be due to the hydrophobic functional groups in their structure, along with hydrophilic groups like alkoxy, aldehyde, hydroxyl, and the 1,2,3-triazole functionalities, makes them well-suited for electrode modification. These hydrophilic groups act as binding groups for metal ions. The metal ion binding and electrode anchoring groups of calixarenes are responsible for their role as conducting-bridge between the transducer (host) and the targeted analyte i.e., HM ions (guest). Calixarenes' ability to bind metal ions and anchor to electrode surfaces make them a useful conducting bridge between the transducer and target metal ions. The surface modification of a GCE by modifier calix[4]arene derivative enhances its capability to detect HM ions present in wastewater samples. This study used calix[4]arene-modified GCE to detect toxic metal ions including As^{3+},Hg^{2+}, Pb^{2+} and Cd^{2+}.

1.6 Sources of HMs in the environment

The entry of HMs in water bodies occurs via natural and anthropogenic sources. Eruption of volcanoes and weathering of rocks are natural sources causing introduction of HMs into the environment. Anthropogenic sources which are the ones to be more concerned about include industrial wastes, combustion, mining, casting, and use of pesticides and fertilizers [27]. Toxic metal ions loaded effluents are released into the ecosystem as industries lack proper waste disposal systems. The use of chemical-based fertilizers, and the burning of non-renewable fossil fuels also leads to HM introduction into the environment.

Commercially available inorganic fertilizers, particularly phosphate fertilizers, have a high tendency to contribute to global heavy metal ion transport from soil to waterways . Fertile lands or agricultural soils receive HMs by the use of inorganic fertilizers. The metals ions might seep, pollute groundwater, and affect the fertility of the land. Phosphate-based fertilizers have a high concentration of hazardous metals. Phosphate rock is used for the manufacturing of phosphatic fertilizer and releases Cd, Cu, Cr, Ni, Pb, and Zn in the environment [28]. The two primary routes for the transport of toxic metals from phosphate-based fertilizers to the living organisms are depicted below:

- Phosphate rock (Raw source) ⟶ Fertilizer (Phosphate based) ⟶ Agriculture soil ⟶ Crop/Plant ⟶ Food ⟶ Primary and Secondary consumer (Animals and humans) [29].
- Phosphate rock (Raw source) ⟶ Fertilizer (Phosphate based) ⟶ Water ⟶ Consumer (Plants, animals, and humans).

Organic fertilizers can sometimes contain heavy metals if they are sourced from contaminated sources as shown in Fig. 1.4. For example, animal manure from livestock that have been exposed to heavy metals in their feed or environment can contain elevated levels of heavy metals such as Cu, Zn, As, Cd [30]. This not only affects the soil productivity but also results in metal migration via leaching and run off water. Similarly, compost made from contaminated materials can also contain heavy metals. Additionally, some organic fertilizers may contain natural sources of heavy metals, such as rock phosphate, which can contain trace amounts of cadmium. Thus, high concentrations of trace metals such as Cr, Ni, Cu, Zn, As, Cd, and Pb have been reported in organic fertilizers [31].

If these organic fertilizers are applied repeatedly to soil, the heavy metals can accumulate and eventually reach levels that can be harmful to plants, animals, and humans. Therefore, it is important to carefully monitor the sources and quality of organic fertilizers and to use them judiciously to prevent the buildup of heavy metals in soil which can prevent leaching to groundwater and as run-off water to waterways. One of the other main sources of HM ion contamination is industrial wastewater, which may contain heavy metals from manufacturing processes. When this wastewater is discharged into the sewage system, the HMs can accumulate in the sludge over time [32], leading to potential contamination of soil and water when the sludge is applied as a fertilizer.

Combustion in engine based automobiles is another source of the most significant anthropogenic source of heavy metal ions in the environment. Emissions from combustion processes are significant anthropogenic sources of HMs. It has been found that during the combustion of coal HMs enter into the environment where cadmium, lead, and arsenic are partly volatile, while, mercury is completely volatile. As per reports from China, coal burning is one of the primary causes of harmful trace element emissions into the atmosphere [33].

HMs are released from different sources such as nickel is released from coal combustion, cadmium enters into the ecosystem from volcanic activity, weathering of rocks and metal mining. Coal combustion may release about 7,000 tons/year of cadmium globally. Excessive use of chemical fertilizers is another source of Cd [34]. Lead comes in the environment from acid batteries, leaded gasoline's combustion, illegal use of tetraethyl lead as a knocking inhibiting agent in gasoline [35], outdated plumbing systems, and lead bullets used in bird shooting games. Other sources of heavy metals can be seen in Table 1.1.

Table 1.1. *Major anthropogenic sources of heavy metals.*

Heavy metals	Sources	References
As, Cu, Hg	Pesticides	[36]
Cd,	Dyes, plastic burning, phosphatic fertilizers	[37]
Hg, Cd, Se,Ni	Mining and burning of coal	[36,38]
Pb	lead battery, herbicides X-ray shielding material	[39]
Ni, Cd, Cu, Pb, Zn, Mn	Industrial wastes, Sewage sludge, House hold waste	[36,40]

1.7 Categories of heavy metals

HMs may be classified as essential or non-essential (Fig. 1.5). Essential metals play crucial roles in living organisms; while those having no known function in living organisms are referred to as non-essential HMs [41]. Zinc, nickel, molybdenum, iron, copper, and cobalt are needed for playing essential roles in biochemical systems and for stress tolerance in humans [42]. Deficiency of any of the essential metals results in diseases/anomalous state. However, it has been found that essential HMs in plants, animals, and microbes, may differ and depend on the living organism taken into consideration. Some HMs might be required for one group of organisms but not for others. Many studies have focused on accumulation of essential HMs in body which can cause damage to living cells. Thus permissible exposure level (PEL) of toxic metals (in mg/m^3) and some of their highly toxic compounds for a length of 8 hours in humans are reported as; arsenic (0.01), cadmium (0.005), lead (0.05), and mercury (0.05) [43]. Some of the same and more HMs with their permissible exposure limit is given in Table 1.2 [43]. It means that a worker should not be exposed to these hazards beyond the mentioned PEL.

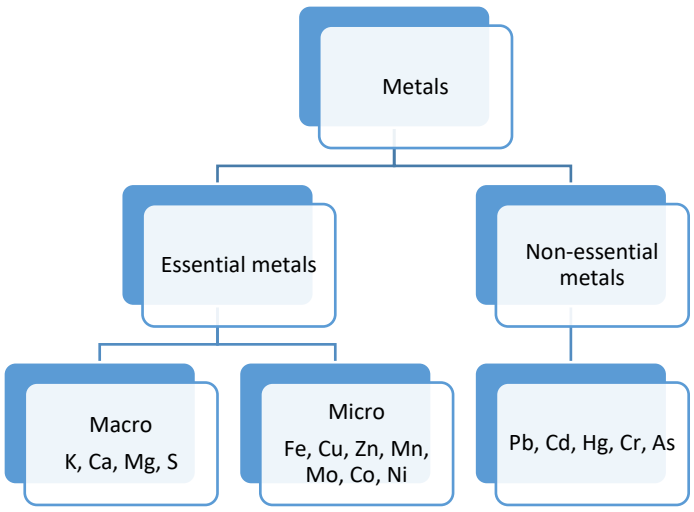

Fig. 1.5. *Classification of heavy metals as essential and non-essential ones . Adapted from reference [44].*

Table 1.2. *The PEL for some important HMs. Adapted from reference [43].*

.

Heavy Metals	PEL
As	0.01 mg/m^3
Cd	0.005 mg/m^3
Cr	0.5 mg/m^3
Cu	0.1 mg/m^3
Pb	0.05 mg/m^3
Zn	5.0 mg/m^3
Mn	1.0 mg/m^3
Hg	0.05 mg/m^3

1.8 The fate and transport of some important HMs

The fate and transport of HMs in the environment refer to the pathways and processes through which these metals move from their sources to different environmental media and their transformation and accumulation in these media. This depends on the form of the metal and the conditions of the environmental media. In general, HMs can exist in different forms, including elemental forms, ionic forms, or bound to other molecules. The fate of these HMs can thus be influenced by various factors such as solubility, reactivity, and mobility. Understanding these processes is essential in assessing the environmental risks posed by HMs and developing effective strategies for their management and remediation. HMs are known environmental contaminants and upon their release from natural or anthropogenic sources contaminate aquatic bodies, sediments and soils. Hence metals such as Pb, Hg Cr, Cd, As, Cu etc are released from their resources into water bodies and soil, where enhanced

accumulation and environmental persistence may result in detrimental effects for life in general. In the modern era, industrialization and urbanization have led to manifold increase in concentration of HMs as untreated industrial waste is introduced into fresh water bodies making it a global issue [45]. This causes contamination of sediments and act as sink to HMs as well its source. Hence the quality of the sediments can be a determinant of the level of contamination in water which is influenced by temperature, pH, redox status, organic matter, microbe content and particle size for adsorption/desorption and subsequent concentration of these HMs in sediments. The pH is one of the important indicators of immobilization of metal ions in sediments. Hence, decreasing pHof the medium results in competition of H^+ ions and metal cations for binding sites. This leads to the dissolution and release of free metal ions in water bodies [46]. In soils, bioavailability of metal ions dictates their fate in environment. This depends on speciation of metals and physicochemical and biological properties of soil. Some important heavy metals and their toxicity is discussed vide infra.

Although Pb is a naturally occurring heavy metal, it is widely found in soil and water due to anthropogenic activities such as lead-based paints, mining, and gasoline with many industrial applications such lead acid batteries, pipes and shielding devices from X-rays. Once released into the environment, Pb can persist for long periods of time and can contaminate soil, water, and air. In soil, lead can remain in the top layer, where it can be ingested by plants and animals. In water, Pb can attach to sediment particles and settle at the bottom, but it can also remain suspended in the water column, where it can be ingested by aquatic organisms. Pb contamination in the environment can have serious consequences for human and animal health [47]. It is a cumulative poison that can build up in the body over time, leading to symptoms such as abdominal pain, anemia, impaired cognitive function, and neurological damage [48]. Efforts to reduce lead contamination in the environment have focused on regulating the use of lead in products such as paints and gasoline, as well as implementing measures to prevent lead contamination from industrial processes. Remediation efforts, such as soil and water cleanup, can also help to reduce lead exposure in areas that have already been contaminated. Arsenic (As) exists in its inorganic forms such as trivalent arsenite which is more toxic than pentavalent arsenate and organic methylated metabolites and so the toxic effects of arsenic can vary depending on its form

and concentration. Its natural sources may include volcanoes and soil erosion while mining and sewage treatment plants with its industrial production for agriculture applications, wood preservatives and even for medicines etc. may introduce it to water bodies [49]. Arsenic can also enter groundwater through leaching from soil and rock formations. Mostly in humans the trivalent arsenite can bind to protein's thiol or sulphydryl group causing inactivation of 200 enzymes. Its toxicity depends on its dose, frequency, gender and individual susceptibilities. Cadmium is a toxic heavy metal that is widely used in industries such as electroplating, mining, and battery production. It can accumulate in the body over time, leading to chronic exposure and adverse health effects such as kidney, bone damage, respiratory and reproductive problems etc. via production of ROS that damages the DNA in body and disrupts body functions [50]. It is classified as a human carcinogen. It's important to note that the severity of cadmium toxicity depends on the dose and duration of exposure, as well as individual susceptibility factors such as age, health status, and genetic makeup. Cd can enter soil and water through industrial discharges, agricultural practices, and atmospheric deposition. Mercury (Hg) is a highly toxic heavy metal that is found in various forms in the environment, including elemental, organic, and inorganic Hg and can enter the environment through natural sources such as volcanic activity and the weathering of rocks, as well as anthropogenic activities such as coal combustion, mining, and waste incineration [51]. It is known that elemental vapors of Hg are very toxic and can be transported via air to long distance and may be deposited through wet or dry deposition on the soil. At the same time some organic Hg compounds such as methylmercury being water soluble can, via the route of aquatic food chain result in bio magnification. This calls for managing risks posed by Hg by reducing its immobilization introduced through anthropogenic activities [52]. Chromium is widely used in industries such as electroplating, tanning, and metal finishing and can enter soil and water through industrial discharges, agricultural practices, and atmospheric deposition. Its solubility and oxidation state are one of the major factors that govern the toxicity of Cr. Cr (III) is less toxic as compared to Cd (VI) and tumors in stomach are attributed to exposure to Cr (VI) in water and other health issues may ensue [53]. Additionally, compared to Cr(VI), Cr (III) has less widespread absorption, which contributes to its toxicity and allows for its crossing the biological membranes.

The transport of these HMs in soil can occur through various processes such as leaching, erosion, and volatilization. These HMs can enter soil through various sources such as deposition from the atmosphere, irrigation water, and agricultural practices. Once in the soil, the metals can be transported to groundwater through leaching, or they can accumulate in the topsoil. The fate of HMs in soil depends on various factors such as the pH of the soil, the presence of organic matter, and the redox conditions. HMs can be immobilized in the soil through adsorption onto soil particles or precipitation as insoluble compounds. Alternatively, they can be taken up by plants and enter the food chain and may result in biomagnification. Once in water, these metals can be transported downstream and accumulate in sediments or be taken up by aquatic organisms. The fate of HMs in water depends on various factors such as temperature, pH, and the presence of other substances that can affect their solubility, bioavailability, and toxicity. These metals are toxic to living organisms and can have harmful effects on human health and the environment. The fate and transport of these HMs in environment are influenced by a physical, chemical, and biological processes.

The solubility of a metal determines how easily it dissolves in water and other solvents. Metals that are more soluble are more likely to be transported by water, whereas less soluble metals tend to stay in the soil and sediment. Thus Lead can be highly soluble in acidic waters, but its solubility decreases as the pH of the water increases. In general, lead is more soluble in soft water than in hard water. Cadmium is relatively soluble in water and can accumulate in aquatic ecosystems through water uptake by plants and animals. Arsenic can exist in various forms, some of which are highly soluble in water. Arsenite is more soluble than the arsenate form and results in leeching to ground water. The solubility of arsenic and mercury is influenced by pH, temperature, and the presence of other chemicals in the water [54].

Adsorption is the process by which metals bind to soil and sediment particles. Metals that are strongly adsorbed are less likely to be transported by water and are more likely to remain in the soil [55]. Generally, HMs that have a high charge or a small ionic radius tend to bind more strongly to soil and sediment particles. Some heavy metals that are known to bind strongly to soil and sediment particles include: Cd has a small ionic radius and can form

strong bonds with soil and sediment particles, especially those containing organic matter. Cu particularly in the presence of sulfides and Pb especially in the presence of high content of organic matter or clay can form strong bonds with soil and sediment particles. It is important to note that the strength of the binding between a heavy metal and soil or sediment particles can also depend on the pH of the soil or sediment, the presence of other chemicals, and the specific properties of the metal and the soil or sediment [56]. The pH of the environment can affect the solubility and adsorption of heavy metals and is an important indicator for bioavailability of metals in soil and their presence in water [57]. Generally, at high pH the metal ion mobility deescalates in soil such as Cd, Zn, Cu and Pb and at low pH the ions becomes less mobile such as Cd, Co, [58]. The presence of organic matter in soil and sediment can affect the fate and transport of heavy metals [59]. Organic matter can bind to metals, reducing their mobility and bioavailability. Natural organic matter is ubiquitous in the environment, and it can form strong complexes with HMs, reducing their solubility and mobility in the environment. This can make it more difficult for HMs to be taken up by plants or animals, reducing their bioavailability and potential toxicity [60]. Organic matter may also result in transformation of metal ions from one form to other such as from more toxic Cr VI to less toxic Cr III [61]. However, these HM complexes can also be broken down under certain conditions, releasing the heavy metals back into the environment. Understanding the processes that govern the complexation and decomplexation of heavy metals with natural organic matter is therefore important for predicting the environmental behavior and potential risks associated with these metals. Moreover, microorganisms in soil can influence the fate and transport of heavy metals through processes such as bioremediation and biomineralization. Microbes can transform metals into less toxic forms or immobilize them in the soil or sediment [62]. Temperature can affect the chemical reactions that occur in the environment, such that higher temperatures can increase the solubility of metals and accelerate chemical reactions. The movement of water in the environment can transport heavy metals from one location to another. Surface runoff, groundwater flow, and erosion can all contribute to the transport of heavy metals in the environment.

The formation of HM-organic matter complexes can also affect the adsorption and desorption of HMs onto soils and sediments. In some cases, HM-organic matter complexes

can increase the adsorption of HMs onto soils or sediments, reducing their transport through groundwater or surface water. In other cases, HM-organic matter complexes can increase desorption of HMs from soils or sediments, increasing their potential to be transported through the environment. Thus, the ions of both nutrients and contaminants are made more mobile in the soil by natural chelating agents (organic acids like citric and acetic), which are generated by plant roots. Plants may typically release the chelating agent back into the soil solution after breaking the chelation bond, absorbing the metal [63]. This can lead to the mobilization and transport of previously immobilized HMs, potentially increasing their bioavailability and toxicity. Therefore, the fate and transport of heavy metals in the environment are complex processes that are influenced by a variety of physical, chemical, and biological factors. Understanding these factors is important for predicting and managing the risks associated with heavy metal contamination in the environment.

1.9 Risks of HMs on human health

Based on the risk, HMs can be categorized as follows:

- Category 1: metals posing a serious safety risk
- Category 2: metals having less safety risk
- Category 3: metals with little safety concern

Cd, As, Cr, and Ni have been classified as category 1 HMs by the International Agency for Research on Cancer. Some metals have also been identified to be possible carcinogens. The harmful effects [64-69] of HMs are displayed in Fig. 1.6 [70].

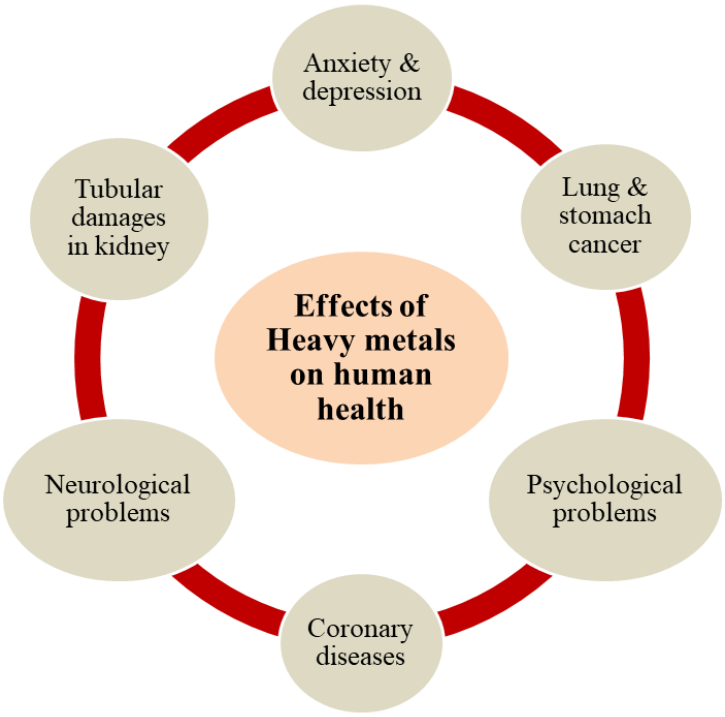

Fig. 1.6. *Health problems associated with heavy metal ions' exposure. Adapted from reference [70] with permission from Frontiers in Environmental Science. Copyright © 2022 Frontiers Media S.A.*

1.10 Toxicity of heavy metals

1.10.1 Arsenic toxicity

In the biotransformation of arsenic, living organisms convert toxic inorganic arsenic molecules to produce toxic methylated arsenicals such as monomethylarsonic acid (MMA) and dimethylarsinous acid (DMA) [71,72]. The biotransformation process is shown in Scheme 1 [73].

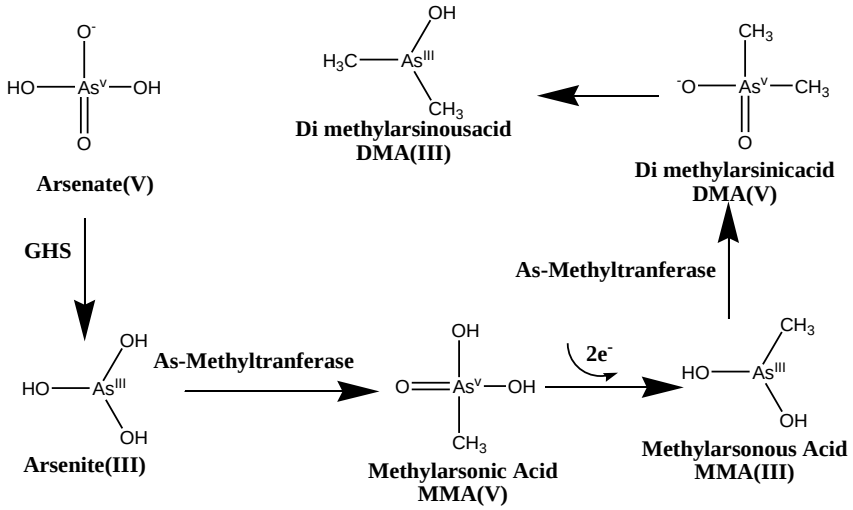

Scheme 1. *Toxicity mechanism of arsenic. Adapted from reference [73] with permission from Journal of Applied Toxicology. Copyright © 1999-2022 John Wiley & Sons, Inc.*

1.10.2 Mercury toxicity

Mercury is an established health hazardous metal, and its toxicity is considered a cause of common acute heavy metal poisoning [74]. Owing to the large stability constants of mercury, it has been found that Hg attaches freely to thiols [75] (Fig. 1.7), which are easily accessible in the body in the form of enzymes, amino acid, glutathione etc [76].

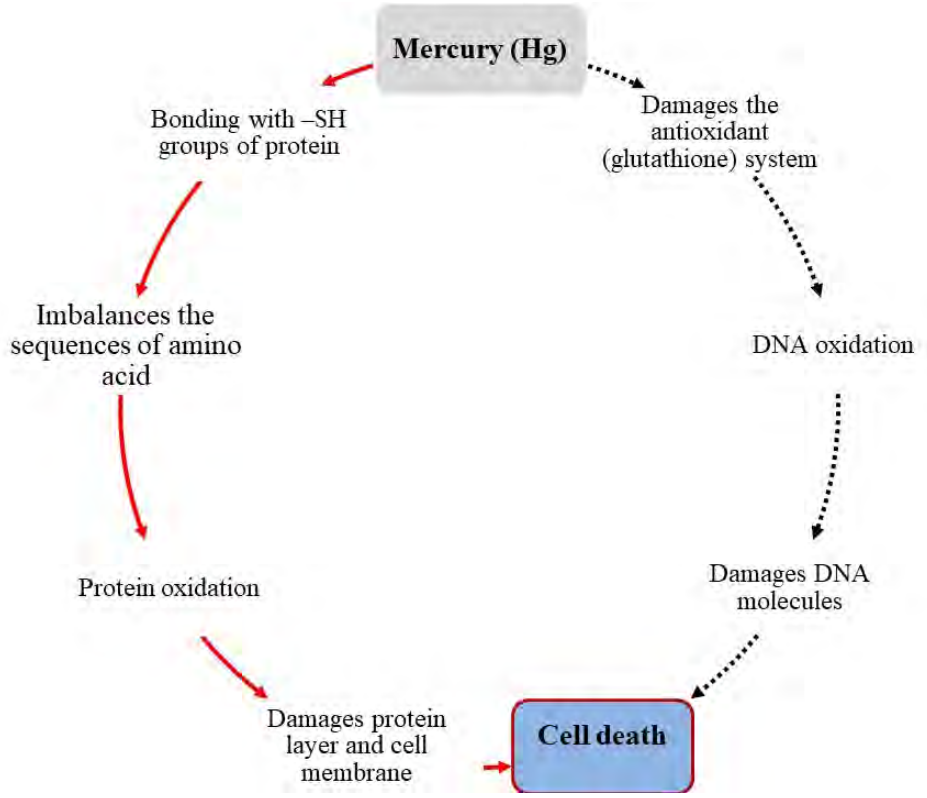

Fig. 1.7. *Mechanism of mercury toxicity in cell. Adapted from reference [75] with permission from Arabian Journal of Chemistry. © 2022 Elsevier B.V.*

Mercury fumes have been found to initiate short-term respiratory issues such as bronchitis and asthma. Mercury affects the tertiary and quaternary protein structure and disrupts the cellular replication and transcription machinery, triggering dysfunctioning of ribosomes, and destroying the endoplasmic reticulum [77]. This results in compromise of the cellular integrity which ultimately leads to the production of free radicals [78]. The mechanism of mercury toxicity is presented in Scheme 1.1 [79].

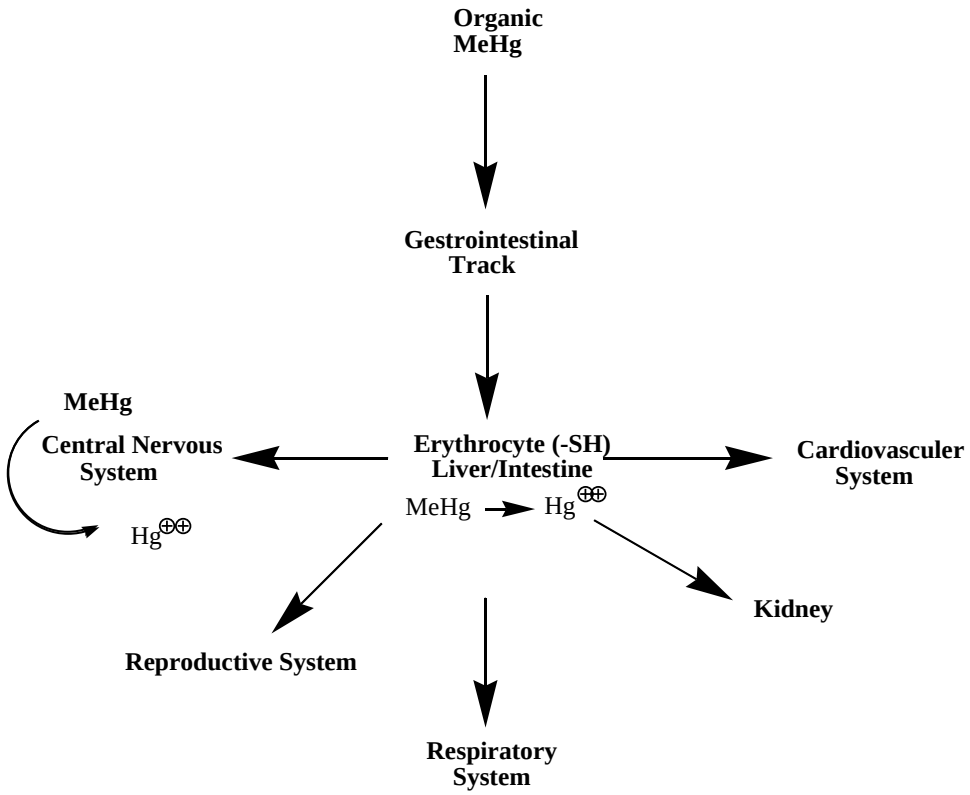

Scheme 1.1. *Molecular mechanism of mercury toxicity. Reproduced from reference [79] with permission from BioMed Research International. Copyright © 2012 Hindawi.*

1.10.3 Cadmium toxicity

The cellular toxic effects due to exposure to cadmium are presented in Scheme 1.2 [80]. It has been found that the concentration of cadmium increases to 3000 times when it attaches itself to a cysteine-rich protein. This interaction results in hepatotoxicity in the liver as reported in literature [81].

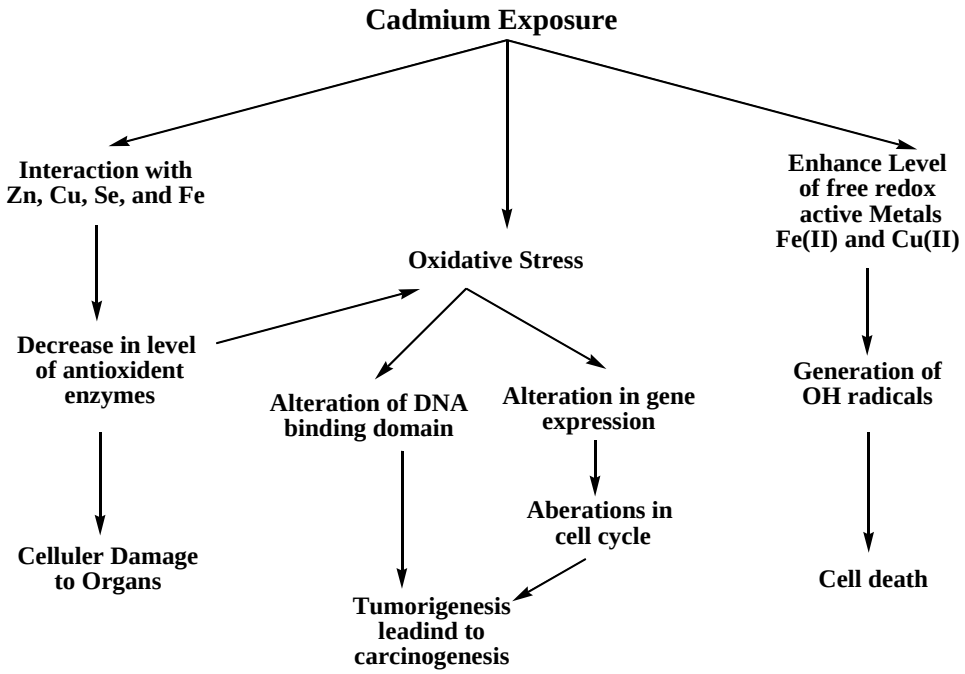

Scheme 1.2. *Mechanism of cadmium toxicity. Reproduced from reference [80] with permission from International Journal of Pharma and Bio Sciences. Copyright © 2009-2015 IJPBS, India.*

1.10.4 Chromium toxicity

Cr(III) is relatively safe, but hexavalent chromium Cr(VI) is highly toxic as it can actively cross the cell membrane as depicted in Fig. 1.8. The interactions of Cr(VI) with biological reductants such as thiols and ascorbate result in osmotic damage in the cell and to the biomolecules [82]. Cr(VI) is far more harmful than Cr(III) because of the ability of Cr(VI) to penetrate cells more easily than Cr(III) and is eventually converted to Cr (III). Cr(VI) is classified as a category 1 human carcinogen due to its mutagenic characteristics [83-89].

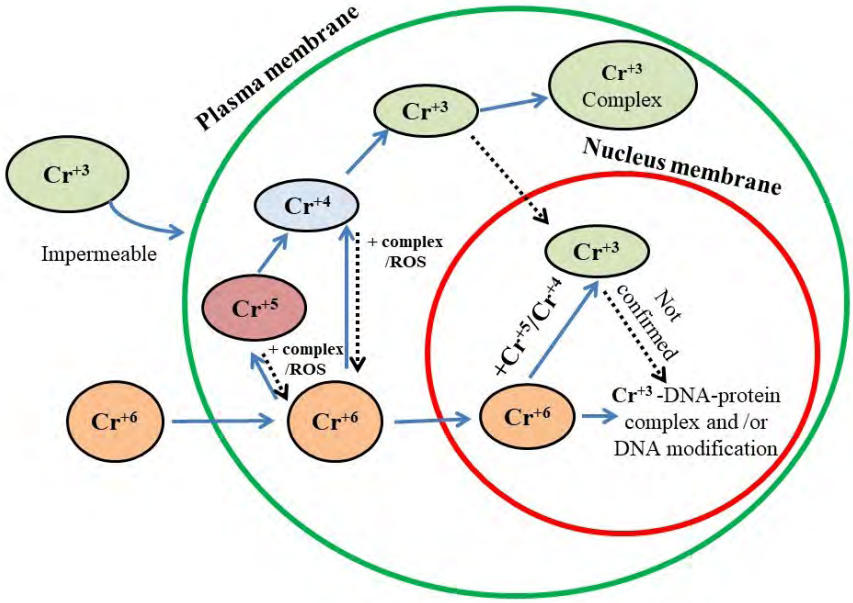

Fig. 1.8. *Schematics of chromium toxicity. Reproduced from reference [90] with permission from Microbial Biodegradation and Bioremediation. Copyright © 2014 Elsevier Inc.*

1.11 Bioaccumulation of HMs

Certain terminology has been proposed to measure the level or degree of heavy metal accumulation in flora and fauna. Bioaccumulation coefficient (BAC), bioaccumulation factor (BAF), bio-concentration factor (BCF), and other quantitative terminology are used. BCF is defined as "the ratio of a heavy metal ion concentration in an organism's tissue to its concentration in an abiotic medium (water and sediments)." BCF is evaluated by the formula 1:

$$BCF = \frac{C_{organism\ tissue}}{C_{abiotic\ medium}} \qquad \text{(Eq.1)}$$

The values of the coefficients such as BCF, BAF, BAC are dependent on the amount of heavy metal in the organism taken into consideration and the concerned medium [17]. The equation 1.1 given below can be used for calculating the BAC [92]:

$$BAC = \frac{C_{plant}}{C_{soil}} \qquad (Eq.\ 1.1)$$

Where C_{plant} corresponds to the concentration of the metal in the plant and C_{soil} denotes the metal concentration in the soil .

HMs accumulate in both aquatic and terrestrial animals owing to their abiotic (non-living) environment and their diet. The factors that affect the accumulation of HMs in animals include behavioral response, nutrition, and physiology [93,94]. The concentration of HMs in invertebrates vary significantly [95]. Their bioaccumulation in insects depends upon the insect's eating patterns. Carnivorous and predatory insects contain more HMs than herbivorous and omnivore insects. The accumulation of HMs in the three insect groups; the predator-dragonfly, the insectivorous-butterfly, and the polyphagous omnivore-grasshopper, reveals that heavy metal content vary in the following order: Dragonfly > Grasshopper > Butterfly [96].

The buildup of toxic metals in aquatic invertebrates have been examined. HMs accumulate in the soft tissue of mussels, commonly consumed as shellfish. Heavy metal bioaccumulation in invertebrates is of particular ecotoxicological importance. Invertebrates can serve as a bio-indicator species for monitoring the HMs contamination in aquatic and terrestrial habitats. Insects are valued bioindicators for monitoring the influence of anthropogenic activities and metal contamination on terrestrial ecosystems since they are the ones directly exposed to harmful metals found in soil and in leaf litter [97].

The estimation of the bioaccumulation of toxic metals in fish is critical because it serves as a measure for assessing water pollution and the possible health risk due to consumption of contaminated fish [98]. HMs find their way into the fish body via three routes including alimentary tract, skin and gills. Metal fractions which are soluble in body fluids accumulate in fish preferably through its gills as illustrated in Fig. 1.9 [99]. Fish gills serve as a key entry point for soluble heavy metal components [100].

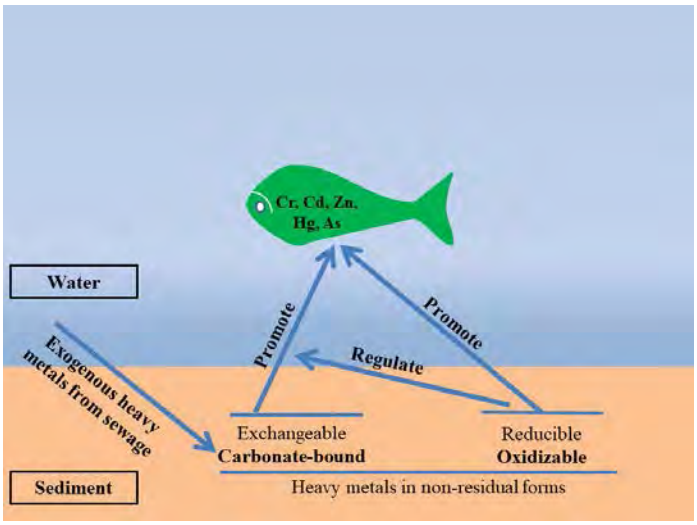

Fig. 1.9. *Mechanistic route showing HMs bioaccumulation in fish. Adapted from [99], with permission from Ecotoxicology and Environmental Safety. Copyright © 2022 Elsevier Inc.*

Owing to the porosity of their skin, Anuran amphibians are most susceptible to the absorption of heavy metal ions [101]. While birds receive HMs through water and food and through geophagy (the behavior of eating soil-like material) [102]. In terms of the influence of eating, heavy metal buildup in the species of birds that differ due to feeding habits vary in the sequence: Carnivorous > Omnivorous and insectivorous > Graminivores [103]. The feathers of birds serve as indicators for the assessment of pollution level due to HMs in the environment [104].

1.12 Detection of HMs

Development of a rapid and precise metal ion detection method is critical. A lot of funds are allocated for the development of sensor technology, biological sensors, or chemical sensors, in addition to traditional procedures. In recent times, the interest in interlinking the concepts of electrochemical methods with the unique set of properties that nano-sized materials have to offer, has been greater than ever before [105]. The present concern is the

monitoring of polluted areas where hazardous metals are expected to exist naturally or released anthropogenically [106]. A number of techniques are used for detection of metal ions.

Spectroscopic techniques are very sensitive techniques such as Atomic Absorption Spectroscopy, Inductively Coupled Plasma Mass Spectrometry, X-ray Fluorescence Spectroscopy, yet are very expensive and require meticulous sample preparation along with trained personnel. Atomic absorption spectroscopy (AAS) is a commonly employed procedure used to measure elements in different environmental media. The underlying concept of AAS is that when light is incident on a sample, the electrons present in the sample atoms undergo a transition from the lower energy levels to higher energy levels. This process of excitation is followed by de-excitation which is facilitated by emission of photons with characteristic frequencies which are distinctive to the individual atoms. The procedure for analysis using AAS requires the material to be atomized first, followed by an examination at the atomic level. The atomization of the material of interest is carried out by using flame and electro-thermal atomizers. The flow of radiation is then monitored and measured after subjecting the atomized sample to radiation. Before the atomization step, the flow of radiation is measured without the sample [107]. The ratio of fluxes of the blank (sample absent) and with the sample can then be computed and converted into an analyte's concentration.[108] It is a commonly used technique for analyzing the concentration of heavy metals in plant samples and groundwater, mixed water and wastewater at ng/mL levels especially when atomization is conducted with graphite furnace mode [109]. Thus in one study Mn, Fe, Cu, Zn, Cd and Pb were studied via AAS and it was found that metal discharged into environmental medium without pretreatment are toxic to health. Such contaminated water can infiltrate the aquifer and pollute the drinking water [110]. The LOD for Pb, Cd, Cu, As and Hg was found to be 0.28, 0.014, 0.49, 0.19 and 0.061 ppm. The World Health Organization permissible limits for HMs in water for the respective ions are 0.05, 0.005, 1.3, 0.05, 0.001 ppm respectively. In wine HMs such as V, and Cr were detected by AAS [111]. Similarly in soil samples very high concentrations of Pb, As, Cu, and Zn determined by AAS confirmed by X-ray Fluorescence Spectroscopy (XRF) were found with an LOD of 13 ppm, 11 ppm, 35 ppm, and 25 ppm, respectively [111]. The limitation of AAS is that it requires a well-equipped laboratory and a skilled operator to carry out the

analysis. Additionally, AAS cannot detect all heavy metals and can only measure one element at a time.

Inductively Coupled Plasma (ICP) is a technique that uses a high-temperature plasma to ionize atoms and molecules in a sample, producing a spectrum of light that can be analyzed to determine the presence and concentration of elements, including heavy metal ions. This is a highly sensitive and accurate technique that is used to detect and quantify a wide range of metals, including heavy metals, in plant and tissue samples up to the nmol/L [112]. It is often used for analyzing trace metals at low concentrations. It combines ICP with a mass spectrometer, which separates and quantifies ions based on their mass-to-charge ratio. Thus a study on fish muscle revealed presence of metal ions resulting in biomagnification through food web. Additionally, cyanobacterial bloom has resulted in release of metals such as As and Se in eutrophic lakes which has been a topic of debate lately with runoff water bringing metal ions into water. With the help of ICP-MS metal ions such Al, V, Cr, Mn, Zn, Fe, Ni, Cu, As, Se, Sr, Mo, Ag, Cd, Hg and Pb were detected in the fish muscle in Argentina which indicated health risk associated with the metals [113]. Yet the technique is very sensitive, it equires expensive equipment and skilled operators. Additionally, ICP-MS cannot distinguish between different oxidation states of an element, which can be important for certain heavy metals.

X-ray Fluorescence Spectroscopy (XRF) is a non-destructive technique that measures the fluorescence of X-rays emitted by metals in a sample. It can be used to analyze the concentration of heavy metals in plant tissues, soil, and other samples. A novel technique by pre-concentrating metal ions on target electrode such as boron doped diamond, followed by elemental identification and quantification through XRF, is developed which improved the sensitivity of the XRF by 4 orders of magnitude. Thus with the in-situ electrochemical X-ray fluorescence (EC-XRF), metals Cu^{2+} and Pb^{2+}, deposition potential was selected as −1.75 V and time for dep was 4000 s with LODs of 0.05 and 0.04 ppb, respectively [114].In situ EC-XRF a multi-metal solution containing 10 μM concentration of Hg^{2+}, Pb^{2+}, Cu^{2+}, Ni^{2+}, Zn^{2+}, and Fe^{3+} with E_{dep}= −1.5 V and t_{dep}= 5 min was possible in one simple measurement with high sensitivity [115]. Though XRF is a non-destructive technique that

can be used to detect heavy metals in solid samples. However, it is not as sensitive as other techniques and cannot detect elements with low atomic numbers.

Electrochemical techniques may require real-time analytics as compared to spectroscopic techniques and hence involve simple procedure. Moreover, they exhibit high LODs and sensitivity as compared to other methods. Electrochemical techniques such as anodic stripping voltammetry (ASV) and differential pulse voltammetry (DPV) can be used to analyze heavy metals in biological samples, soil by using extraction solution and water. These methods involve applying an electrical potential to a sample, which causes the metals to oxidize and reduce, resulting in a measurable current that can be used to determine the metal concentration. Yet due to small diameter of the electrode, a fraction of analyte reacts which can be overcome by modifying the electrode surface to enhance surface active area and availability of active sites at the sensing platform. Here voltammetry technique where applied potential is swept across the WE while keeping the potential difference constant between the WE and reference electrode has been most commonly used for detection of metal ions. Thus functionalized rGO on Glassy carbon electrode GCE was used as a modified electrode for multiplex detection of Cd^{2+}, Pb^{2+} and Cu^{2+} in aqueous media with high sensitivity and selectivity by engaging differential pulse anodic stripping voltammetry (DPASV). The LOD for the respective ions was found to be 0.17, 0.18 and 0.69 μg/L, respectively [116]. Hg is toxic to environment hence usage for detection purposes is to be curtailed. Thus Hg free electrode by employing Quercetin was carried out that acted as a complexing agent for the metal ion as well as reducing agent for green synthesis of rGO on GCE which led to simultaneous detection of Cd^{2+} and Pb^{2+} electrochemically by ASV. The Cd^{2+} was detected in a linear range of 0.19 to 2.5 μgL^{-1} with LOD of 0.05 μgL^{-1} and Pb^{2+} ions from 0.19 to 3.1 μgL^{-1} with an LOD of 0.06 μgL^{-1} [117] A surfactant modified GCE was used to simultaneously detect Cd^{2+}, Cu^{2+}, Hg^{2+}, Pb^{2+}, Zn^{2+}, and Sr^{2+} ions by ASV with an LOD of 6.45, 7.85, 9.15 , 11.0 , 16.9 , and 178.8 nM respectively [118]. Electrochemical methods, such as ASV, are highly sensitive and can detect trace levels of heavy metals in various samples [119]. However, they are limited to certain types of samples, such as liquids and solutions, and may require special preparation of the sample. Currently electronic tongues are used for sensing and quantification of toxic metals. The electronic tongue is a device that uses electrochemical methods such as potentiometry, voltammetry, and

chronoamperometry to image complex liquids. This sort of advancement has the potential to fill the gap between detection and the remedial technologies [120]

1.13 Modified electrodes for pharmaceuticals detection

Pharmaceutical drugs are used for prevention and treatments of disease and to protect public health. However the effluents discharged in water bodies from pharmaceutical industry are infused with drugs and their metabolites which are toxic for living organisms if present in amount greater than their threshold limit. In under developed countries drugs disposal regulations are not strictly followed and as a result some drugs find their way to water bodies. Proper management of water loaded with pharmaceutical wastes is obligatory for the protection of flora and fauna [121]. Release of pharmaceuticals in sewage water via urine and wastes end up in plants and aquatic life. Their absorption by water dwelling species would have a significant detrimental influence on public health [122]. The interference effect between pharmaceuticals makes it impossible to evaluate their concentration during formulation in particular applications, causing substantial challenges in their manufacturing processes. Moreover, measurements of the active ingredients in pharmaceutical formulations must be taken on the production line for quality control. Furthermore, many drug classes, such as addictive drugs, require 24-hour monitoring to avoid misuse or overdose. To achieve these goals, extremely sensitive, quick-responding, and selective pharmacological detection approaches are required [123,124]. To make a contribution in the field of tuberculosis treatment, a sensitive and rapid method called square wave voltammetry was utilized to analyze the effectiveness of isoniazid (INZ), a widely used drug for treating tuberculosis [125]. INZ, also known as pyridine-4-carboxylic acid hydrazide, a well known inhibitor of Mycobacterium Tuberculosis (MBT), the bacteria responsible for causing tuberculosis [126] . Monitoring the concentration of INZ in biological fluids is crucial to ensure the medication level remains stable and effective in tuberculosis therapy [127, 128]. Bimetallic cobalt-iron diselenide nanorods were used as modifier of the GCE surface for detecting INZ. Metal chalcogenides, especially metal diselenides (MSe_2) (M = Ni, Cu, Mo, Fe, and Co), have sparked a lot of interest due to their efficient electrocatalytic role in electrochemical applications [129,130]. $FeSe_2$ and $CoSe_2$

have been the most studied metal diselenides because of their outstanding electrical conductivity, low ion and electron diffusion duration, high specific capacitance, mechanical resilience, substantial recycling capacity, and low charge transfer resistance [131,132]. During the electrocatalytic phase, the transfer of electric charge is improved due to the presence of 3D electrons with low spin in cobalt (Co), resulting in enhanced metallic properties of $CoSe_2$ [133]. The synergistic effect between Fe and $CoSe_2$ leads to enhanced electrocatalytic behaviour of the $FeCoSe_2$. The development of hetero-metallic bonds enables fine-tuning of the bonding patterns between the catalyst surface and analyte molecules [134]. Bimetallic structures have powerful metal-metal interactions that change their electrical and mechanical properties. These peculiar characteristics make them suitable for a range of electroanalytical applications. Hence, $FeCoSe_2$/GCE was utilized for the electrochemical sensing of INZ.

A sensing platform was also created to detect venlafaxine (VEN), a selective serotonin and norepinephrine reuptake inhibitor (SSNRI) commonly prescribed to children experiencing nightmares, cataplexy, and narcolepsy. VEN is chemically called as 1-[2-(dimethylamino)-1-(4-methoxyphenyl) ethyl] cyclohexanol [135]. The recommended daily dosage range for the drug VEN is between 75 to 375 mg. If taken in excess, an overdose can lead to severe health complications. These complications include serotonin syndrome, cardiac arrhythmias, depression, coma, hypertension, hypotension, and, sometimes, even death may occur. As a result, it has become increasingly important to clinically assess the drug's toxicity, potential interactions with other medications, and the effectiveness of any necessary treatments. Monitoring VEN levels in biological fluids has become a necessary aspect of this process to ensure that patients receive safe and effective care. The electrochemical sensing platform developed for VEN detection offers a promising approach to aid in this monitoring process and improve patient outcomes [136]. In this regard a nanosensor made of modified-GCE with Co-Pd@Al_2O_3, utilized for the analysis of the VEN in water and biofluids.

Metal NPs have been widely used in electrocatalytic studies owing to the exceptional characteristics like higher electrical-conductivities and a larger-surface-area. These characteristics make them highly effective in catalyzing electrochemical reactions, and

their small size allows for enhanced sensitivity in detection methods. Additionally, the surface chemistry of metal NPs can easily be modified to optimize their performance for specific applications, further increasing their usefulness in electrocatalytic studies. In electrochemical studies, supported metal catalysts play a crucial role in the development of new electrode materials, mainly because of the advantages provided by the support material. By using a support material, the catalyst is provided with a greater surface area, thereby increase the number of active-sites accessible for electrochemical reactions. This feature leads to better metal dispersion, enabling the catalyst to exhibit superior catalytic activity, selectivity, and stability. Additionally, the support provides good electrical conductivity, allowing for efficient electron transfer process between the electrode material and catalyst. The higher stability of supported metal catalysts also ensures their long-term performance, and they possess better mass transfer properties, facilitating the transport of molecules to and from the catalytic surface. All these factors make supported metal catalysts an essential component of electrochemical studies and the development of advanced electrode materials [137]. Gamma alumina has emerged as a preferred support material because of the exclusive characteristics. It possesses a mesoporous structure, providing higher-surface-area and narrower pore-size distributions, which enhances the dispersion of metal nanoparticles. Furthermore, it exhibits good mechanical strength, allowing it to withstand the high pressure as well as temperature. The oxide groups of alumina, such as hydroxyl and carboxyl, exhibit a proton-donating nature, which helps improve the sensitivity of many materials by reducing overpotential, resulting in more efficient electrocatalytic activity. Metal nanoparticles supported on gamma alumina have demonstrated superior performance in various electrochemical applications. For example, PdCo/C, Ni/graphite, Au/C, and Pt-Co/CNT modified electrodes have extensively been used in electrochemical sensing, fuel cells, and other applications. The incorporation of metal NPs with gamma alumina support provides several benefits, including high stability, catalytic activity, and conductivity, thereby making them a popular choice for developing advanced electrochemical materials [138,139]. In recent years, the focus has been on utilizing various metal oxides for electrochemical sensing of venlafaxine. In this study, we have synthesized bimetallic Co-Pd@Al_2O_3 nanoparticles and deposited them on a GCE to create a sensor capable of detecting venlafaxine in human serum samples. This is the first

report of quantifying venlafaxine using a GCE that has been modified with Co-Pd@Al_2O_3 nanoparticles. These nanoparticles exhibit excellent performance in venlafaxine oxidation with a lower limit of detection and wider linearity range. The superior performance of the nanoparticles can be credited to their greater electrical conductivity along with the collaborative-effect of the bimetallic structure.

1.14 Research Plan

Certain events, during human history have shaped the fate of mankind in such a way that catapulted its status from being primitive hunter-gatherer to the present-day de facto ruler of the planet. The industrial revolution is one of such events that has uplifted the status of life by bringing comfort and luxury but it has also led to environmental pollution. Rapid increase in industrialization to meet the needs of ever-growing population has endangered the ecosystem owing to the excessive and unregulated discharge of toxic wastes into the environment, especially water bodies. Wastes from electronics manufacturing, painting, and metal forming industries are usually rich in heavy metal ions which are the sources of acute toxicity due to their persistent and bio-accumulative nature. While the effluents discharged into aquatic environment from pharmaceutical industry and personal care products are infused with xenobiotics of pharmaceuticals and their metabolites. This is due to poorly treated wastewater owing to insufficient resources and lack of environmental awareness in under developed countries where drugs disposal regulations are not strictly followed. Most of the pharmaceuticals are active chemicals that exert specific curing effect on targeted organ, however, they can also affect non-targeted aquatic biota and adversely cause disturbance on the integrity of body systems. Pharmaceutical effluents contain mixture of various classes of organic and inorganic micropollutants that are capable of inducing toxicological effects on aquatic organisms. Proper management of water loaded with pharmaceutical wastes and heavy metal ions is obligatory for the protection of aquatic life and public health. In this regard donor agencies should play their role in awareness campaign about safe ways of wastes disposal and they should invest in countries which cannot afford high standard equipment for analysis and waste treatment. In fact the United Nations has set seventeen sustainable development goals (SDGs) for addressing major

global issues. One of these SDGs is directly related and two are indirectly linked with water cleanliness . The current work exploring efficient environmentally friendly approaches for the detection of water contaminants is expected to be a useful addition to the existing knowledge economy on this topic and a valuable contribution to water purification SDGs. The foremost goal of the present research work is to synthesize electrode modifiers that can effectively enhance the sensitivity of the transducer surface in electrochemical sensors. The focus of the study is on developing improved methods for modifying the electrode's surface to enhance the performance of electrochemical sensors.

1.14.1 Research objectives and goals

This study has set out to accomplish a number of specific goals, which are:

1. Creating fast-responding and operationally stable electrochemical sensors.
2. Utilizing the prepared sensors for drug analysis and detection of toxic HM ions.
3. Examining various modifiers and selecting the most suitable one to meet the application requirements of the sensors.
4. Optimizing conditions to obtain well-defined electroanalytical response of the analytes for quantitative analysis.
5. Assessing the validity and reliability of the proposed sensors in real samples.
6. Investigating the anti-interference ability, accuracy, and stability of the sensing platforms.
7. Testing the feasibility of the proposed protocols for analyzing target analytes in biological specimens.

1.14.2 Research methodology

- **Electrode Modification**: Utilize drop coating approach for modifying glassy carbon electrode (GCE) with selected modifiers based on their transducer anchoring and toxin binding capabilities.
- **Characterization:** Employ SEM, TEM, EDX, and XRD analysis to characterize synthesized electrode modifiers.

- **Electrochemical Studies:** Conduct EIS, CV, and SWASV to assess charge transport, electrode active surface area, and electrocatalytic role of the recognition layer in the presence of target analytes.
- **Optimization:** Optimize parameters such as scan rate, pH, deposition time, modifier concentration, accumulation potential, and supporting electrolyte to enhance electroanalytical signals.
- **Performance Evaluation:** Evaluate sensors' performance in the presence of interfering agents, assess selectivity, and conduct real sample analysis to validate practical applicability and determine percentage recoveries.
- **Long-Term Stability:** Assess repeatability and long-term stability of sensors through prolonged electrochemical experiments.

Chapter 2

EXPERIMENTAL BACKGROUND

This chapter presents chemicals and techniques used for investigation of the samples. Moreover, it presents the details of materials and their synthetic protocols. The methods of electrode modification are also explained.

2.1 Instrumentation

XRD was performed on Rigaku D/max 2500 with a Cu Kα1 radiation source (λ=1.54056 Å). Morphologies of the prepared samples were probed at Hitachi S-4800 Scanning Electron Microscope at an accelerating voltage of 30 KV. Energy dispersive X-ray spectra were obtained on Oxford Material Analysis equipped on SEM and TEM. The 302 Eco Chemie Auto lab PGSTAT 12 (Utrecht, The Netherlands) and Metrohm Auto lab B.V, PGSTAT 302N, ADC164, External, DIO48 running with software NOVA were used for electrochemical studies. A conventional three-electrodes setup comprising of a working, a reference along with a counter electrode was used. A double-walled glass cell with an adjustable plastic covering at the top, containing five tapper ports was employed. These ports facilitated the inlet and outlet for argon gas, which was used to displace the dissolved electroactive oxygen from the solution. The remaining three ports were used for the electrodes employed during experiments [140].

For minimizing the IR drop to the applied voltage, the WE was placed at the center of the electrochemical cell, ensuring the least distance between the working and the reference electrodes [141]. For the WE, a clean bare GCE with an effective surface area of 0.071 cm^2 and modified GCE were utilized. This electrode could function both as anode or a cathode, depending on whether oxidation or reduction is occurring at its surface. The results obtained from the unmodified GCE were compared with those obtained from a GCE that had been modified with appropriate modifiers [142]. Glassy carbon electrode was selected

as it has high resistance for temperature and chemical attack [143], and it can provide a wide potential range, thus, permitting greater degree of analyte characterization.

In electrochemistry, a reference electrode is an essential component of an electrochemical setup that provides a stable potential as a reference point for controlling and measuring the voltage of the WE. [144]. The study utilized the Ag/AgCl (3 M KCl) electrode as a reference electrode, which is one of the three most preferred reference electrodes alongside the saturated calomel electrode and the normal hydrogen electrode.

In electrochemical analysis, a counter electrode, also known as an auxiliary electrode, is an essential component of an electrochemical cell that completes the circuit and enables the flow of current. In order to prevent any limitations to the kinetics of the electrochemical reactions, it is significant that the counter electrode's total surface area must be greater than the WE. In the present investigation, a platinum wire with a considerably larger surface area than the WE was used as the counter electrode in order to ensure that the half-cell reaction proceeds rapidly enough to avoid restricting the kinetics of the electrochemical process occurring at the working electrode [145,146]. The schematic diagram of the electrochemical cell used for electrochemical analysis is displayed in the Fig. 2.1.

Fig. 2.1. *Diagram experimental setup (A,B) and the electrochemical cell (C) used for electrochemical analysis [145].*

2.2 Chemicals used

The chemicals used are broadly categorized into solvents, supporting electrolytes, analytes, and electrode modifiers.

Table. 1.3 List of required chemicals with supplier information and purity percentage.

S. No	Chemicals required	Supplier	Percentage purity (mass%)
1.	Acetone	Riedel-deHaen	99
2	DMSO	Sigma-Aldrich	≥99.0%
3	Isopropanol	Sigma-Aldrich	≥99.0%
4	Boric acid	Sigma-Aldrich	≥99.0%
5	Distilled water	-	-
6	HCl	BDH	98%
7	Potassium chloride	Sigma-Aldrich	-
8	Sodium chloride	Merck	-
9	Sodium hydroxide	Fluka	97%
10	Sodium nitrate	BDH	98.0%
11	Sulphuric acid	BDH	98.0%
12	$CoCl_2.6H_20$	Sigma-Aldrich	97%
13	$FeCl_2.4H_2O$	Sigma-Aldrich	99%
14	EDTA	Sigma-Aldrich	99%

2.2.1 Solvent and supporting electrolytes

Solvent selection was made on the basis of two main criteria. Firstly, the solvent must be able to dissolve the electrode modifiers as well as the analytes. Secondly, the solvent should be stable and must not undergo any oxidation/reduction reactions during the selected voltage range of the voltammetric investigations. To meet these criteria, doubly distilled water and analytical-grade dimethyl sulfoxide (DMSO) were selected as solvents for the preparation of stock solutions of analytes and electrode modifiers. These solvents are stable under the voltammetric measurement conditions. The use of analytical grade solvents ensured that the electrochemical measurements are reliable, as any impurities in the solvents could potentially interfere with the analysis.

Supporting electrolytes are electrochemically inert in the chosen voltage range and possess good electrical conductivity and ionic strength [147,148]. These are extensively utilized in electrochemical studies to achieve various objectives such as regulating the electrode potential to eliminate the IR drop effect, increasing the conductivity of the solution, inhibiting the migration of analytes, sustaining a consistent ionic strength, and stabilizing the pH level of the solution. In recent years, pH determination has been improved by the use of Britton-Robinson Buffer (BRB) solutions. These acidic mixtures have reduced strength, and their pH values continuously vary from approximately 2 to 12 during the neutralization process. BRB solutions are prepared by mixing 0.04 M H_3BO_3, 0.04 M CH_3COOH, and 0.04 M H_3PO_4 and titrating the resulting mixture against solution of NaOH (0.2 M) to achieve the pH required for electroanalytical measurements [149]. Supporting electrolytes increase the conductivity of the analyte's solution and decrease the migration factors [150,151].

2.2.2 Analytes and electrode modifiers

The list of analytes and electrode modifiers is given in Table 2.2. The analytes isoniazid and venlafaxine drugs were acquired from Sigma-Aldrich and utilized without any additional purification. To enable the selective detection of isoniazid, bimetallic cobalt-iron diselenide nanorods were employed as a modifier. Bis(imidazo[4,5-f][1,

10]phenanthroline) appended bis-triazolo calix[4]arene, multifunctional bis-triazole-appended calix[4]arene was synthesized according to Scheme 2.1 and Scheme 2.2 respectively. Bimetallic cobalt-iron diselenide nanorods were prepared according to Scheme 2.3. For the preparation of Co-Pd /ɤ-Al_2O_3, the support ɤ-Al_2O_3 was prepared according to Scheme 2.4, followed by simple wet impregnation method for Co-Pd /ɤ-Al_2O_3 according to Scheme 2.5. Bis(imidazo[4,5-f][1, 10]phenanthroline) appended bis-triazolo calix[4]arene and multifunctional bis-triazole-appended calix[4]arene were used as modifiers for the preparation of electrochemical platforms for the detection of HM ions (Cd^{2+}, Hg^{2+}, Pb^{2+}, Zn^{2+}, and As^{3+}) simultaneously.

Table 2.2. *The list of analytes and recognition layers containing electrode modifiers.*

S.No	Analytes	Electrode modifier as recognition layer of the sensor
1	Cd^{2+}	Bis(imidazo[4,5-f][1, 10]phenanthroline) appended bis-triazolo calix[4]arene
2	Pb^{2+}	• bis(imidazo[4,5-f][1, 10]phenanthroline) appended bis-triazolo calix[4]arene • multifunctional bis-triazole appended calix[4]arene
3	Hg^{2+}	• bis(imidazo[4,5-f][1, 10]phenanthroline) appended bis-triazolo calix[4]arene • multifunctional bis-triazole appended calix[4]arene
4	As^{3+}	multifunctional bis-triazole appended calix[4]arene
5	Zn^{2+}	multifunctional bis-triazole appended calix[4]arene
6	INZ	Bimetallic cobalt-iron diselenide nanorods
7	VEN	Co-Pd@Al_2O_3 nanoalloy

2.2.2.1 Procedure for synthesis of Bis(imidazo[4,5-f][1, 10]phenanthroline) appended bis-triazolo calix[4]arene

The tweezer like fluorescent Bis(imidazo[4,5-f][1, 10]phenanthroline) appended bis-triazolo calix[4]arene (8) was efficiently synthesized *via* condensation of the bis-triazolo diabenzaldehyde derivative **5** with the 1, 10 phenanthroline-5,6-dione **7**. The

phenanthroline dione **7** was first synthesized by oxidation of 1, 10-phenanthroline **6** in the presence of concentrated HNO_3, H_2SO_4 and KBr at reflux in 3 h. The hot reaction mixture was then poured into ice cold water and pH was adjusted between 6 and 7 using a highly concentrated aqueous NaOH solution. The aqueous neutralized reaction mixture was then extracted with EtOAc (3× 20 mL) and the organic phase was dried over $MgSO_4$. The final mixture was then concentrated under reduced pressure and was finally purified through column chromatography using silica gel as the stationary phase and a mixture of EtOAc and hexane (4:6, v/v) as the mobile phase. The desired phenanthroline dione **7** was obtained as yellow solid with 67 % yield. Compound **7**, the dialdehyde **5,** and ammonium acetate (20 equivalents) in acetic acid (10 mL) were added and refluxed for 3 h. The hot reaction mixture was then poured into ice cold water which yielded yellow precipitate of the desired product. The precipitates were filtered, washed with excess distilled water and dried under vacuum. The completely dried precipitates were grinded into fine powder which were consequently washed with ethyl acetate (15 mL), acetone (10 mL) and ethanol (10 mL). Our desired tweezer like calix[4]arene bridging Bis(imidazo[4,5-f][1, 10]phenanthroline) **8** was obtained in 71% isolated yield without any further purification. The synthesis was confirmed by mass spectrometry, ^{1}HNNMR and ^{13}C NMR analysis and the molecular mass was deduced from its MALDI-TOF-MS analysis, where a strong peak for $[M + Na]^+$ was observed at *m/z,* 1539.20 as shown in Fig. 2.2 and 2.3. The atomic mass of Na^+ (22.9897) when subtracted gave molecular mass of 1516.21, which is consistent with molecular mass 1515.84, calculated for $C_{94}H_{94}N_{14}O_6$. ^{1}H NMR (Fig. 2.4) recorded in DMSO-$_{d6}$ revealed a broad singlet at 13.56 ppm corresponding to imidazole-N<u>H</u>, the triazole-C<u>H</u> as sharp singlet at 8.36 ppm, and the characteristic Ph-O-C<u>H</u>$_2$- also as sharp singlet at 5.27 ppm. All other peaks in ^{1}H NMR were compared which unambiguously justified the structure of our desired product. Similarly, the ^{13}C NMR (DEPT-135) also recorded in DMSO-$_{d6}$ showed the five different kinds of methylene carbon atoms at ppm; 72.92, 61.25, 64.45, and 31.18, and 30.22 (Fig. 2.5).

2.2.2.2. Synthesis of precursors 2-7

The synthesis of precursors **2-5** (shown in **Scheme 2.1**) has already been published by our research group, where the mentioned molecules were used to synthesize a novel

macrocycle as highly fluorescent photochemical sensor for selective detection of Cu^{2+} ions in water. Similarly, 1, 10-phenanthrolinedione **7** was synthesized according to the published protocol [15].

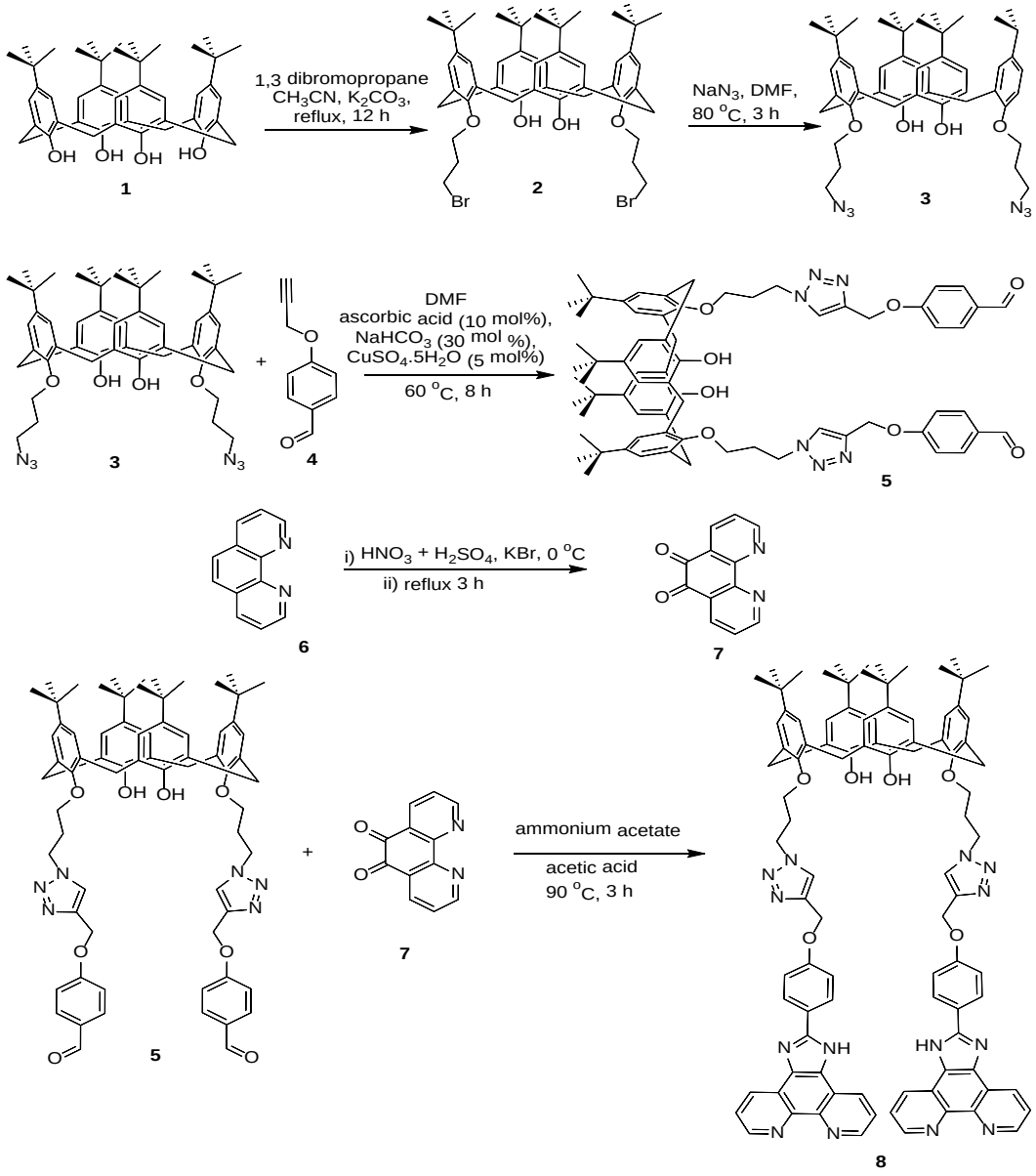

Scheme 2.1*. Synthesis of bis(imidazo[4,5-f][1, 10]phenanthroline) appended bis-triazolo calix[4]arene*

2.2.2.3. Characterization of the synthesized (bis(imidazo[4,5-f][1, 10]phenanthroline) appended bis-triazolo calix[4]arene

Compound 5 (Scheme 2.1) or compound 8 (Scheme 2.1) (100 mg, 0.08 mmol), 1, 10-Phen-5, 6-dione **7** (55.5 mg, 0.26 mmol), and ammonium acetate (123 mg, 1.60 mmol) were stirred in 5 mL of glacial acetic at 90 ^{0}C for 3h. The reaction mixture was then poured into ice cold distilled water (~ 15 mL in a small beaker) which formed yellow precipitates of the desired product. The precipitates were filtered, washed with acetone (10 mL), EtOAc (10 mL), and MeOH (10 mL).

Yield: 71 mg, 71%. m.p. 254-256 ^{o}C; MALDI-TOF-MS: observed, $[M+H]^{+}$, *m/z* 1517.21, $[M+Na]^{+}$, *m/z,* 1539.20, and calc for [$C_{94}H_{94}N_{14}O_6$ + Na], *m/z,* 1539.23. ^{1}H NMR (DMSO-*d6*, 300 MHz): δ (ppm); 13.56 (bs, 2H, imidazole-NH), 8.96 (s, 2H, ArH), 8.84 (d, 4H, ^{3}J = 7.5 Hz, ArH), 8.50 (s, 2H, PhOH) ,8.36 (s, 2H, triazole-CH) , 8.18 (d, 4H, ^{3}J = 7.8 Hz, ArH), 7.75 (s, 4H, ArH), 7.21 (d, 6H, ^{3}J = 7.8 Hz, ArH), 7.09 (d, 6H, ^{3}J = 5.1 Hz, ArH), 5.27 (s, 4H, Ph-O-CH_2), 4.84 (br s, 4H, Ph-O-CH_2-CH_2-), 4.86 (bs, 4H, -NCH_2CH_2), 4.13 (d, 4H, J_{gem} = 12.3, bridge CH_2), 3.92 (bs, 4H, -OCH_2CH_2CH_2-), 2.32 (bs, 4H, -OCH_2CH_2CH_2-), 1.13 (s, 18H, *t*-butyl-H), 1.03 (s, 18H, *t*-butyl-H).13CNMR (DMSO-*d6*, 300 MHz): δ (ppm); 159.11, 150.60, 149.94, 149.31, 147.67,147.57, 147.36, 143.57, 142.76, 141.69, 135.69, 133.15, 129.54, 127.76, 1^{26}.16, 129.45, 127.76, 126.16, 125.68, 125.36, 124.69, 123.70, 123.29, 123.06, 122.94, 119.28, 115.19, 72.93, 61.29, 64.47, 31.34, 31.18, 30.79, and 30.22.

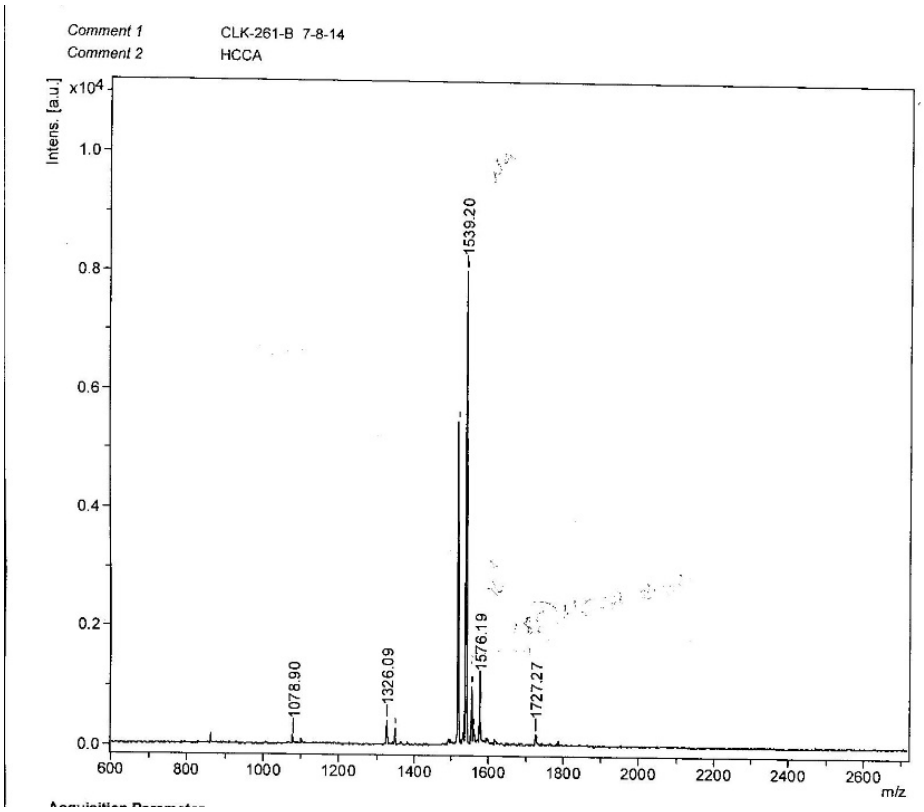

Fig. 2.2. *MALDI-TOF mass spectrum of (bis(imidazo[4,5-f][1, 10]phenanthroline) appended bis-triazolo calix[4]arene*

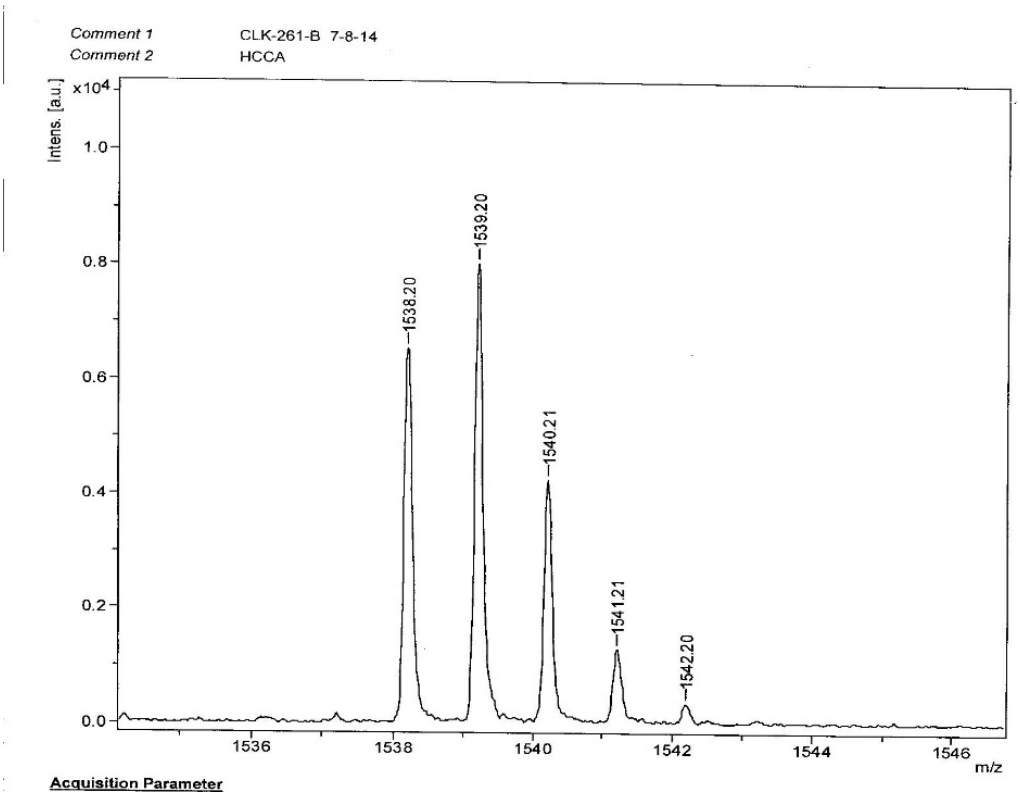

Fig. 2.3*. MALDI-TOF resolved molecular ion peak for bis(imidazo[4,5-f][1, 10]phenanthroline) appended bis-triazolo calix[4]arene.*

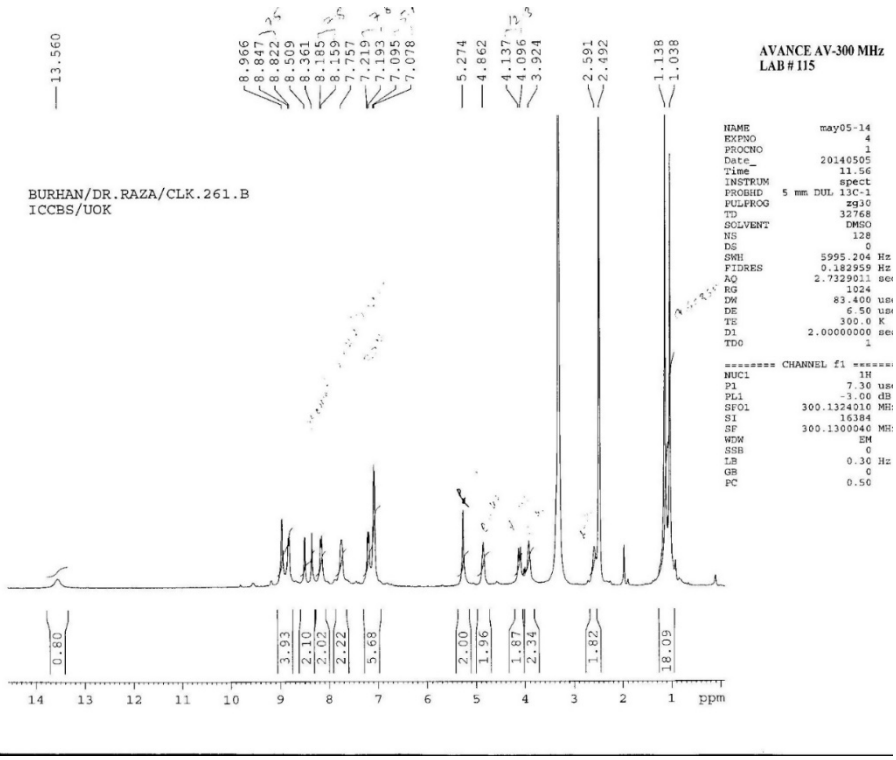

Fig. 2.4. *^{1}HNMR Spectrum of bis(imidazo[4,5-f][1, 10]phenanthroline) appended bis-triazolo calix[4]arene.*

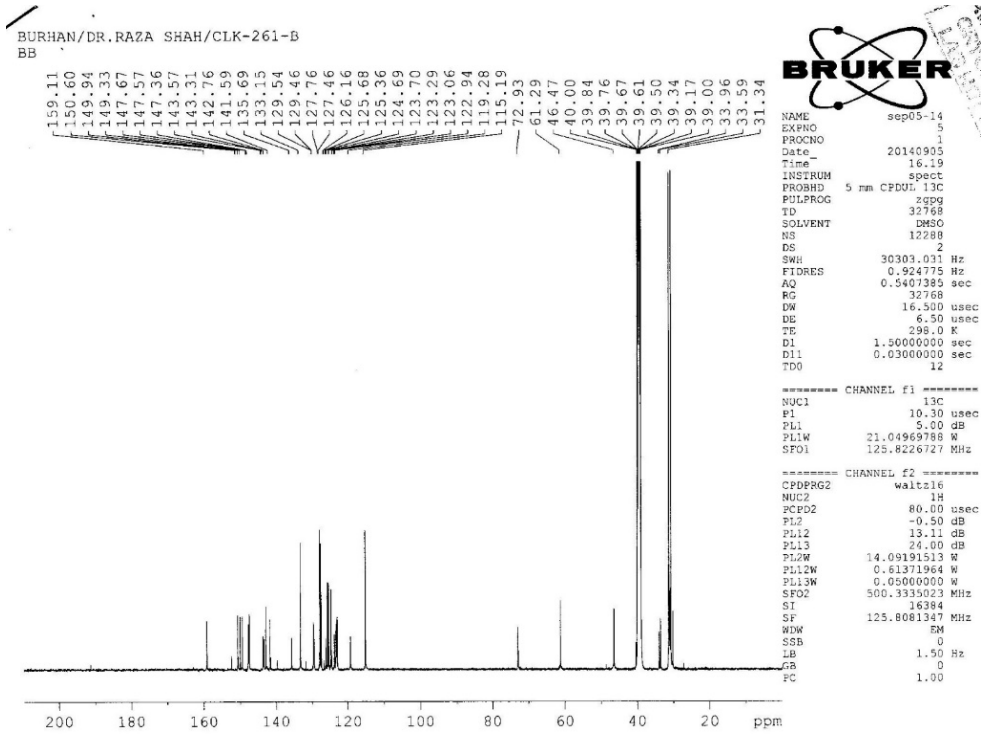

Fig. 2.5. *^{13}CNMR, Broad band spectrum of (bis(imidazo[4,5-f][1, 10]phenanthroline) appended bis-triazolo calix[4]arene*

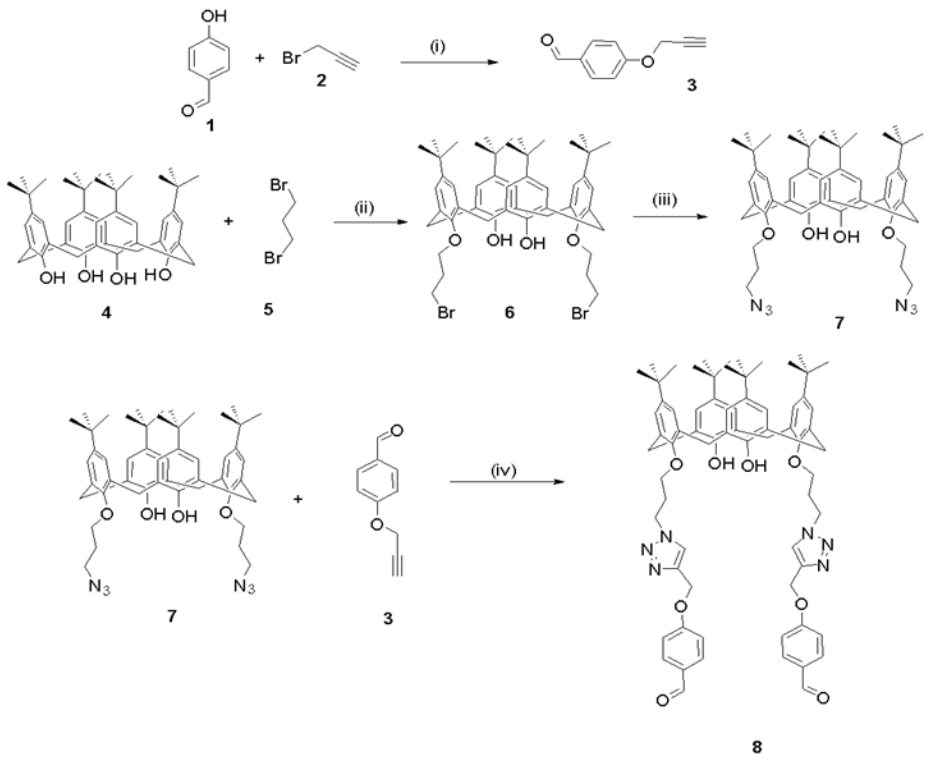

Scheme 2.2. *Synthesis of BTC (8) (i) Acetone, K_2CO_3, 60˚C, 3h, 91%, (ii), CH_3CN, K_2CO_3, 70˚C , 4h, 68% (iii) DMF, NaN_3, 70˚C, 1h, 90% (iv) DMF, sodium-ascorbate, $CuSO_4.5H_2O$, 2h, 73%.*

Scheme 2.3. *A diagrammatic representation of the process for synthesizing $FeCoSe_2$.*

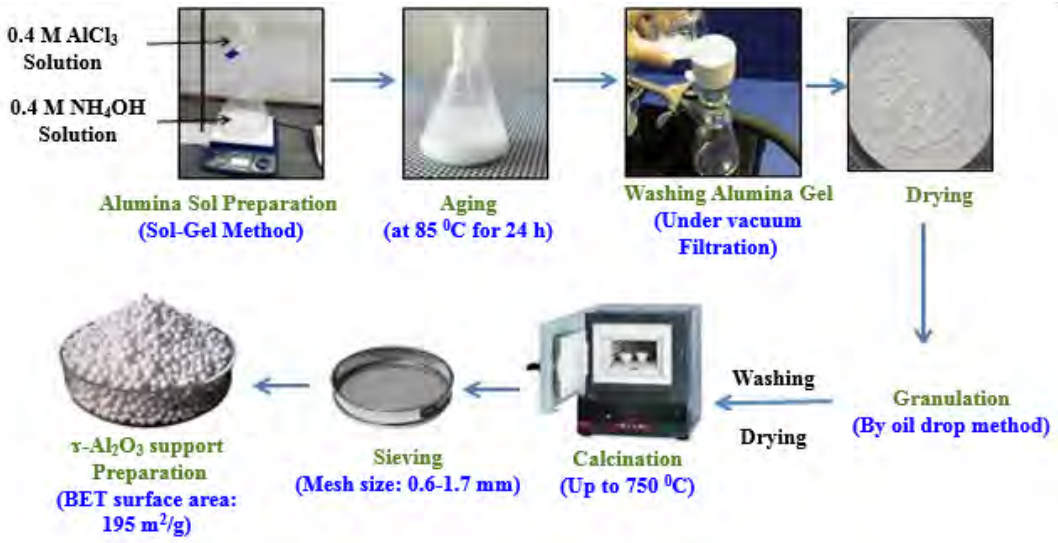

Scheme 2.4. *The diagram depicting multiple steps for the synthesis process for producing the ɤ- Al_2O_3 support.*

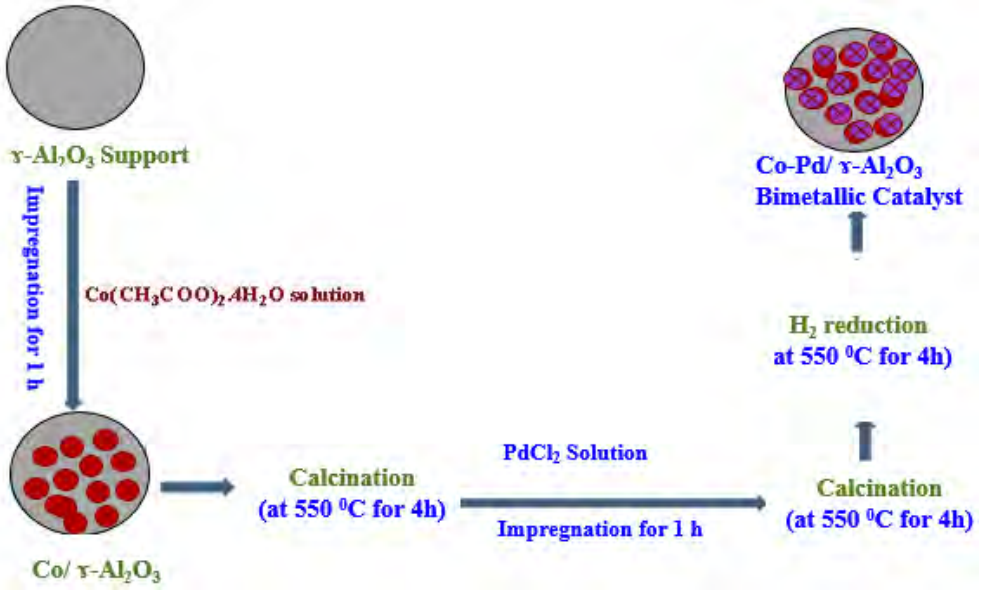

Scheme 2.5. *The wet impregnation method employed to prepare the Co-Pd/ɤ-Al_2O_3 catalyst.*

2.3 Preparation of electrochemical sensors

2.3.1 Sensor 1: BTC modified GCE

To detect Zn^{2+}, Pb^{2+}, As^{3+} and Hg^{2+}, individually and simultaneously, the GCE surface was prepared by polishing it with a nylon-buffing-pad and 0.05 μm α-Al_2O_3 powder until it achieved a shiny and smooth surface. Afterward, a mixture of HNO_3 (1:1, v/v), ethanol, and doubly distilled water was prepared followed by immersing GCE in the mixture. The GCE was then sonicated for a few minutes, washed with distilled water, and dried in air. The stock solution of BTC was prepared in DMSO, and the modification of the GCE was done by using drop casting method. To remove any molecules that were only loosely attached, the electrode coated with BTC was thoroughly washed with doubly-distilled water. Afterward, the prepared electrode was inserted into an electrochemical cell that contained the analyte solution, and a voltammetric analysis was carried out following the steps outlined in Scheme 2.6. In the beginning, the electrode surface underwent an electroreduction process to electroplate metal ions onto it. Following that, multiple scans of SWASV were performed, measuring the resulting current during the stripping steps. To establish a comparison, the electroplating of metal ions and stripping analysis of their electroreduced forms were also carried out using a bare GCE.Surface Characterization of bare and modified electrodes was done by SEM as shown in Fig. 2.6.

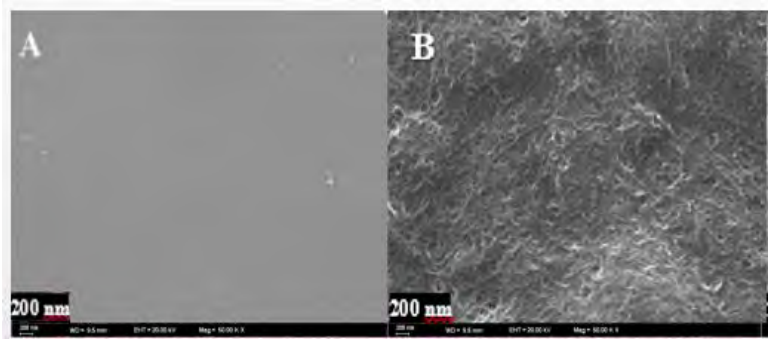

Fig. 2.6. *SEM micrographs of (A).Bare GCE, (B) BTC-modified GCE*

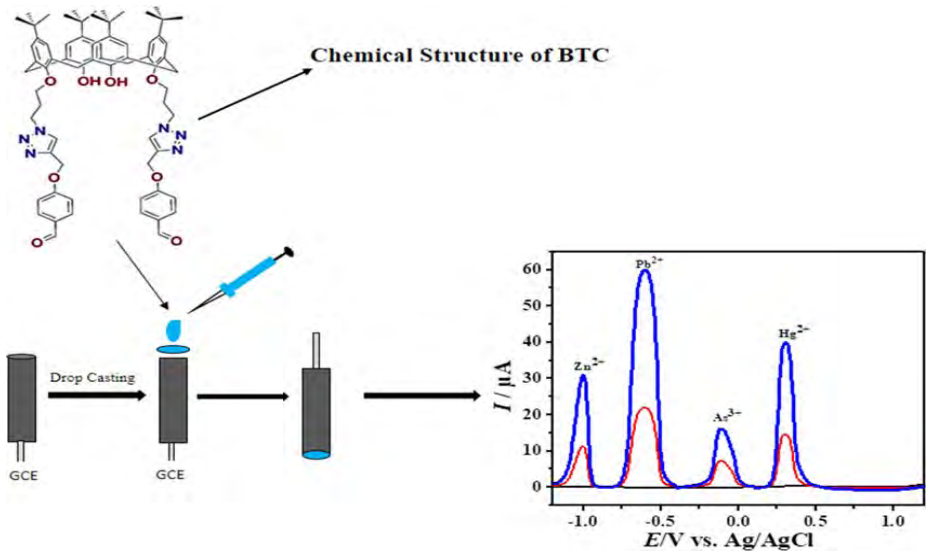

Scheme 2.6. *Multifunctional bis-triazole appended calix[4]arene based electrochemical sensor preparation and application.*

2.3.2 Sensor 2: BPTC modified GCE

To detect Cd^{2+}, Pb^{2+}, and Hg^{2+} ions electrochemically, bis(imidazo[4,5-f][1,10]phenanthroline) appended bis-triazolo calix[4]arene was immobilized over the surface of GCE. Firstly, a smooth and polished surface for the GCE was achieved by polishing it with α-Al_2O_3 powder (0.05 µm), utilizing a nylon buffing pad. Then, a 0.5 mM solution of modifier (BPTC) was prepared in DMSO and after that a 5 µL drop of this solution was applied onto the clean GCE surface, which was then air dried. The modified GCE was then cleaned with deionized water to take away any loosely bound molecules. The molecules of BPTC interacted with the chemical functionalities on the surface of GCE to form a recognition film. Evaporation of solvent led to anchoring of the BPTC with the GCE during the modification process. Insolubility of the modifier in aqueous solution of target analyte prohibited its leaching from the electrode surface. The complexing head groups of the modifier molecules led to binding with the target metal ions. Consequent preconcentrating role of the recognition layer generated intense signals of electroreduced metals in stripping step of pulse voltammetry. Fig. 2.7 displays the chemical structure of

the modifier and comparison of the metal ions sensing performance of bare and modifier GCE. Surface characterization was modified GCE was done by SEM as shown in Fig. 2.8.

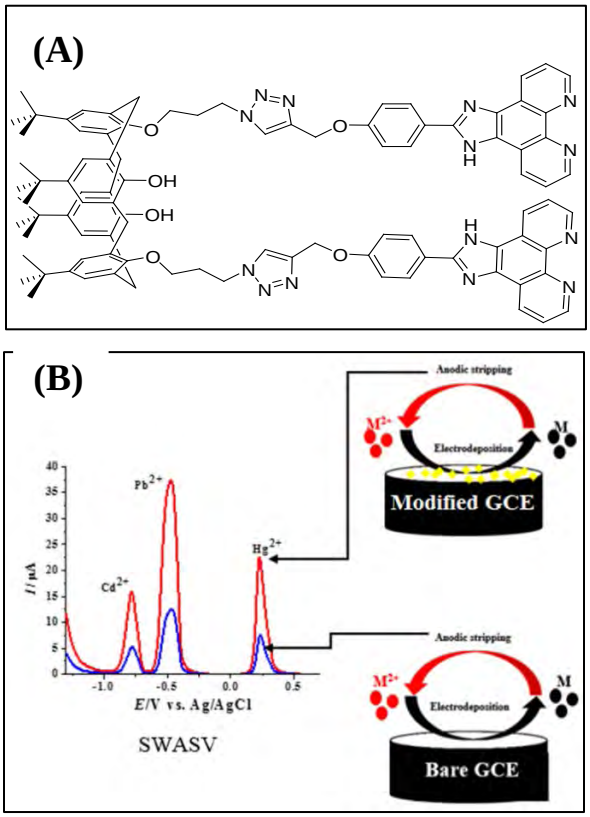

Fig. 2.7. *(A) Molecular structure of BPTC (B) the electrochemical response of the bare compared to modified electrodes investigated for the simultaneous detection of Pb^{2+}, Cd^{2+} and Hg^{2+}.*

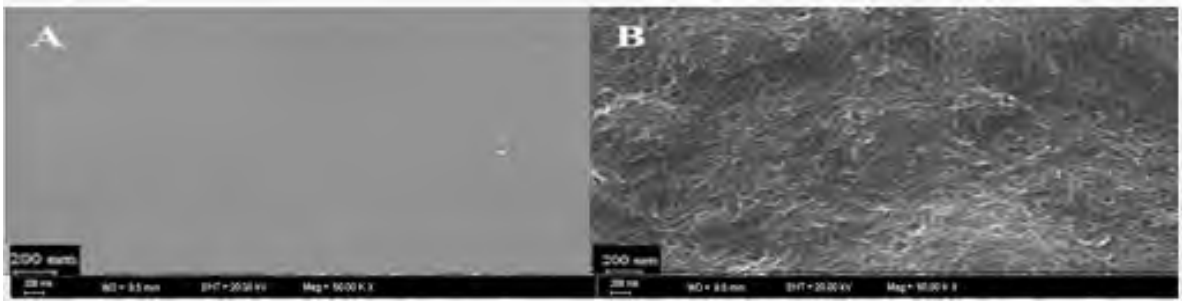

Fig. 2.8. *SEM micrographs of (A) Bare GCE and (B) BPTC-modified GCE.*

2.3.3 Sensor 3: GCE modified with cobalt–iron diselenide nanorods

To prepare $FeCoSe_2$/GCE electrode, 1 mg of $FeCoSe_2$ was dispersed in 1 mL of isopropanol by ultrasonication for 30 minutes. Next, 5 µL of the $FeCoSe_2$ solution was drop cast onto the polished surface of the bare GCE (0.071 cm^2). Before modification of surface of the GCE, it was first polished using alumina powder (0.05 µm) followed by washing it with doubly distilled water. After drop casting 5 µL of the $FeCoSe_2$ solution on the polished surface of the bare GCE, the modified electrode was washed with a mixture of nitric acid and acetone (1:1) to remove any impurities, followed by rinsing thoroughly by doubly distilled water. The cleaned GCE was dried in a desiccator while the modified electrode was dried at room temperature for 20 minutes and then completely dried in an oven at 50°C for 30 minutes. The as prepared $FeCoSe_2$/GCE electrode was employed for the electroanalysis of INZ under optimized conditions. Fig. 2.9 shows significantly enhanced signal of INZ at the $FeCoSe_2$/GCE vs., bare-GCE. Surface characterization of modified GCE was done by SEM as shown in Fig. 2.10.

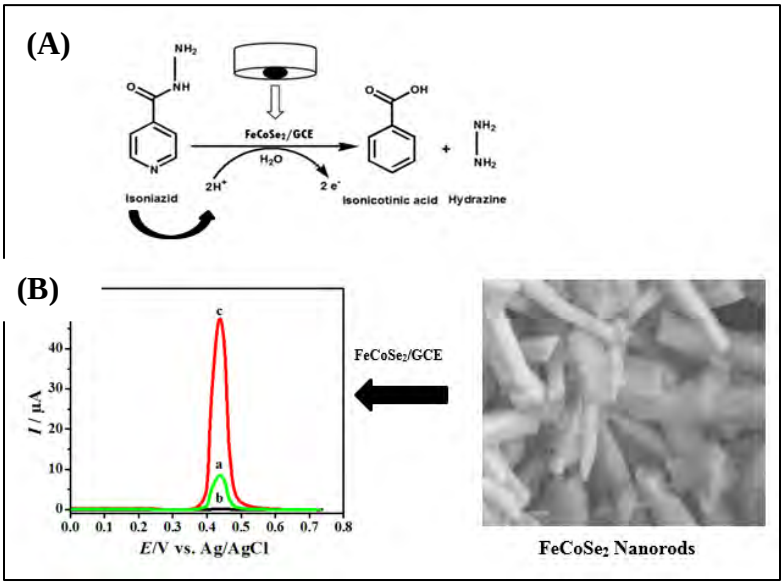

Fig. 2.9. *(A) Electrochemical oxidation mechanism of INZ over modified $FeCoSe_2$/GCE. (B) Electrochemical oxidation peak of INZ over modified $FeCoSe_2$/GCE.*

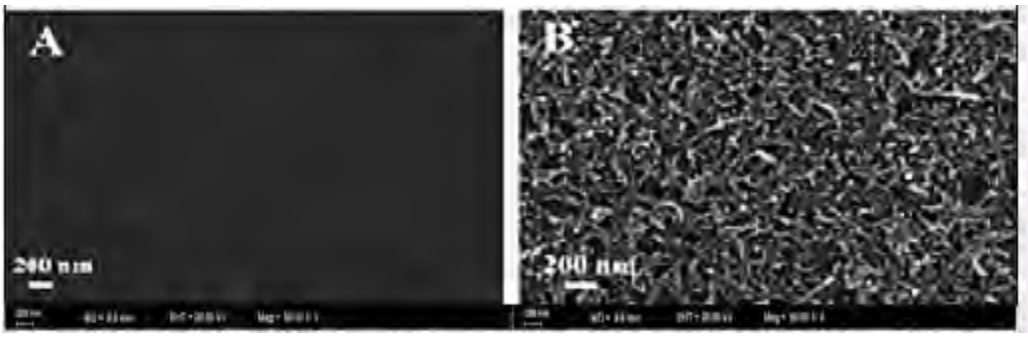

Fig. 2.10. *SEM micrographs of (A) Bare and (B) $FeCoSe_2$/GCE.*

2.3.4 Sensor 4: GCE modified with Co-Pd@Al_2O_3 nano-alloys

To modify the cleaned GCE surface, Co-Pd@Al_2O_3 nanoparticles were coated on the surface of GCE. For this purpose a milligram of the catalyst powder was dispersed in 5 microliters of ethanol by using ultrasonication for 20 minutes. Subsequently, 5 microliters of the suspension that was obtained were applied onto the electrode surface using a drop-casting method. Finally, the electrode was coated with 2-3 drops of Nafion solution. The modified electrode was allowed to completely dry at room temperature before use. Fig. 2.11 shows GCE modification and comparison of its VEN detection performance with unmodified GCE. Surface characterization of Co-Pd@Al_2O_3/GCE was done by SEM and is shown as in Fig. 2.12.

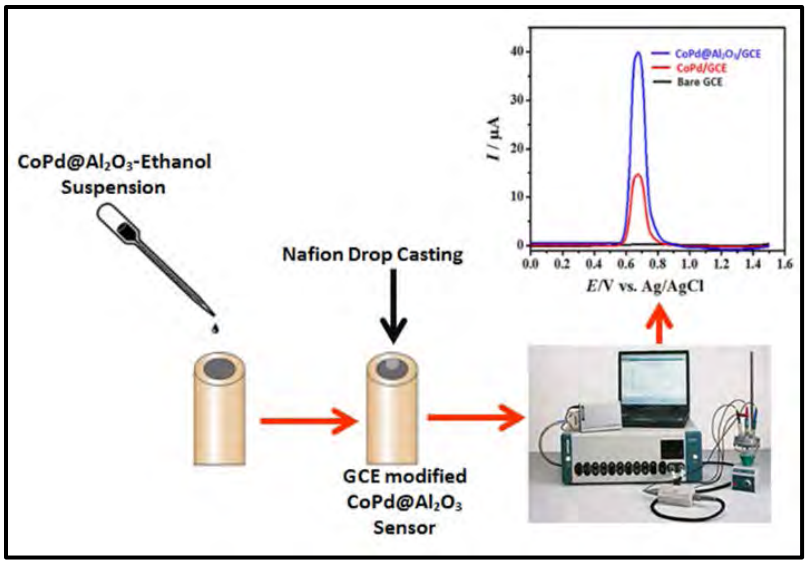

Fig. 2.11. *Stepwise procedure for electrode modification with Co-Pd@Al_2O_3 and performance test for VEN sensing.*

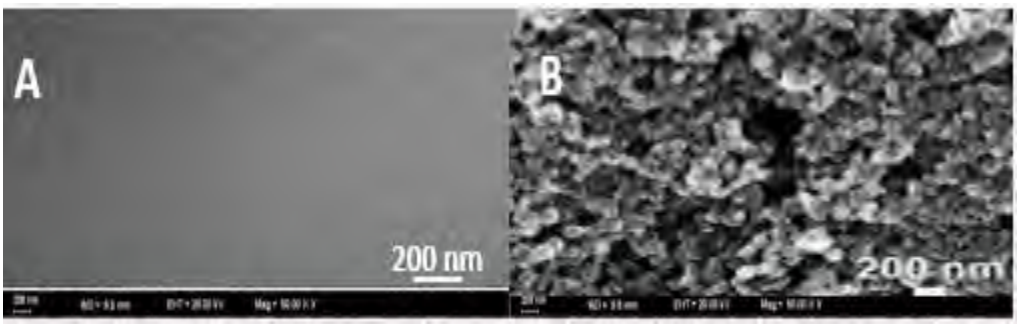

Fig. 2.12. *SEM micrographs of (A) Bare and (B) Co-Pd@Al_2O_3/GCE*

2.4 Electrochemical measurements

The stock solutions of analytes were prepared in 100 mL volumetric flask with their respective solvents. Then, in an electrochemical cell, 10 mL of the stock solution and 10 mL of stripping electrolyte was added up and the total volume was made with 20 mL at a constant 1:1 (v/v) ratio of respective stock solutions and buffer for the water toxins analytes working solution preparation. While, for the drug working solutions, the stock solutions were diluted with a constant 20/80 (v/v) ratio of their respective solvents and buffer to

avoid any solubility problems. The fabricated electrode was inserted in an electrochemical cell for the concurrent sensing of multiple analytes in supporting electrolyte by SWASV method. At deposition potential, the analytes get accumulated onto the sensor surface under stirring of solution for giving deposition time. Afterward, an equilibrium time of 5 s was retained in quiescent solution, and then SWASV scan was run from a desire potential window at 20 Hz frequency, by an increment of 0.5 mV potential, 100 mVs^{-1} scan rate and 20 mV pulse amplitude. Voltammograms were recorded and the oxidation peaks of the targeted analytes were measured. Blank voltammograms of the buffer + solvent systems were also taken at each modified electrode as verification that the voltammetric signal is due to analytes and not the solvent/modifier.

2.5 Theoretical background of the experimental techniques

The theoretical principles of the techniques employed in the present research work are presented in this section. The developed sensors and their analytical performance were characterized and examined by various techniques, including CV, Pulse Voltammetry, EIS, SEM, TEM and XRD [152-154]. Square wave voltammetry was utilized for the detection of analyte species in biological samples and water samples, while stripping voltammetry was employed to preconcentrate analytes for highly sensitive detection. [155,157]. The surface characteristics of the sensing surfaces were examined from SEM images. Further information regarding the specific methodologies employed have been discussed in the following sections.

2.6 Cyclic Voltammetry

The CV technique involves measuring the changes in potential of an electrode over a period of time. This change occurs when the electrode is exposed to a controlled potential waveform. It is a method of studying the behavior of charged species in solution and how they interact with an electrode. It is a commonly employed technique for the determination

of the reduction and oxidation potentials of species in a solution, as well as for investigating the kinetics of electrochemical reactions. [158-161]. Cyclic voltammetric analysis involves measuring the current in response to a periodically changing potential. During CV, the voltage is usually scanned in a triangular-waveform amongst two defined values, E1 and E2, at a controlled potential scan rate. The resulting current is recorded, and this data is subsequently utilized to analyze the chemical behavior and electrochemical reactions occurring within a sample.

In cyclic voltammetry, the triangular potential sweep drives the flow of ions and electrons in the sample, leading to a variation in the total charge. The resultant current produced is directly proportional to the rate of change of charge can be used to identify chemical processes, such as oxidation and reduction, and to determine the rate constants and redox potentials of species in the sample. The cyclic voltammogram, a graph of current versus potential, provides a visual representation of the electrochemical behavior of the sample [162-164].

The International Union of Pure and Applied Chemistry (IUPAC) has set guidelines according to which cathodic currents are assigned negative values and denoted as I_c. The maximum value of the cathodic current is denoted as the cathodic peak current (I_{pc}), and the voltage upon which the analytes are fully reduced is called the cathodic peak potential (E_{pc}). On the other hand, anodic currents are considered positive and referred to as I_a. The anodic peak current (I_{pa}) corresponds to the highest value of the anodic current observed during cyclic voltammetry, while the anodic peak potential (E_{pa}) represents the potential at which the analyte is fully oxidized at the working electrode surface. [165,166].

The relationship between potential (E) and the reaction quotient (Q) for a reversible redox reaction can be shown by the Nernst equation.

$$E = E_{\mathrm{o}} - 2.303RT\ nF\ logQ \qquad \text{(Eq. 2.1)}$$

The standard cell potential is denoted by E_o in electrochemical reactions, and the values of R, T, and F are defined according to their standard definitions. The variable "n" represents the number of electrons that are involved in the reaction, while Q represents the concentration ratio of oxidized and reduced species.

Cyclic voltammetry can discriminate among reversible, irreversible, or quasi-reversible processes. By utilizing cyclic voltammetry, it is possible to gain knowledge about both the thermodynamics and kinetics of electrode processes [167]. This valuable information includes the rate of heterogeneous charge transfer, as well as rate constants and equilibrium constants of electron transfer and any resulting chemical reactions [168]. The technique is also useful for understanding the fate of redox products, transport properties, and mechanistic features of electroactive species at different redox potentials [169-170].

Depending on several criteria, cyclic voltammograms can be classified in various ways, including the shapes and positions of the redox peaks, the ratio of peak currents, and the alterations in peak currents when the scan rate is varied. The voltammograms can be classified into three types: reversible, irreversible, and quasi-reversible [171-173].

2.6.1 Analyzing nature of redox reactions via CV

Redox reactions that involve the transfer of a single electron can be classified into reversible, quasireversible and irreversible categories. Reversible process refers to a redox reaction that can occur in both the forward and reverse directions with equal ease. When examining a reversible process in a cyclic voltammogram, the anodic and cathodic peaks will be positioned symmetrically with a distinct separation between them. The peak currents (Ipa/Ipc) of reversible redox reactions will have a ratio close to one, and their peak currents will increase in a linear fashion as the scan rate is increased. These informations are useful for the assessment of thermodynamic and kinetic parameters of redox events, as well as for studying the behavior of redox-active species in solution [174-178].

Peak potentials and half peak potentials are interrelated as;

$$E_{\mathrm{pa}} = E_{1/2} - (1.109 \pm 0.002)RT/nF \qquad \text{(Eq. 2.2)}$$

$$E_{\mathrm{pc}} = E_{1/2} - (1.109 \pm 0.002)RT/nF \qquad \text{(Eq. 2.3)}$$

Where

$$E_{1/2} = 0.8817\ I_{\mathrm{p}} \qquad \text{(Eq. 2.4)}$$

With the change in scan rate peak potential does not change in case of reversible reactions. When broad peaks are observed, the half-wave potential ($E_{p1/2}$) is often utilized instead of the peak potential (E_p). These two values are related as follows:

$$E_{\mathrm{p1/2}} = E \pm 28/n(mV) \text{ at room temperature} \qquad \text{(Eq. 2.5)}$$

Positive sign (+ stands for reduction and negative sign (–) for oxidation

The relationship between the number of electrons transferred in an electrode reaction and the peaks separation can be expressed using the following equation:

$$\Delta E_{\mathrm{p}} = E_{\mathrm{pa}} - E_{\mathrm{pc}} \approx \frac{0.059}{n}\ V \qquad \text{(Eq. 2.6)}$$

An irreversible cyclic voltammetric process refers to a redox reaction that proceeds predominantly in one direction, and the reverse reaction is either very slow or does not occur at all. When examining an irreversible process in a cyclic voltammogram, the anodic and cathodic peaks will not be symmetrical, and the separation between them will increases as the scan-rate increases. The values of peak current will increases accordingly with increase in scan-rate, but the ratio of the anodic to cathodic peak currents will be significantly different from unity, due to the mostly one-way charge transfer process. Irreversible processes are often encountered in systems involving the adsorption of species onto electrodes, or in situations where one of the reaction products gets strongly adsorbed on the electrode surface, it can hinder or prevent the reverse reaction from occurring. Investigating irreversible processes is crucial in understanding the electrochemical behavior of the electroactive species on electrodes and the kinetics of electrode processes. It can provide valuable information on the nature of electroactive species and the mechanisms of their electrochemical reactions.

Irreversible processes refer to those reactions that have slow electron transfer and result in peaks with a potential separation greater than 59/n mV. The I_p value for such processes can be calculated as:

$$I_p = (2.99 \times 10^5)\ \alpha^{1/2}\ n^{3/2} A C D^{1/2} v^{1/2} \qquad \text{(Eq. 2.7)}$$

For irreversible electron transfer reactions, the peak-potential changes with change in the scan rate, and the peak width is described by a relationship involving the square root of the scan-rate.

$$\left|E_{\mathrm{p}} - E_{\mathrm{p}/2}\right| = 1.857RT/\alpha nF \qquad \text{(Eq. 2.8)}$$

Rate constant of irreversible reaction is evaluated according to Reinmuth expression:

$$I_{\mathrm{p}} = nFAC_0^* k_{sh} \qquad \text{(Eq. 2.9)}$$

k_{sh} represents standard-heterogeneous-rate-constant with values less than 10^{-5} cms^{-1} for the irreversible reactions.

In a quasi-reversible reaction, the forward and reverse reactions are not completely reversible. The reaction does not reach to a state of dynamic equilibrium. Forward reaction occurs much faster than the reverse reaction, but the reverse reaction is still significant enough to be observed in the cyclic voltammogram. These reactions fall between irreversible and reversible systems. In cyclic voltammogram of such reactions signal appears in reverse scan but with a lower magnitude than the signal in the forward potential scan. Peak separation of such reactions increases with increasing the scan rate. The values of E_p-$E_{p/2}$ of the redox reactions with fast heterogeneous charge transfer rates typically fall within the range of 60-100 mV, with k_{sh} values ranging from 10^{-1} to 10^{-5} cm/s. Fig. 2.13 provides a comparison of the electron transfer processes in all three types of redox reactions.

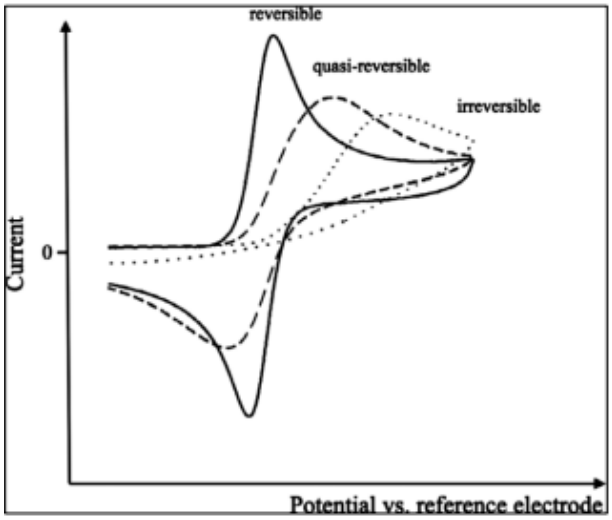

Fig. 2.13. *Comparison of cyclic voltammograms for reversible, irreversible and quasi-reversible electron transfer processes [179].*

2.7 Pulse voltammetric techniques

When studying fast redox reactions at low current levels, square wave pulse voltammetric techniques are highly useful for analyzing the kinetics and thermodynamics of these reactions. Unlike cyclic voltammetry, pulse techniques involve application of a series of brief, high-amplitude potential pulses to the electrode instead of a continuous waveform [180]. These techniques can also be employed to study the electrochemical behaviors of the electro-active species at electrode surface, and to determine the relative standard reduction potentials of redox species in solution. There exist various pulse voltammetric techniques, which include:

2.7.1 Normal pulse voltammetry (NPV)

NVP is a commonly-used tool in electroanalytical chemistry and electrochemical engineering. During each pulse, the potential is incrementally increased and the resulting current response is measured until a predetermined final value is reached. The data collected from these pulses can be useful to analyze the kinetics and thermodynamics of

the redox reaction in solution and determine the relative standard reduction potentials of redox species. NPV is particularly advantageous for studying fast oxidation/reduction reactions and investigating the behavior of electroactive moieties at electrodes [181,182]. By utilizing NPV technique, electrochemists can achieve a deeper understanding of the complex mechanisms that are involved in these reactions. This, in turn, facilitates the development of more efficient electrochemical systems that can be applied in a wide range of applications. Ultimately, the technique of Normal pulse voltammetry provides researchers with a valuable analytical tool for advancing the field of electrochemistry [183].

2.7.2 Differential pulse voltammetry (DPV)

The technique of Differential Pulse Voltammetry (DPV) is of great significance in the field of electrochemical analysis, owing to its broad applicability to a diverse range of analytes. As such, DPV has emerged as a crucial tool in the domain of analytical chemistry [184, 185]. DPV involves introducing a small potential pulse to the baseline potential, followed by the measurement of the resulting current response. Typically, the potential pulse ranges from 10 to 100 mV and is applied for a brief period, usually between 1 to 100 ms. As the potential is changed, the current response is recorded and a current versus potential plot is generated [187, 188].

DPV is useful for studying the kinetics and thermodynamics of redox reactions in solution. By analyzing the current response at different potentials, information about the reaction rate, the potential at which the reaction occurs, and the relative standard reduction potential of the redox species can be obtained. DPV is particularly useful for studying redox reactions that occur at low current levels, and enables electrochemists to investigate the mechanistic behavior of electroactive species at the electrode surface.

One of the advantages of DPV is its clear discrimination between Faradic and non-Faradic current and owing to this peculiar characteristic this technique finds wide applications in limit of detection determination. Although it is a slow technique, yet it is highly sensitive. It is used to study a variety of systems, including biological systems, metal-ion complexes,

and electroactive organic compounds. With its superior peak resolution, DPV is an exceedingly sensitive technique that facilitates the detection of analytes in the nano, pico, and even femto molar range. The current response yielded by DPV can be employed to calculate the number of electrons engaged in an electrochemical process, utilizing a particular expression (Eq. 2.10).

$$W_{1/2} = 3.52RT/nF \qquad \textit{(Eq. 2.10)}$$

In Fig. 2.14, the application of DPV involves the provision of a specific magnitude pulse to the WE, followed by the current measurements, before and after the pulse. Through the analysis of the linear correlation between the concentration of the analyte and the peak current, it becomes possible to assess critical analytical parameters such as the LOD and LOQ. Additionally, each species has a unique peak potential that can be correlated to the half-wave potential. By accurately correlating the peak-potential values to the half-wave potential, it is possible to identify and quantify the analyte under investigation using Eq. 2.13.

$$E_{\mathrm{p}} = E_{1/2} - \Delta E/2 \qquad \text{(Eq. 2.11)}$$

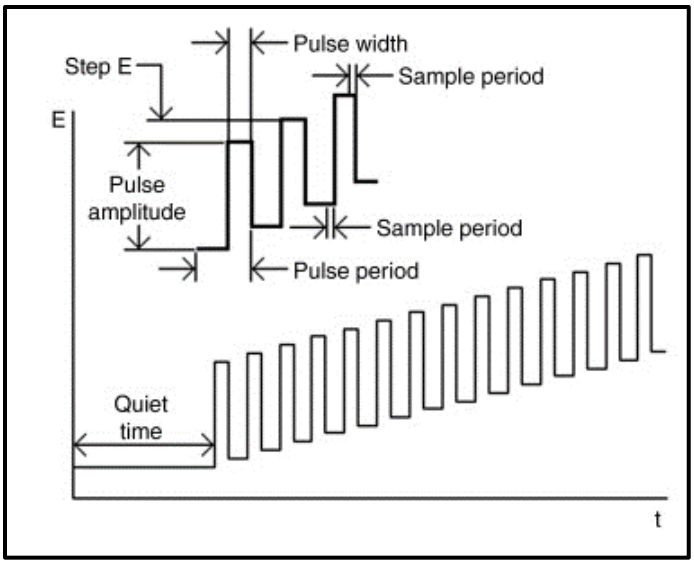

Fig. 2.14. *Diagram illustrating pulse parameters of differential pulse voltammetry and application in electrochemical analysis [188].*

2.7.3 Square wave voltammetry

SWV is a fast electroanalytical method that is frequently used to identify and quantify various species in a sample solution. This technique applies a staircase base potential to the working electrode and then superimposes regular square waves on it. To obtain the net current (Inet) centered on the redox potential of the process, it is necessary to measure the resulting current and then calculate the disparity between the forward and backward current components (Inet = If – Ib). Fig. 2.15 shows that the potential applied to the electrode is systematically varied, and the resulting current is both measured/recorded in a controlled manner.

In SWV, the application of regular square waves onto the staircase base potential creates a current response that is characterized by a series of peaks and valleys. The concentration of the analyte species present in the sample can be directly measured using the peak height, which is the difference between the maximum and minimum current obtained from SWV. In addition, the shape and position of the peaks provide valuable insights into the electrochemical behavior of the analyte, including its redox potential and reaction kinetics.

SWV is one of the highly sensitive technique that can detect analyte species at very low concentrations, with typical detection limits in the parts-per-billion range. The technique is also highly selective, with the ability to distinguish between different analyte species based on their electrochemical behavior. Additionally, SWV is relatively fast and requires minimal sample preparation, making it a valuable tool for various analytical applications.

Thus, SWV is a powerful and versatile technique that offers numerous advantages for electroanalytical measurements. Its ability to provide quantitative information about analyte species in a fast, sensitive, and selective manner makes it a valuable tool for many fields, including analytical chemistry, environmental monitoring, and biomedical research [189,190].

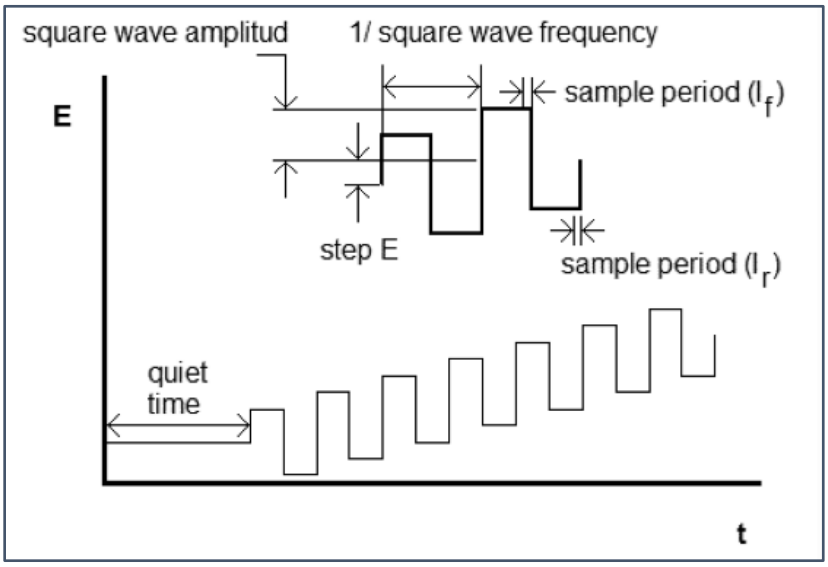

Fig. 2.15. *A typical potential waveform for SWV [191].*

2.8 Stripping voltammetry

With its exceptional sensitivity, stripping voltammetry is used to identify and quantify trace concentrations of metal ions in solution. Among the stripping techniques ASV is particularly utilized for the determination of toxic HM ions in solution. This method allows practical detection limits in parts per trillion range. Moreover, ASV has the potential of detecting multiple metal ions simultaneously. It involves three main steps:

Deposition step: In this specific step of the stripping voltammetry, a suitable potential is applied to the electrode, which induces the reduction of metal ions present in the sample solution on the surface of the electrode. As a result, a thin layer of metal is created on the surface of the electrode. This step is critically dependent on mass transport, which can be enhanced by stirring. After deposition, a rest period of around 10-15 seconds is typically provided to ensure maximum electroreduction.

$$M^{n+} + ne^- \rightarrow M \qquad \text{(Eq. 2.12)}$$

Stripping step: After deposition, the electrode is scanned over a potential range, causing the metal ions to be stripped off from the electrode surface and oxidize back to their original ionic state. The current that emerges is then measured as a function of the potential that is applied.

$$M \rightarrow M^{n+} + ne^- \qquad \text{(Eq. 2.13)}$$

Analysis step: The recorded currents versus potential data are analyzed to determine the concentrations of the metallic ions in the solution. This is typically done by comparing the peak current or peak area to a calibration curve generated from known concentrations of the metal ions.

Hence, stripping voltammetry is an effective technique for trace metal ion analysis owing to its high sensitivity, selectivity, and capacity to deliver quantitative data [192,193]. Fig. 2.16 demonstrates the working principle of ASV.

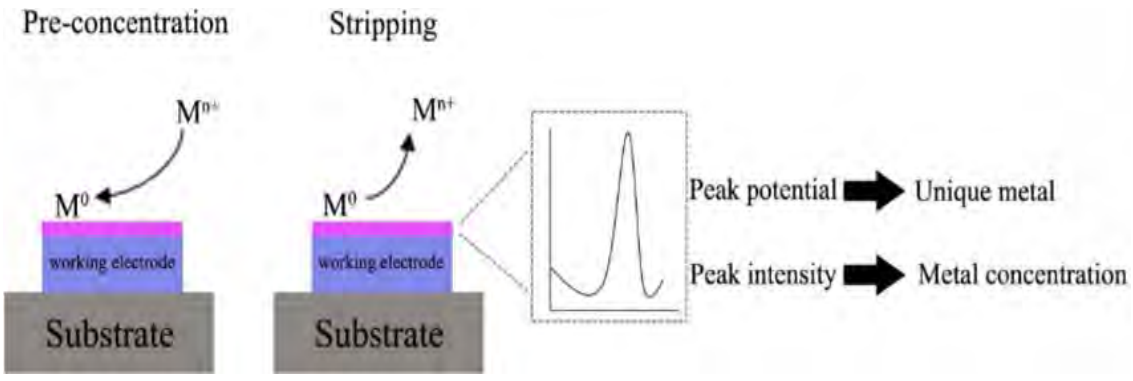

Fig. 2.16. *Steps of Anodic Stripping Voltammetry [194].*

2.8.1 Electrochemical impedance spectroscopy (EIS)

EIS involves perturbing analytes with electrochemical sinusoidal waves of different frequencies and measuring their response in terms of current and potential phase shifts. As a non-destructive method, it provides important info about the properties and behavior of the analyte under study. This technique is beneficial for studying various electrochemical redox reactions at the electrode surface, including their rates, charges transduction behavior, diffusion-limited processes, and capacitance. EIS is used for the analysis of biosensors, battery materials, corrosion fuel cells, surface features, and kinetics of electron transfer reactions.

Ohm's Law (R=V/I) is used to relate electrical resistance to voltage and current in DC circuits. However, in complex AC circuits, electrical impedance depends on the frequency of the AC signals and includes contributions from resistance, capacitance, and/or induction. Therefore, electrical impedance is a complex number consisting of a real component (resistance) and the imaginary components (inductance and capacitance) as shown in Eq. 2.14 [195,196].

$$Z = \frac{V}{I} = Zo\ exp^{I\varphi} = Zo\ (Cos\varphi + isin\varphi) \qquad \text{(Eq. 2.14)}$$

In EIS, an AC voltage is applied to a sample at different frequencies, which leads to the production of electrical current. The changes in amplitude and phase shift at different frequencies are used to estimate impedance components in the sample.

The Nyquist plot of presenting EIS data consists of a semicircle and a linear segment. In a Nyquist plot obtained from EIS data, the semicircular portion observed at higher frequencies is indicative of the charge transfer resistance (R_{ct}), whereas the linear portion observed at lower frequencies corresponds to the diffusional-limited process. A larger diameter of the semicircle indicates slower kinetics of electrochemical reactions with larger Rct values at the electrode surface, while a smaller diameter indicates faster kinetics. At lower frequencies, a linear portion appears in the Nyquist plot, which characterizes the diffusional-limited process. Fig. 2.17 shows that the solution resistance (R_s) is represented

by the intersection of the semicircle with the x-axis at the far left side. The frequency at the apex of the semicircle represents $\omega = C_{dl}R_{ct}$. The sum of $R_s + R_{ct}$ indicates the total impedance of the electrochemical system [197-199].

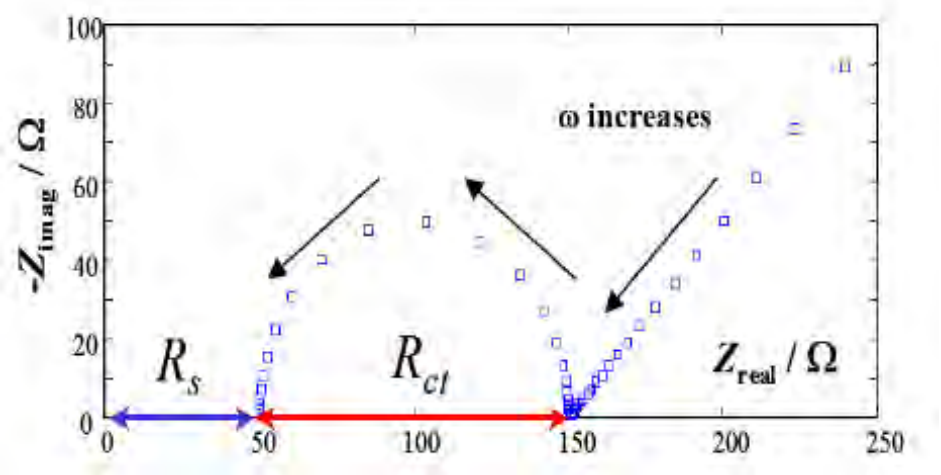

Fig. 2.17. *Nyquist plot showing solution resistance, charge transfer resistance and diffusion controlled process [200]*

A suitable circuit model is chosen for fitting with the experimental EIS data shown as Nyquist plot. Each element in the circuit model corresponds to a specific electrochemical activity and is assigned a physical parameter. One or more equivalent circuit models can be used to associate the mechanistic parameters of the electrochemical system with the impedance plot to extract numerical information. There are several circuit models available for fitting the impedance parameters, but the Randle's circuit model is the most commonly used (Fig. 2.18).

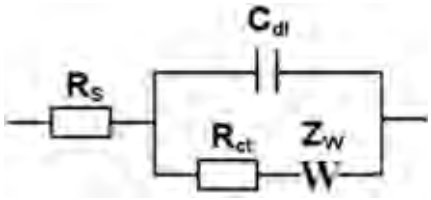

Fig. 2.18. *Randle's equivalent circuit for a charge transfer reaction followed by diffusion limited process.*

The equivalent circuit model used in EIS analysis typically consists of several components arranged in a specific order. It begins with a R_s in series with a R_{ct}, followed by a Z_w, and a C_{dl} in parallel, as shown in Fig. 2.18. Each element of the circuit model is related to a specific electrochemical activity and has a physical parameter assigned to it. The R_{ct} represents the charge transport at the electrode/electrolyte interface, while R_s represents the uncompensated resistance of the solution between the WE and reference electrode. The Cdl is the capacitance associated with the electrical double-layer formed around the surface of the electrode, while the Warburg impedance (Zw) corresponds to the impedance associated with diffusion-controlled mass transfer.

2.9 Physical Characterization Techniques

2.9.1 Scanning electron microscopy (SEM)

SEM offers information about the morphology of the surface, texture, and structure of various materials. It offers magnifications ranging from 10x to 1,000,000x, making it a valuable tool for the characterization of nanomaterials, biological samples, and various surfaces [201,202]. SEM is also capable of identifying surface defects, cracks, and other surface features. Achieving high-resolution images using SEM involves coating the sample with a conductive material like gold or carbon to prevent charging during imaging. The sample is then placed inside the vacuum chamber of the SEM, and an electron beam is used to scan it. The signals generated from the electrons that are scattered back or emitted from the sample are used to create an image of the surface.

In addition to imaging, SEM can also be utilized to analyze the chemical compositions of the samples by utilizing the energy-dispersive X-ray spectroscopy (EDS). EDS detects the characteristic X-rays emitted by the sample upon exposure to the electron beam, allowing for the determination of the elemental composition of the sample. SEM can provide information on the morphology, topography, crystallography, grain orientation, composition, and other characteristics of a sample material. The spatial resolution of SEM can be as high as 1 nm, and the magnification can reach up to 300,000 times. In addition to surface morphology and composition, SEM can also provide information on magnetic,

electrical, and crystallographic properties of materials [203,204]. The instrument consists of several components, including the electron gun, the condenser lens, the objective lens, the scanning coil, aperture, sample container, and detector, as illustrated in Fig. 2.19.

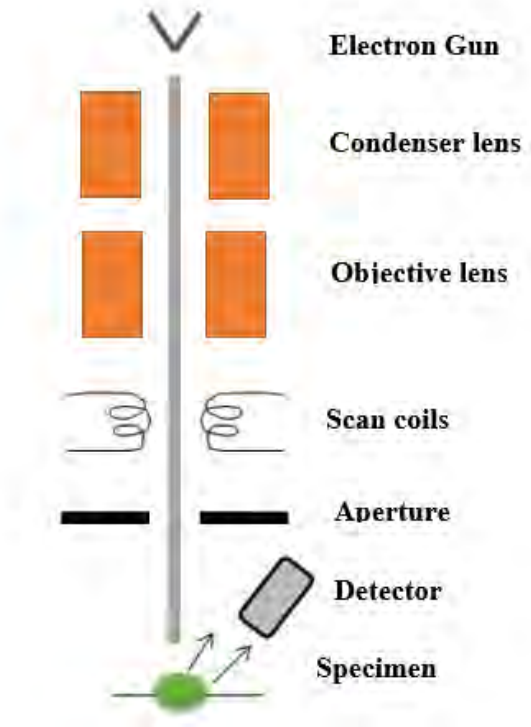

***Fig. 2.19**. Representation of a typical scanning electron microscope [204].*

2.9.2 Transmission electron microscopy (TEM)

TEM is a high-resolution imaging technique that utilizes a focused electrons beam to visualize the ultrastructure of materials. It involves transmitting the electron beam through an extremely thin sample, and the resulting interaction between the electrons and the sample generates a high-resolution image of sample's internal structure. This imaging technique is useful for analyzing the internal structure of solid-state materials as well as biological samples. The basic components of a TEM include an electron gun, which produces the electron beam, a series of electromagnetic lenses, which focus and control the beam, and a fluorescent screen or detector, which captures the image formed by the transmitted electrons. The sample is typically prepared by cutting a very thin section using

a microtome and placing it on a thin support film that can withstand the vacuum conditions of the microscope.

TEM has several advantages over other microscopy techniques. It can provide very high-resolution images with sub-angstrom resolution, allowing researchers to visualize individual atoms and molecular structures. It can also be used to analyze the crystal structure and defects of materials, and to observe the dynamics of biological samples at the nanometer scale. However, TEM has some limitations, such as the need for specialized sample preparation techniques, the requirement for high vacuum conditions, and damage of the sample by the electrons beam. Despite these limitations, TEM remains an essential tool in materials science and biological research. Fig. 2.20 presents the schematics of TEM and its essential components [205].

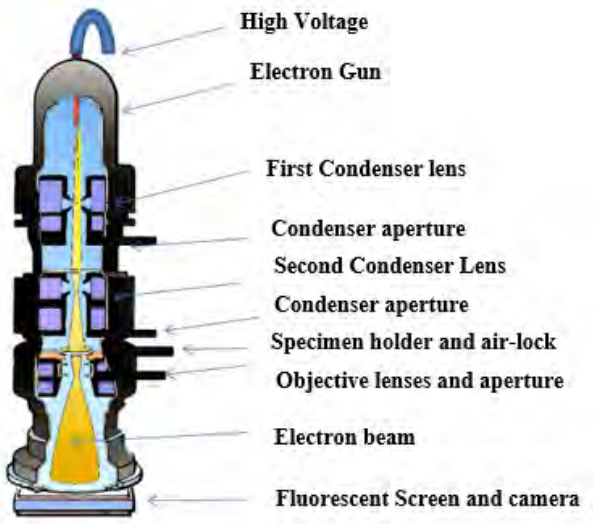

***Fig. 2.20**. Diagram of a transmission electron microscope [205].*

2.9.3 X-ray diffraction analysis

XRD is used to analyze the structural features of samples. The XRD pattern, which is a material's unique "fingerprint," is used for getting information about crystal structure. XRD is based on Bragg's law, which relates the angle of incidence, the wavelength of the X-rays,

and the distance between the atomic planes in crystal lattice. When X-rays are incident on a sample, they are diffracted at an angle (θ) determined by the inter-planar spacing (d) between the atoms in the crystal lattice. The shape of the unit-cell is used to establish the h, k, and l indices of the inter-planar spacing. These indices are essential in determining the angles (2θ values) where diffraction will occur. The intensity of the XRD signals relies on the atoms' nature, location, and density in the unit cell. By analyzing the XRD pattern, the sample's crystalline phase structure can be determined based on its unit cell dimensions and purity. Additionally, unknown materials can be identified by comparing their XRD patterns with reference cards. Debye Scherer's formula (**D = Kλβ /cosθ**) is used to determine the crystallite size. The interaction of X-rays with electrons in crystalline material is the core concept of XRD. According to Bragg's rule, parallel X-rays incident on parallel planes with inter-planar spacing (d) are diffracted at an angle (θ) with the path length of an integral multiple of wavelengths (Fig. 2.21). The inter-planar spacing (d), also known as the h, k, and l indices, is determined by the form of the unit cell and determines the two values at which diffraction occurs. The kind of atoms, their position, and density in the cell unit all influence the intensity of XRD signals. The XRD pattern may be used to detect the crystalline phase structure of a sample, sample purity, and to identify an unknown substance by comparing its XRD pattern to a reference card [206].

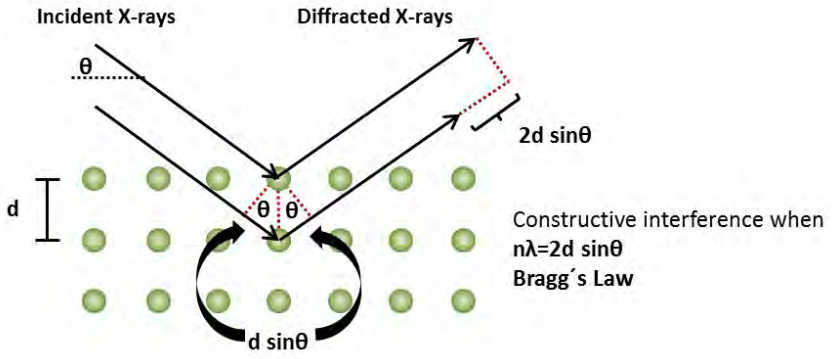

***Fig. 2.21**. Schematic representation of X-ray diffraction from crystal planes [206].*

Chapter 3

RESULTS AND DISCUSSION

This chapter presents details of the results obtained at the designed sensing platforms. Electrochemical impedance spectroscopy and voltammetric studies provide proof of the improved responsiveness of modified GCE interface. Results of the selectivity, sensitivity, repeatability and reproducibility of the sensors and pH dependent redox mechanistic behavior of the investigated drugs are presented in this chapter. Moreover, it encompasses details of the influence of the electrode modifier, supporting electrolytes, pH of the solution, deposition time and deposition potential. A comprehensive discussion on the experimental results of all four sensors is provided in the subsequent sections:

3.1 Sensor 1: BTC/GCE for the detection of Zn^{2+}, Pb^{2+}, As^{3+} and Hg^{2+}

Experimental parameters were optimized for getting intense signals of targeted analytes at the GCE that was modified with multifunctional-bis-triazole-appended-calix[4]arene (BTC). The optimization process involved adjusting the concentration of the modifier, pH of the medium, deposition time and potential, and the supporting-electrolytes used. The outcomes of the optimization process revealed that the modified electrode exhibited exceptional sensitivity towards heavy metal ions, with the ability of detecting their concentrations upto picomolar levels. Experimental evidences of the characterization and performance of BTC/GCE sensor are given below:

3.1.1 Electrochemical characterization of BTC modified GCE

CV and EIS were used for surface characterization of GCE modified with BTC. CV was performed at the bare as well as BTC modified with GCE in a solution mixture of 5 mM $K_3[Fe(CN)_6]$ and 0.1 M KCl. A significant increase in the redox signals of redox probe was noticed on BTC/GCE as compared to bare-GCE (Fig. 3.1(A)). This enhanced response can be credited to the improved surface area of the modified GCE and catalytic role of the

modifier in facilitating electron transfer between the redox probe and transducer. These results indicate that the assembly of BTC on GCE acts as an effective electrode modifier for improving the sensing response.

EIS carried out with optimized parameters showed a semicircular arc and a linear segment in the Nyquist plot. The diameter of the semicircle indicates the charge transfer mechanism at the electrode-electrolyte interface. Upon modification of GCE with BTC, a prominent reduction in the semicircle diameter (Fig. 3.1(B)) suggests improved charge transfer kinetics through BTC/GCE surface. Thus, both CV and EIS outcomes reveal efficient electron transfer through the modified GCE than the unmodified electrode.

As, the $Fe(CN)_6^{3-/4-}$ redox couple consists of ferricyanide ($Fe(CN)_6^{3-}$) and ferrocyanide ($Fe(CN)_6^{4-}$) ions, which contain the central iron (Fe) atom surrounded by cyanide (CN) ligands. The negatively charged redox probe interacts favorably with surfaces that have an affinity for metal cations due to the central role of the iron atom in the redox couple.

When the glassy carbon electrode is modified with the BTC the surface properties are tailored to bind metal cations effectively. This results in a higher local concentration of metal cations, particularly iron ions from the $Fe(CN)_6^{3-/4-}$ redox couple, due to the specific interaction between the redox-active species and the modified electrode surface.

The binding of metal cations to the modified surface promotes a more concentrated and efficient electron transfer process, thereby enhancing the electroactivity or sensitivity of the $Fe(CN)_6^{3-/4-}$ redox probe. The affinity of the modified electrode for metal cations creates an environment that is particularly conducive to the redox reactions involving the metal-centered species, thereby leading to a more pronounced electrochemical response.

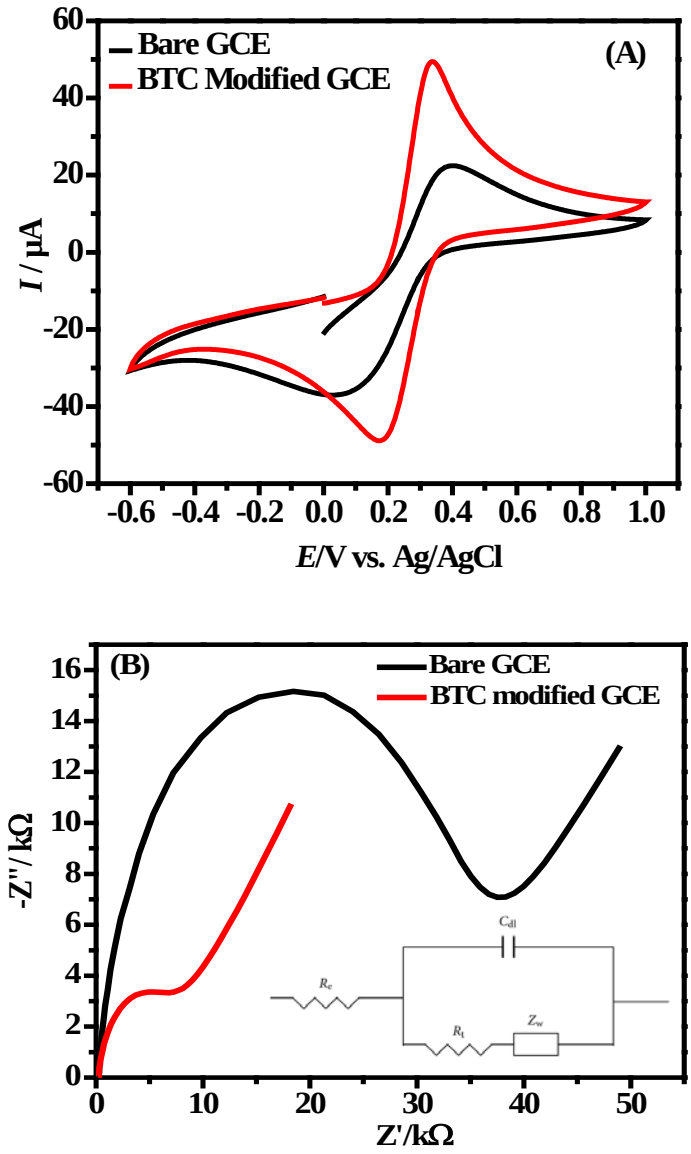

Fig. 3.1. *(A) The obtained (A) cyclic voltammograms and (B) Nyquist plots were generated for a solution containing 5 mM $K_3[Fe(CN)_6]$ and 0.1 M KCl, using both bare and BTC/GCE.*

To further explore the impact of BTC modification on metal ion detection, SWASV analysis of a solution mixture consisting of Zn^{2+}, Pb^{2+}, As^{3+}, and Hg^{2+} was conducted on

in a 50% BRB solution (pH=3) via bare as well as BTC modified GCEs. As obvious from Fig. 3.2 the current response for all four metal ions are more pronounced at the GCE modified with BTC in comparison to the unmodified GCE. Based on the results, it can be inferred that the hydroxyl, carbonyl, and triazole functional-groups in the chemical structure of the BTC are effectively preconcentrating the metal ions at the electrode surface. By serving as a conducting medium between the metal ions and the transducer, the immobilized layer of the BTC facilitated a more rapid electron transfer process. The existence of electron-rich functional groups in the BTC molecules offered sites for the adsorption of metal ions, resulting in the formation of a metal atom-metal ion pair that boosted the current response. The outstanding conductivity of the BTC electrode modifier may be due to the fact that its water-soluble parts are oriented towards the solution, and that they are capable of bending and serving as a linking-bridge amongst the analytes and the transducer. Moreover, the hydrophobic groups of BTC made it insoluble in water, allowing it to remain on the electrode surface during analyte detection and preventing any leaching into the analyte solution.

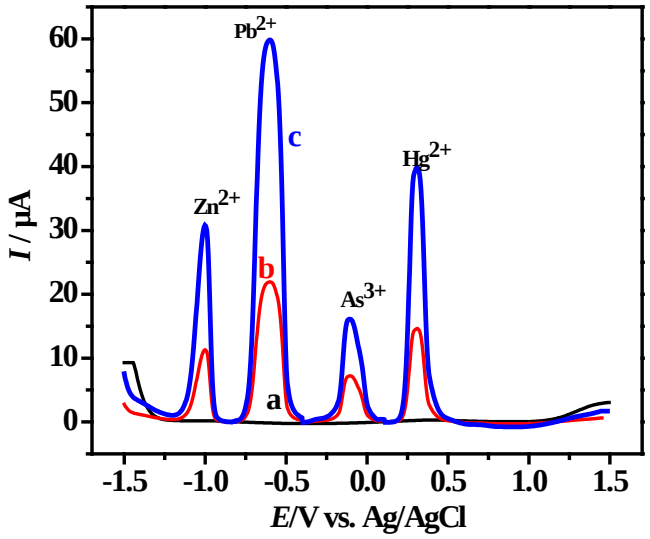

Fig. 3.2. *The SWASV measurements performed under optimized conditions (a) the BTC/GCE in solvent mixture of water and BRB of pH 3.0, (b) the bare-GCE in solvent mixture (water + BRB of pH 3.0), and (c) the BTC/GCE in a 1.2 µM solution of* Zn^{2+}, Pb^{2+}, Hg^{2+}, *and* As^{3+}

3.1.2 Parameters optimization

The study investigated a range of experimental parameters to optimize the stripping conditions for the successful detection of targeted HM ions on BTC/GCE. The study examined several parameters, such as the modifier amount, sample pH, scan rate, the supporting electrolyte, deposition potential and time to get intense signals of the analyte species at the sensing platform.

Firstly, the impact of varying BTC concentrations on metal ion sensing response was investigated. The peak currents were found to increase until a saturation point approached. The observed improvement in the current signals suggests that the modifier plays an electrocatalytic role and lead to increase in the active surface area of the modified-electrode surface. After a certain point, increasing the concentration of molecules of the BTC on the GCE surface led to the formation of multiple layers, which hindered efficient electron transfer as evidenced from the decrease in the peak current responses. The maximum peak current values were noticed at a 1 mM concentration of BTC for stripping electroplated metals into corresponding Zn^{2+}, Pb^{2+}, Hg^{2+}, and As^{3+} ions, as shown in Fig. 3.3.

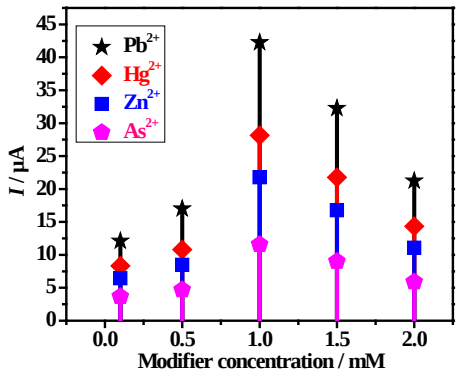

Fig. 3.3*. The impact of the amount of the BTC immobilized on GCE on the peak current responses of Zn^{2+}, Pb^{2+}, Hg^{2+}, and As^{3+} metal ions during the stripping process*

For optimization of the stripping conditions for detecting Zn^{2+}, Pb^{2+}, Hg^{2+}, and As^{3+} ions, the influence of accumulation potential and time was probed. The sensitivity of modified-GCE was significantly influenced by the deposition time, which was investigated by performing SWASV over a range of 10 to 60 seconds. The graph in Fig. 3.4 displays a relative increase in the current responses as the accumulation time prolongs, indicating the electroreduction of more number of metal ions on the modified GCE surface. When the accumulation time was increased beyond the optimal limit, the peak current signal showed a decline. The optimal accumulation time of 50 seconds yielded the highest current response, indicating its effectiveness for maintaining this accumulation time in further electroanalytical experiments.

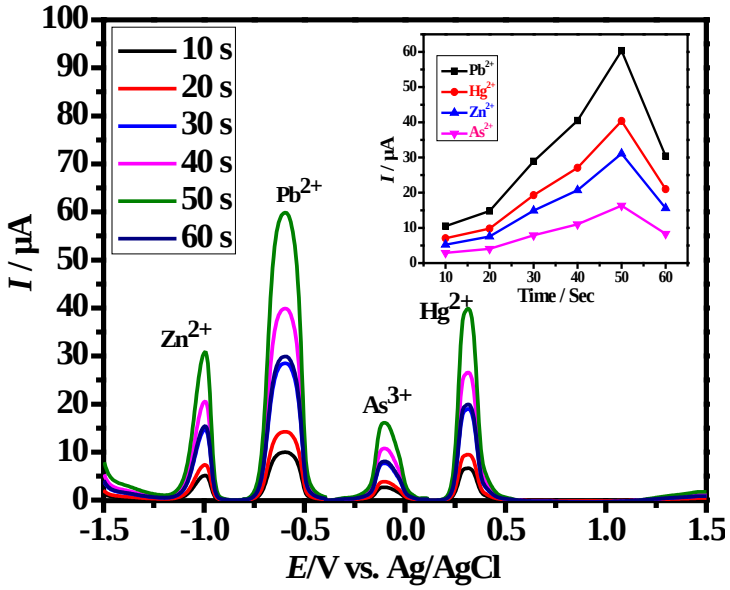

Fig. 3.4. The impact of deposition time on current signals for detection of Zn^{2+}, Pb^{2+}, Hg^{2+}, and As^{3+} (1.2 µM) using a BTC/GCE in BRB of pH 3 as supporting electrolyte and 50 mV/s as the scan rate, by SWASV. An inset plot showing, relationship between Ip vs. t_d.

To determine the optimal potential range for detecting Zn^{2+}, Pb^{2+}, Hg^{2+}, and As^{3+}, the study was conducted to examine how changes in the deposition potential can impact the sensitivity of an BTC/GCE. The current signals increased in the potential range between −1.0 to −1.2 V. However, beyond this potential, i.e., in the potential range (−1.2 to −1.4 V) sensitivity decreased due to the evolution of hydrogen gas caused by water splitting. In order to achieve best sensing outcomes and to avoid evolution of the H_2 gas, experiments were conducted at an optimal deposition potential of −1.2 V as demonstrated in Fig. 3.5.

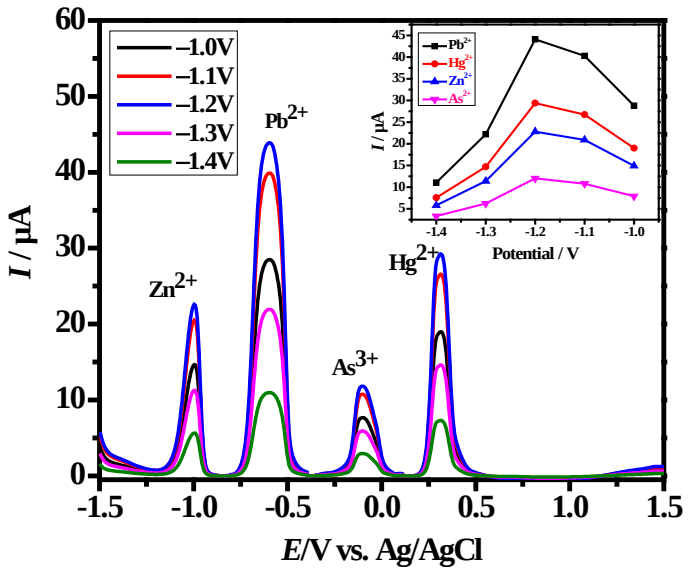

Fig. 3.5. *The influence of various accumulation times on SWASV current signals of 0.9 mM Zn^{2+}, Pb^{2+}, Hg^{2+}, and As^{3+} solutions were investigated using BTC/GCE. (inset :the data plotted as I_p versus E_d).*

The detection capability of BTC/GCE towards metal ions was evaluated to investigate the impact of different supporting electrolytes. For this purpose multiple electrolyte solutions such as KCl, HCl, CH_3COOH, H_3PO_4, and BRB with pH 3 were examined. The results of the study depicted in Fig. 3.6, reveals that the BRB solution of pH 3 provides the highest current signals, thus indicating its effectiveness as a supporting electrolyte for subsequent experiments using the BTC/GCE sensor.

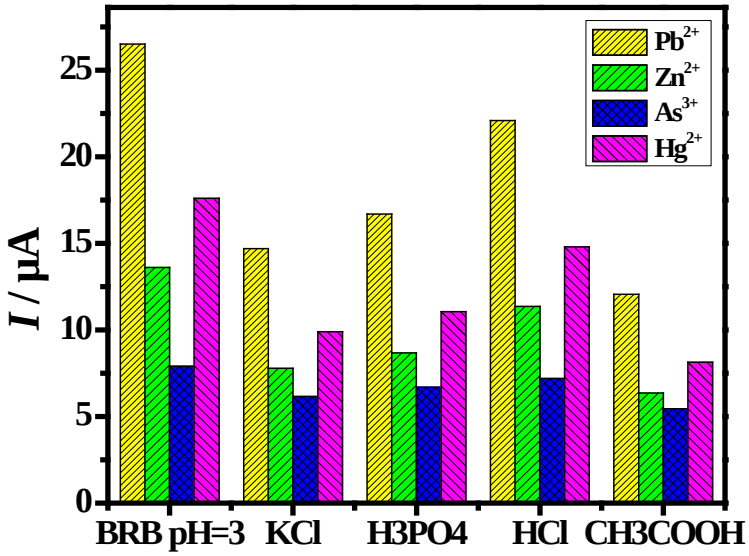

***Fig. 3.6**. The SWASV peak current of a 0.5 µM solution of Zn^{2+}, Pb^{2+}, Hg^{2+}, and $As^{3+}$was studied using BTC/GCE under optimized.*

The response of the BTC/GCE towards HM ions was examined in media of different pH. Fig. 3.7 demonstrates that the highest response is achieved at pH 3, which can be explained by the ionization of the functionalities within the BTC compound structure that are accountable for the HM ions binding. The exchange of HM ions with protons produced by the ionization of functionalities of the modifier occurs is expected in acidic pH. With the increase in pH of the analyte solution there is a decrease in the ionization of functional groups, which in turn reduces the number of available ion-exchange sites for metal ions. Consequently, this results in a decline of current signals. Based on these findings, a medium of pH of 3 was deemed to be the most suitable for rest of the electroanalytical experiments conducted on BTC/GCE.

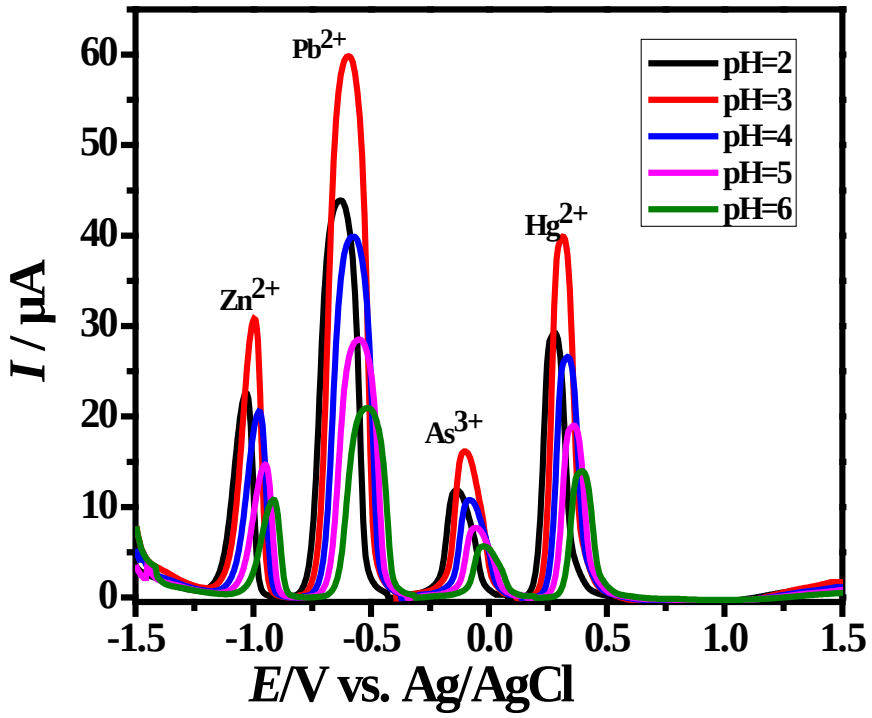

Fig. 3.7. *The influence of pH variation on the current signals of a 1.2 µM solution of Zn^{2+}, Pb^{2+}, Hg^{2+}, and As^{3+} was examined using the BTC/GCE under optimized conditions in BRB with pH values ranging from 2 to 6.*

The capability of the electrochemical sensors to analyze real sample was evaluated by studying the impact of competitive metal ions; Cr^{2+}, K^{+}, Na^{+}, Mg^{2+}, Co^{2+}, Cu^{2+}, Cd^{2+}, on the signals intensity of Zn^{2+}, Pb^{2+}, Hg^{2+}, and As^{3+}. Interfering agents were introduced at concentrations twice that of the analytes. Fig. 3.8 illustrates that the current signals of Zn^{2+}, Pb^{2+}, Hg^{2+}, and As^{3+} are minimally affected by the interfering agents, indicating the applicability of the sensor for analyzing the chosen metal ions in complex samples.

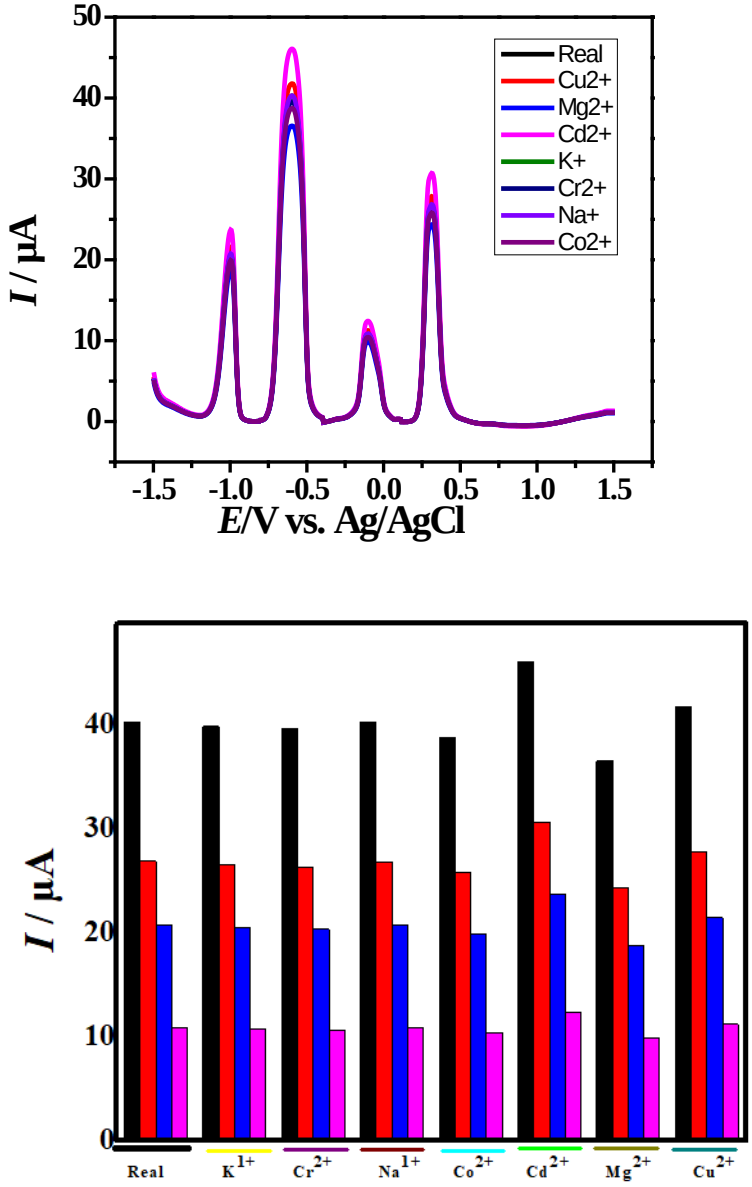

***Fig. 3.8**. The effect of various interfering agents on the stripping peak current of analytes using BTC/GCE*

3.1.3 Assessing the Reproducibility of the BTC/GCE

Figure 3.9 demonstrates reproducibility of the electrode through six measurements of stripped metal ions using SWASV on the BTC-modified GCE. The resulting stripping current values for 0.8 µM Zn^{2+}, Pb^{2+}, Hg^{2+}, and As^{3+} show no significant differences,

indicating reproducibility of the modified electrochemical sensing platform. Therefore, BTC/GCE holds promise for repeated electrochemical measurements of heavy metal ions.

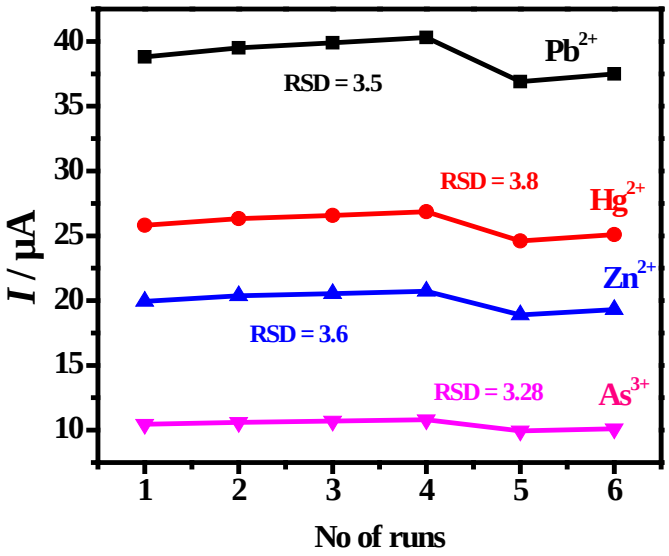

***Fig. 3.9**. The reproducibility of the BTC/ GCE evaluated by conducting six successive measurements of a 1 µM solution of Zn^{2+}, Pb^{2+}, Hg^{2+}, and As^{3+}.*

3.1.4 Simultaneous Detection of Zn^{2+}, Hg^{2+}, $Pb^{2+}$and As^{3+}

Optimized conditions were utilized to enable the concurrent detection of Zn^{2+}, Pb^{2+}, As^{3+}, and Hg^{2+} through SWASV, resulting in distinct responses as depicted in Fig. 3.10. Linear calibration curves were obtained for Pb^{2+}, Zn^{2+}, Hg^{2+} and, As^{3+} in the concentration range of 7 nM to 0.9 µM with regression coefficient values of 0.99, 0.99, 0.99, and 0.998, correspondingly. The LOD for Zn^{2+}, Pb^{2+}, As^{3+}, and Hg^{2+} are presented in Table 3.1. The LOD values are quite promising as compared to documented values in prior literature [207-214].The LOD is obtained in pico Molar range, as it is calculated based on sensitivity of instrument used, the standard deviation of blanks (s) and the slope of linear caliberation curve (m), its not necessarily tied to any data point on calibration curve.

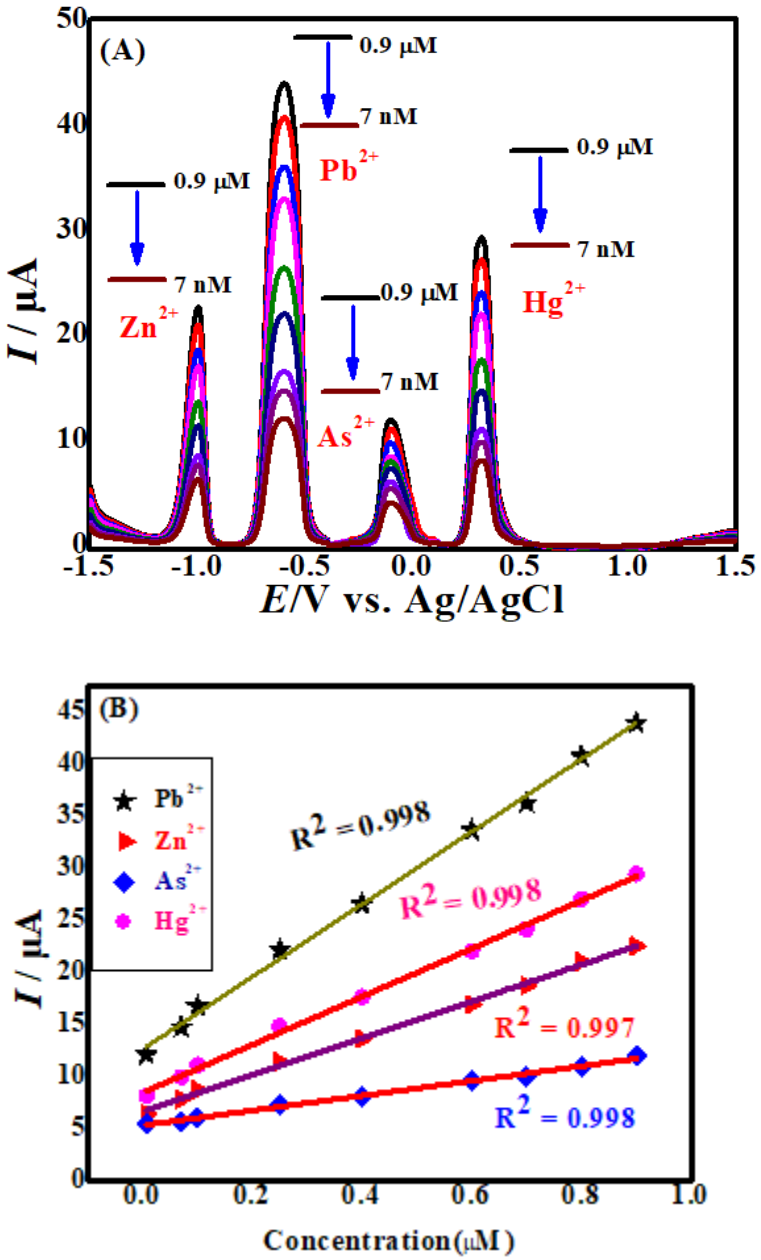

Fig. 3.10. *(A) SWASV curves acquired in the 7 nM to 0.9 µM, concentration range for simultaneous detection of Pb^{2+}, Zn^{2+}, Hg^{2+}, and $As^{3+}$by BTC/ GCE. (B) Linear calibration curves generated for Zn^{2+}, Pb^{2+}, Hg^{2+}, and As^{3+} in the concentration ranging between 7 nM -0.9 µM.*

Table 3.1. *A comparison between the newly designed sensor and other already reported sensors for the simultaneously determination of Hg^{2+}, Zn^{2+}, Pb^{2+}, and As^{3+}.*

Modified electrode	Method	LOD Zn^{2+}	LOD Pb^{2+}	LOD As^{3+}	LOD Hg^{2+}	Supporting electrolyte	Refs.
$[Ru(bpy)_3]_2$+-GO /GE	DPV	–	1.41 nM	2.30 nM	1.60 nM	Citrate buffer / pH 5	[215]
Graphene/CeO_2 /GCE	DPASV	–	0.1057 nM	–	0.28 nM	Acetate buffer / pH 5.0	[216]
HAP-Nafion /GCE	DPASV	–	0.049 µM	–	0.03 µM	NaAc-HAc / pH 3.0	[217]
BiFEs	SWASV	615 nM	192 nM	–	–	Acetate buffer / pH 4.45	[218]
Ƴ-AlOOH@SiO_2/Fe_3O_4 /GCE	SWASV	0.04 µM	0.002 µM	–	0.02 µM	NaAc-HAc / pH 5.0	[219]
HMDE	DPASV	2.1×10^{-8} M	7.1 nM			KNO_3	[220]
AuNPs/CNFs /GCE	SWASV	–	0.1 µM	–	–	PBS	[221]
BTC/GCE	SWASW	14.6 pM	28.8 pM	71.9 pM	66.3 pM	BRB / pH 3.0	This work

3.1.5 Real samples analysis

For validation of the sensor performance, real water samples obtained from various sources, including Rawal dam Lake in Islamabad, tap water samples, and drinking water samples were analyzed using the BTC-modified GCE. The water samples were prepared for analysis by diluting them with 50% BRB (pH 3) without any additional treatment [222]. The concentrations of Zn^{2+}, Pb^{2+}, Hg^{2+}, and As^{3+} in the water samples were detected and recorded using the standard addition technique, where the known quantities of these metal ions were spiked into the samples for analysis. The results showed excellent recoveries for all the analytes in the three types of water samples as presented in Table 3.2.

***Table 3.2**. The outcomes of the recovery experiment indicating satisfactory recoveries for all the analytes in the three types of water samples.*

Samples		Lake Water	Drinking water	Tap water
Pb^{2+} (μM)	Original	-	-	-
	added	0.9	0.6	0.3
	Found	0.89	0.59	0.298
	Recovery	98.9%	98.3%	99.3%
Zn^{2+} (μM)	Original	-	-	-
	added	0.9	0.6	0.3
	Found	0.89	0.58	0.3
	Recovery	98.9%	98.3%	100%
As^{3+} (μM)	Original	-	-	-
	added	0.9	0.6	0.3
	Found	0.88	0.59	0.3
	Recovery	97.8%	98.3%	100%
Hg^{2+} (μM)	Original	-	-	-
	added	0.9	0.6	0.3
	Found	0.89	0.6	0.3
	Recovery	98.9%	100%	100%

3.2 Sensor 2: BPTC/GCE

The GCE surface was immobilized with BPTC for HM ion analysis by employing anodic stripping voltammetry. The stripping signals of Hg^{2+}, Cd^{2+}, and Pb^{2+} at BPTC/GCE were found to have a rapid electron transfer as confirmed by SWASV. The sensor's effectiveness was further evaluated in real water samples obtained from local drinking water sources. The details of BPTC/GCE characterization and its applications are presented below:

3.2.1 Electrochemical characterization of BPTC/GCE

The electrochemical behavior of ferricyanide and ferrocyanide interconversion at the BPTC/GCE and bare-GCE was compared as shown in Fig. 3.11(A). Observation of the voltammograms reveals that the oxidation and reduction peaks of the redox couple at the BPTC/GCE have higher current intensity than at the surface of the bare-GCE. The much improved current response can be related to the BPTC's ability to accumulate the redox probe at the electrode and electrolyte interface, thereby creating active sites that promote the maintenance of equilibrium between ferrocyanide and ferricyanide ions. The reversible behavior of the oxidation/reduction process of the redox couple at the surface of the electrode was confirmed by ratio of the cathodic and anodic peak current values that were found equal to 1. Using the Randles Sevcik equation (Eq. 3.1), the electroactive surface area (ECSA) was calculated for both unmodified GCE and the BPTC/GCE. Based on the results it can be inferred that the BPTC/GCE has a greater ECSA compared to the bare GCE, which could improve the electrode's performance in various electrochemical applications.

$$I_p = 2.69 \times 10^{5} A D^{1/2} n^{3/2} \upsilon^{1/2} C \qquad \text{(Eq. 3.1)}$$

The obtained ECSA value for the bare and BPTC GCE were found to be 0.06 cm^2 and 0.17 cm^2 respectively. EIS was also used to investigate the faster charge transport through

BPTC/GCE. The Nyquist plots constructed from EIS data exhibited a semi-circular section at higher frequencies and a linear section at lower frequencies. The diameter of semicircle represents R_{ct}, and the linear part relates to the diffusion process of the products of redox probe. The information displayed in the Table 3.3 depicts that the BPTC/GCE exhibits a lower R_{ct} compared to the bare GCE, indicating a more facile process of charge transfer. The lower value of resistance of the electrolytic solution (R_e) at BPTC/GCE indicates promising conductivity. The constant phase element (CPE) with value lower as compared to bare GCE indicates a smoother surface with a more homogeneous distribution of active sites, resulting in faster electron transfer. The higher number density of active sites (n) for the BPTC/GCE indicates the availability of greater number of available electroactive sites for redox species. These results further support the improved electrochemical performance of BPTC/GCE related to the unmodified GCE.

Table 3.3. *EIS parameters calculated obtained from Nyquist plot.*

EIS parameters	Bare-GCE	BPTC /GCE
R_e / 10^2 (Ω)	4.5	3.6
R_{ct} / 10^3 (Ω)	5.6	5.2
CPE / 10^6 (F)	1.9	1.7
N	0.5	0.9

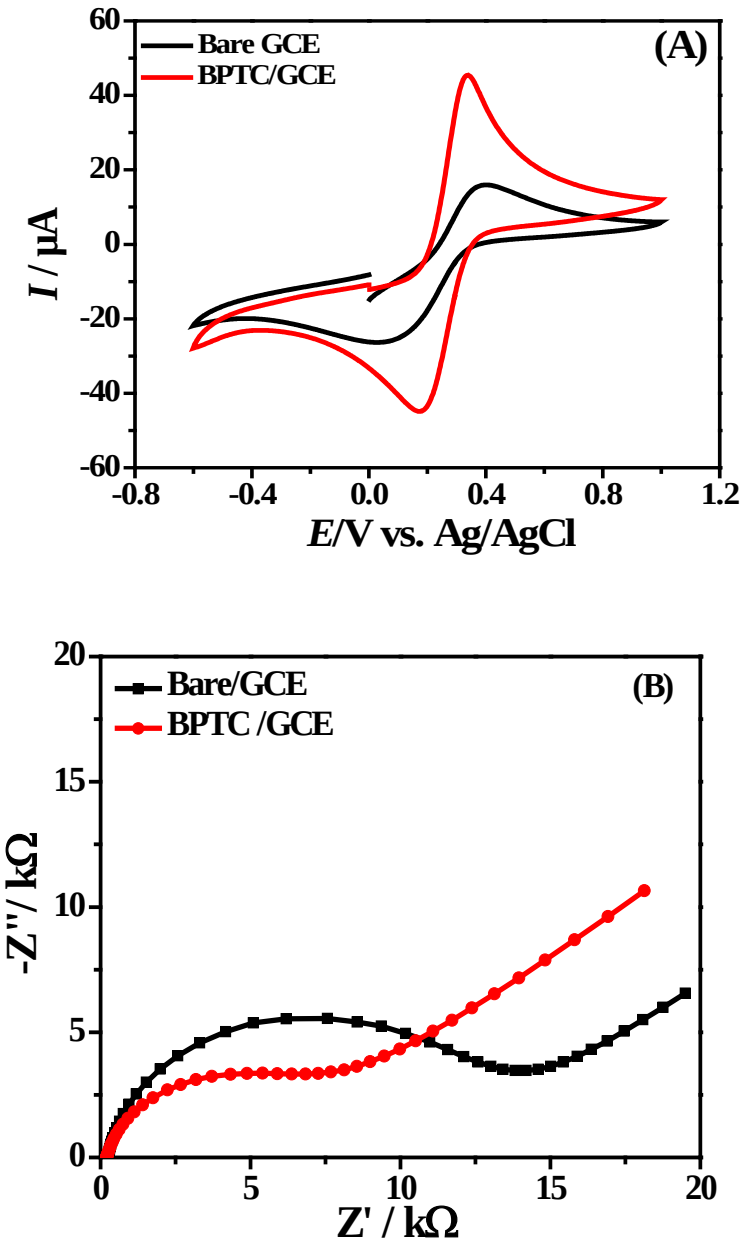

Fig. 3.11. *Depicts (A) the cyclic voltammograms, (B) and Nyquist plot, generated from electrochemical impedance spectroscopy measurements taken at both bare and BPTC/ GCEs in in 5 mM solution of* $K_3[Fe(CN)_6]$.

3.2.2 SWASV for electrochemical analysis through BPTC/GCE

SWASV was employed to investigate the response of Cd^{2+}, Pb^{2+}, and Hg^{2+} at the BPTC/GCE. Significantly sharper and enhanced current responses of metal ions were noticed at BPTC/GCE as compared to the unmodified-GCE (indicated by the blue line). The reason can be linked to the role of the modifier in pre-concentrating the targeted analyte species at the interface between the electrode and electrolyte via host-guest-complexation. In addition, the modified-GCE exhibited remarkable specificity towards all the three metal ions, as their signals were detected at unique potentials without any overlap. This indicates that the BPTC/GCE has great potential as a recognition material for HM ions detection. Additionally, the higher conductivity of the BPTC/GCE may also contribute to the enhanced observed current response. The outcomes of the study suggest that the BPTC/GCE has the potential to serve as a useful and effective analytical tool for the detection of HM ions.

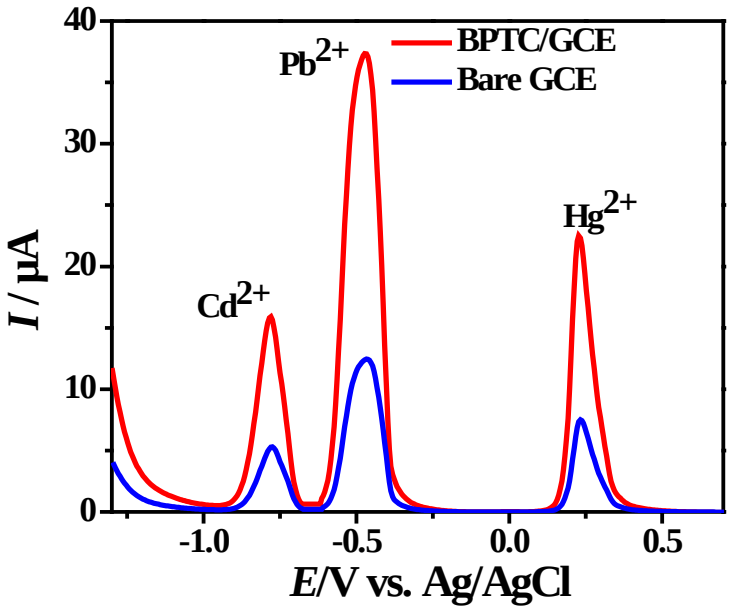

Fig. 3.12. *SWASV was performed to measure the response of a 10 µM solution of Hg^{2+}, Cd^{2+}, and Pb^{2+}, at both bare-GCE and BPTC/GCE under optimized experimental conditions.*

3.2.3 Optimizing parameters for HM Ions sensing at BPTC/GCE

Assessing the sensing capability of BPTC/GCE platform for HM ion detection, the concentration of the modifier was investigated as a key factor that could affect the analytical performance. The current signals corresponding to Cd^{2+}, Hg^{2+}, and Pb^{2+}, increased as the amount of BPTC increased as shown in Fig. 3.13, and reached a maximum at 0.5 mM. However, amount of the modifier greater than 0.5 mM resulted in a decline in the current signals of the analytes, which may be due to the formation of a thick multilayer film of BPTC leading to impeding the electrical conductivity. The study determined that the most effective concentration of BPTC for the detection of Cd^{2+}, Hg^{2+}, and Pb^{2+} is 0.5 mM. These findings suggest that BPTC/GCE is an effective analytical tool for detecting as well as quantifying HM ions in various environmental samples.

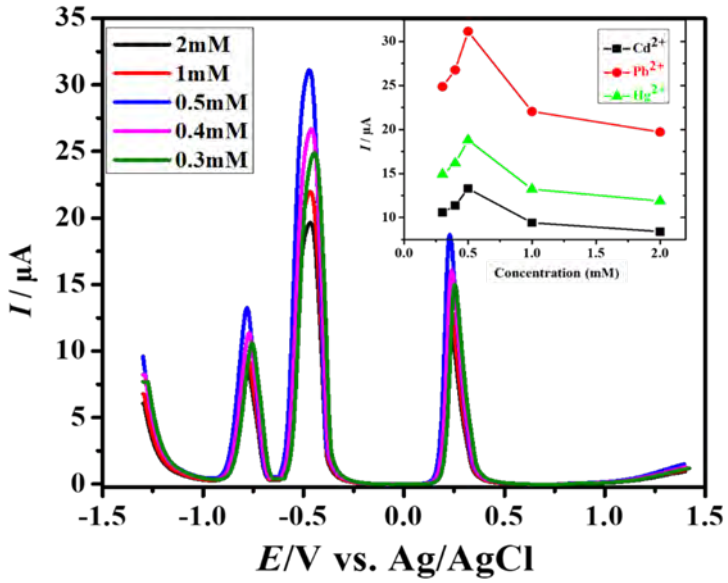

Fig. 3.13. *Under optimized conditions, different concentrations of BPTC were employed to determine the SWASV responses for detection of Hg^{2+}, Pb^{2+}, Cd^{2+}, and (7 µM) at the BPTC/GCE.*

Optimization of several parameters was done to provide suitable conditions for BPTC/GCE to simultaneously detect Hg^{2+}, Pb^{2+} and Cd^{2+}. In order to find a suitable supporting electrolyte, three different electrolytes including 0.1 M acetic acid-sodium acetate, 0.1 M ammonium chloride-hydrochloric acid, and BRB of pH 4 were tested. In the BRB electrolyte, metal ions exhibited the highest current response at the sensor surface as shown in Fig. 3.14(A), indicating BRB as preferred electrolyte the other two electrolytes. Consequently, it was selected for electroanalytical experiments conducted for LOD determination.

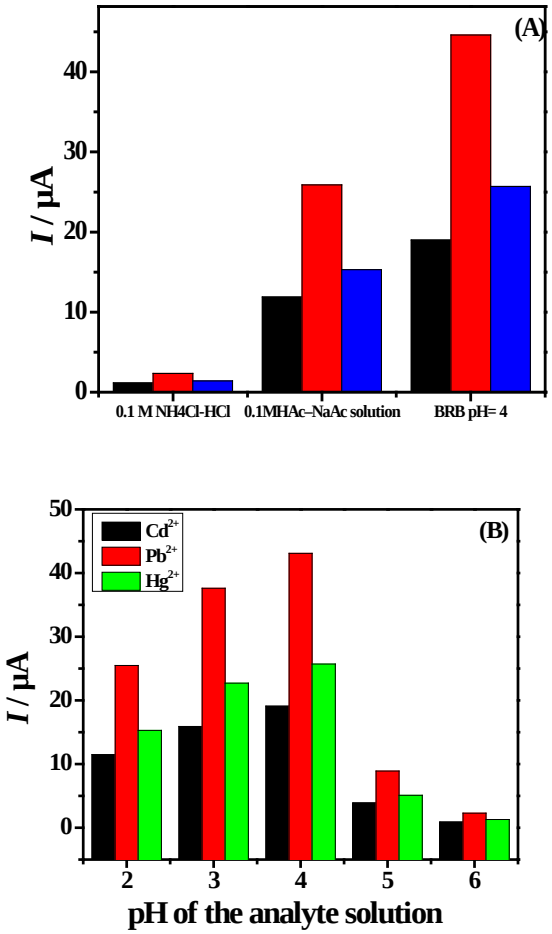

Fig. 3.14. *The impact of various factors on SWASV current signals of Cd^{2+}, Hg^{2+}, and Pb^{2+} (10 µM) investigated, and the results are presented showing impact of the (A) different supporting electrolytes, (B) the pH values of the solution medium, as determined under optimized conditions at BPTC/GCE.*

The impact of the pH of solution on the current intensity of HM ions was examined. The solutions pH was changed between 2 to 6, and the corresponding peak current values were noted. Fig. 3.14(B) illustrates pH dependent variation in the peak current values under optimized conditions at BPTC/GCE. The outcomes demonstrate that the current values increases steadily with pH level reaching maximum at pH 4, and then drop as pH level further increase beyond 4. Thus, pH 4 was selected as the optimum pH level for subsequent electroanalytical experiments. The fluctuations in peak current values with pH can be explained by alterations in the speciation and activity of the target analytes, as well as variations in the electrode's surface characteristics. At lower pH values, there are more hydrogen ions in the solution, which can hinder metal ions binding to the available sites on the surface of electrode, leading to lower peak currents. When pH levels rise, the concentration of hydrogen ions tends to decrease, allowing more binding sites to become available for the metal ions, leading to an increase in peak currents. However, as the pH continues to increase, the metal ions can form hydroxide complexes, as a consequence, there is a reduced likelihood of hydrogen ions binding to the surface of electrode, which can lead to reduction in the peak current signals. pH 4 is likely the optimal pH because it balances the competing effects of increased metal ion binding at higher pH values with the potential formation of hydroxide complexes at even higher pH values.

The peak current values observed during HM ion detection using the BPTC/GCE modified electrode demonstrated enhancement as the accumulation time increased. The reason for the increase in current response with longer accumulation time is due to the larger volume of HM ions which are accumulated at the surface of electrode during this time. However, when the accumulation time was prolonged beyond a certain limit, the electrode surface could become saturated with metal ions, which lead to a decline in the current signals. Thus, the best accumulation time was determined based on achieving the highest possible accumulation of metal ions on the electrode surface, leading to the highest current signal. In this study, the optimal accumulation time for detecting Hg^{2+}, Cd^{2+}, and Pb^{2+} using the BPTC/GCE modified electrode was found to be 20 seconds, as depicted in Fig. 3.15(A), where the highest peak current value was obtained.

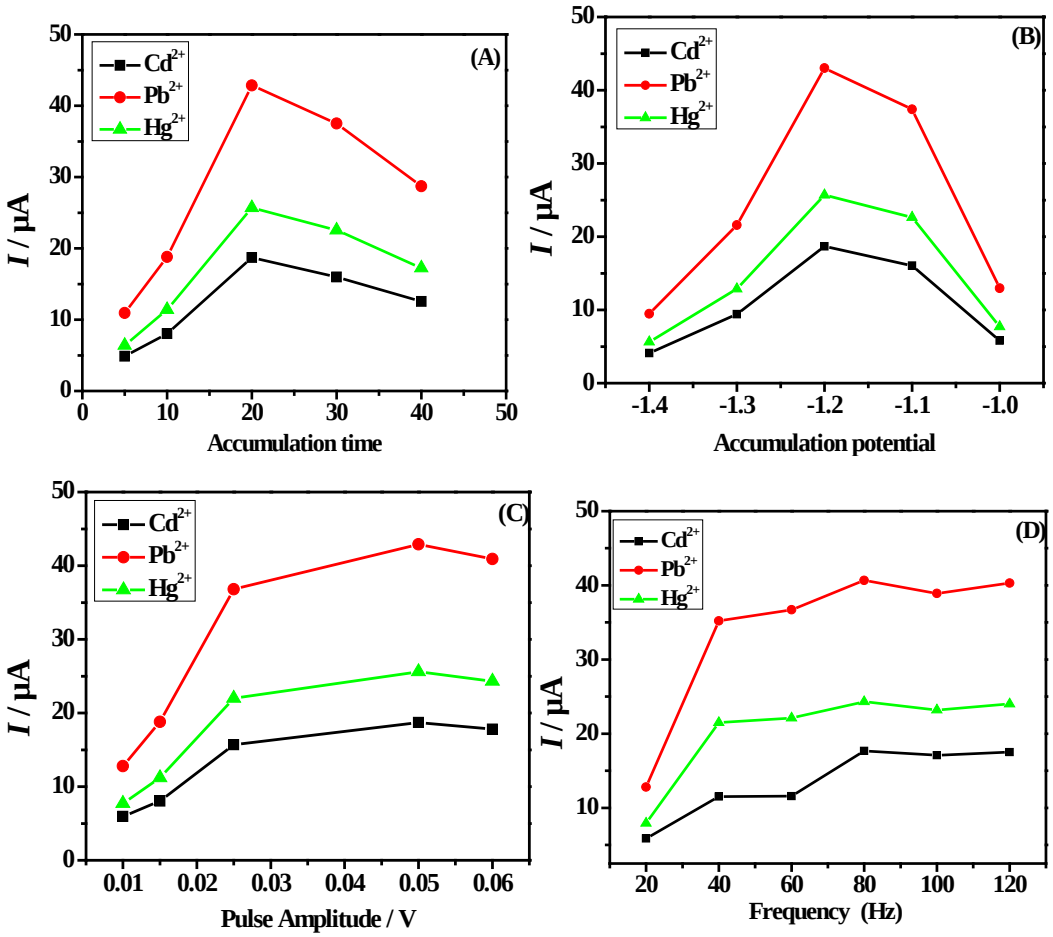

Fig. 3.15. *The SWASV current response of* Cd^{2+}, Pb^{2+}, *and* Hg^{2+} (*10 µM*) *on BPTC/GCE affected by different factors, including (A) accumulation time, (B) accumulation potential, (C) pulse amplitude, and (D) frequency.*

The selection of an appropriate deposition potential is crucial in stripping voltammetric analysis, as it directly affects the current response of the target analytes. In this study, a deposition potential range between −1.0 to −1.4 V was investigated to determine their effect on the stripping current responses of Cd^{2+}, Hg^{2+}, and Pb^{2+}. According to the results, it was observed that the current response was positively correlated with more negative deposition potentials. The rise in current response with potential value becomes more negative, can be credited to the advantageous reduction and accumulations of HM ions at the surface of modified GCE. However, the deposition potential of −1.4 V can result in water splitting and lead to H_2 gas release, which can compromise the surface of electrode

and affect measurement repeatability. Therefore, after careful evaluation, a deposition potential of −1.2 V was determined to be the optimal condition for detecting Hg^{2+}, Cd^{2+} , and Pb^{2+} using the BPTC/GCE. The selected potential offered the most effective stripping current response for the electroreduced metal ions, while also ensuring measurement reliability.

The choice of instrumental parameters, such as amplitude and frequency, is crucial in obtaining accurate and reliable results in stripping voltammetric analysis. The impact of amplitude and frequency on the peak current responses of Cd^{2+}, Hg^{2+}, and Pb^{2+}, was studied, and the optimal values were determined and depicted in Fig. 3.15(C) and 3.15(D). An amplitude of 50 mV was found to produce the maximum current signals, indicating that it is the optimum amplitude for detection of the Cd^{2+}, Hg^{2+}, and Pb^{2+} simultaneously. The effect of frequency was also studied, and it was observed that increasing the frequency resulted in higher current signals up to 80 Hz, after which the current response decreased. However, a frequency of 80 Hz also introduced a significant amount of noise into the current signal, limiting its usefulness. Consequently, after examining the influence of amplitude and frequency on the peak current signals of Cd^{2+}, Pb^{2+}, and Hg^{2+}, a frequency of 20 Hz was chosen as the optimal value to achieve an exceptional signal-to-noise ratio for the current responses. After assessing different instrumental parameters, the optimal values were found to be, −1.2 V as accumulation potential, 20 s as accumulation time, 50 mV as pulse amplitude, and a 20 Hz frequency. These parameters were then implemented to find the analytical parameters of the targeted analyte species using the developed sensing platform, guaranteeing precise and dependable outcomes.

3.2.4 Electroanalytical detection parameters of Hg^{2+}, Cd^{2+}, and, Pb^{2+} using BPTC/GCE

The electro-analytical performance of the BPTC/GCE sensor was examined under experimental conditions optimized for the detection of Hg^{2+}, Cd^{2+}, and Pb^{2+} using SWASV. The concentration range of 1.0 nM to 2.5 μM was used to construct linear calibration plots for the simultaneous detection of the three metal ions, with obtained regression coefficient

values of 0.992, 0.993, and 0.991, for Hg^{2+}, Pb^{2+}, and Cd^{2+} respectively. Fig. 3.16 shows the results of electroanalysis at the designed sensing platform.

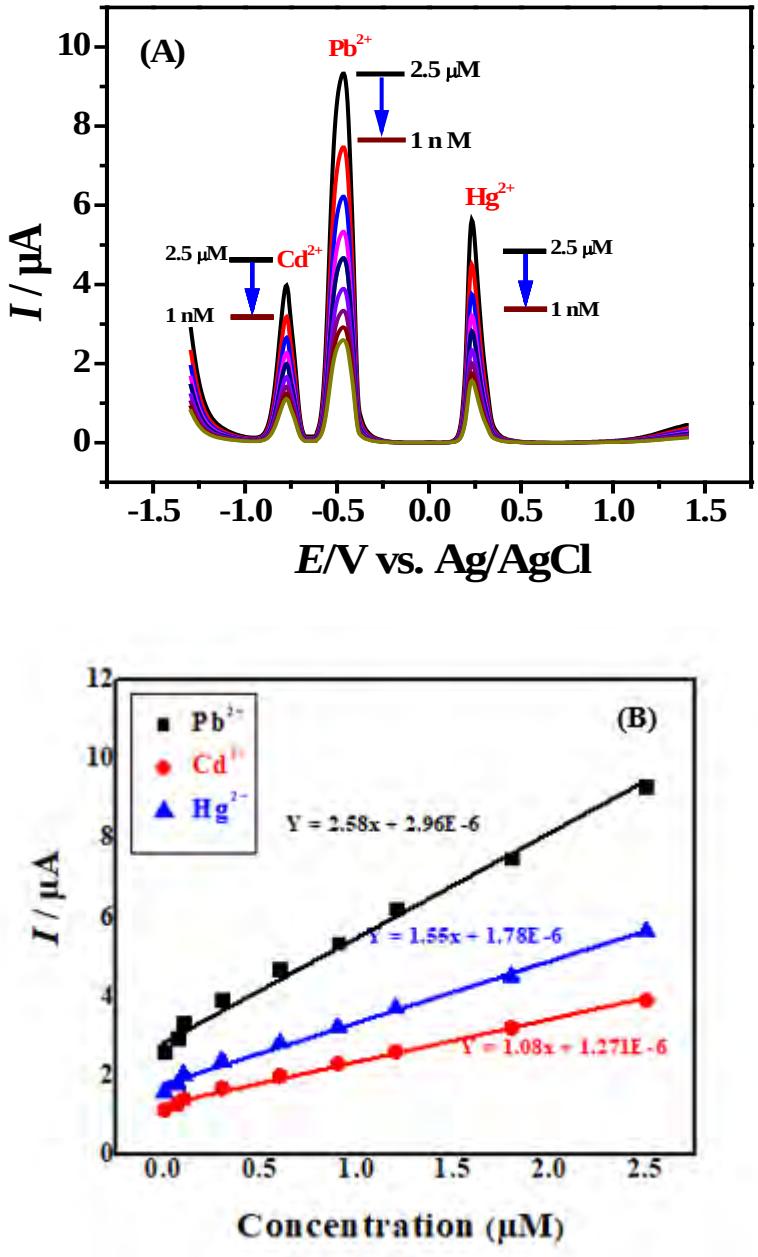

Fig. 3.16. *(A) SWASV used to determine the concentration of the targeted analytes, Cd^{2+}, Pb^{2+}, and Hg^{2+}, simultaneously using BPTC/GCE. (B) Calibration curves constructed for Hg^{2+}, Cd^{2+}, and Pb^{2+}, simultaneously at BPTC/GCE.*

The LODs of a targeted analyte at the sensor is evaluated from LOD = 3s/m and LOQ = 10s/m, where 's' denotes standard deviation of multiple voltammograms of the sensor in blank solution and 'm' the calibration curve slope. Hence, the LODs for Hg^{2+}, Pb^{2+} and Cd^{2+}, were determined to be 25.7 pM, 15.5 pM , and 37.1 pM respectively. These values represent high sensitivity of modified-GCE. Table 3.4 presents a summary of the comparison of the detection performance of our designed sensor as compared with LODs achieved with various modified electrodes as reported in literature.

Table 3.4. *The LODs achieved by BPTC/GCE for Hg^{2+}, Cd^{2+} and Pb^{2+} detection were compared with previously reported methods, showing similar or improved LODs for all three ions.*

Electrode	Techniques Used	LODs			Ref.
		Cd^{2+}	Pb^{2+}	Hg^{2+}	
SnO_2-reduced graphene oxide nanocomposite-GCE	SWASV	110 µM	184 µM	279 µM	[223]
NG-GCE	DPSV	-	5 nM	50 nM	[224]
Bi-ERNGO-GCE	SWASV	2 nM	0.8 nM	-	[225]
NH_2-CMS-GCE	SWASV	1.07 µM	0.38 µM	0.37 µM	[226]
Mn_3O_4-GCE	DPASV	48 pM	96.6 pM	56 pM	[227]
F-MWCNT-Fe_3O_4-0.5% Nafion-GCE	SWV	14 nM	8.4 nM	3.9 nM	[228]
ERGO-GCE	SWASV		97 µM	4.99 nM	[229]
BPTC-GCE	SWASV	37.1pM	15.5 pM	25.7 pM	This work

3.2.5 Interference study

To assess the potential impact of coexisting metal ions on the sensor performance for detecting Hg^{2+}, Pb^{2+}, and Cd^{2+}, interference experiments were conducted. Also, We conducted interference study to recognize the significance of investigating the presence of heavy metals (HMs) in forms other than metal ions in water, particularly those associated with organic matter or already chelated, and also to ensure the efficacy of BPTC in sensing these diverse forms. This study assess the selectivity and sensitivity of the electrochemical method in the presence of potential interferents, providing insights into the ability of BPTC to detect and quantify HMs in complex environmental samples.

This involved spiking known concentrations of metal ions such as Ni^{2+}, Ca^{2+}, Cr^{2+}, Al^{3+} and Zn^{2+} and Cl^{1-}, to the standard solution of target metal ions, with the aim of determining the sensor's ability to retain integrity of its analytes signals when interfering ions are present in solution. By conducting this experiment, the selectivity and specificity of the sensor for detecting the target metal ions in complex sample matrices was evaluated.

The outcomes of the experiment displayed that the current signals remained relatively unchanged even when the competitor ions concentration was increased up to three-fold for chloride, cobalt, nickel, and zinc ions, and two-fold for chromium and aluminum ions as compared to target analytes concentration. According to the findings of the interference study, the sensor showed excellent selectivity towards the target metal ions, and the presence of other metal ions in the solution could not significantly affect its performance. This indicates that the sensor is capable of accurately detecting Hg^{2+}, Cd^{2+}, and Pb^{2+}, even when if interfering ions are present. These findings point to the applicability of the sensor for determining of the Hg^{2+}, Pb^{2+}, and Cd^{2+} in real-world samples which may contain various other metal ions. The results of interference study are presented in Fig. 3.17.

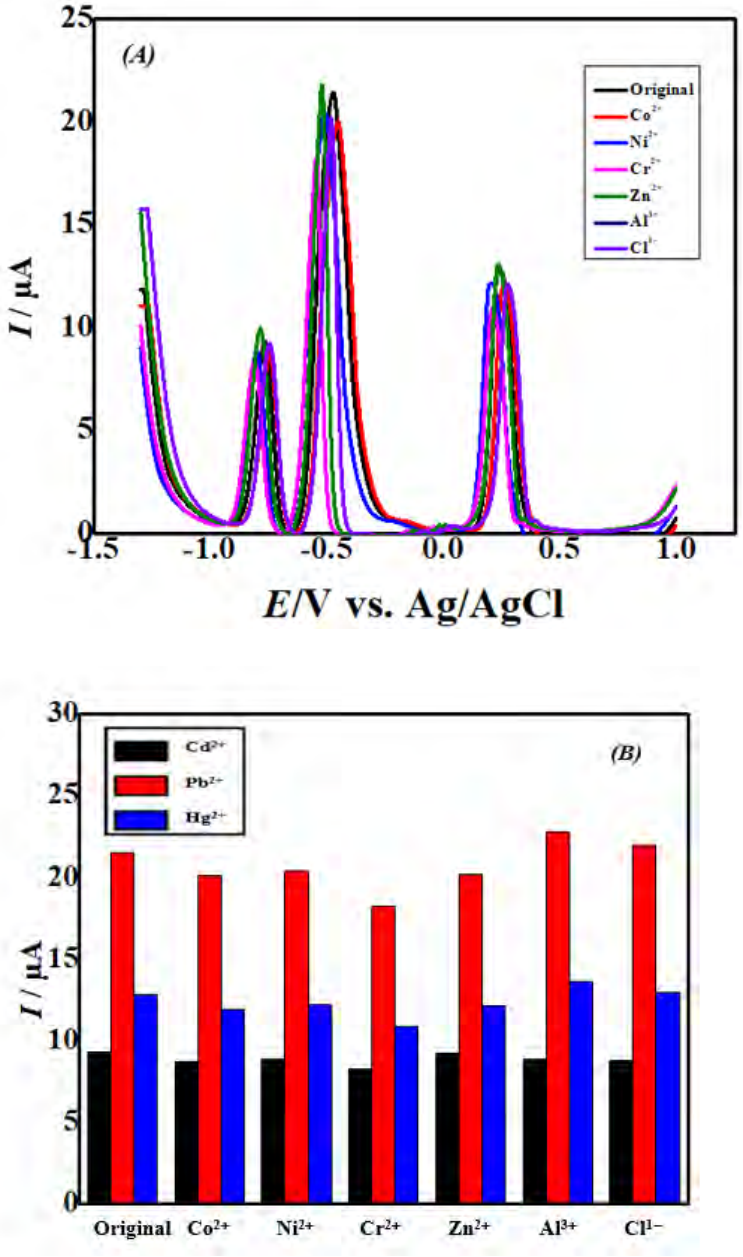

Fig. 3.17. *(A) The impact of potential interfering species on detection of the Hg^{2+}, Pb^{2+}, and Cd^{2+}, simultaneously, investigated by adding cobalt, nickel, chloride, zinc and chromium, aluminum ions to the solution in concentrations up to three times and two times, respectively, and compared to the detection in the absence of interfering agents. (B) The results presented in bar graphs for a clear comparison of the impact of potential interfering-agents on the detection of the target HM ions.*

3.2.6 Reproducibility and stability of the designed sensing platform

To ensure the reliability of the BPTC/GCE for the determination of Hg^{2+}, Pb^{2+}, and Cd^{2+}, several experiments were conducted to evaluate its reproducibility and precision. Six repeated experiments were carried out on the same day, and triplicate detection was performed for three consecutive days to check intraday and inter-day precisions. It was found that the BPTC GCE had decent reproducibility, with RSD of 1.46% and 2.51% for intra-day and inter-day precision, respectively. Based on these results, it can be inferred that the developed sensor exhibits excellent precision, suggesting its potential utility for the quantitative determination of the target analytes. Moreover, to assess the stability of the BPTC/GCE, multiplexed detection was performed after one complete week using the same electrode. Results demonstrated promising promising stability. These results demonstrate that the BPTC/GCE has reliable and stable performance, making it a useful tool for the detection of Hg^{2+}, Pb^{2+} and Cd^{2+} simultaneously in various samples.

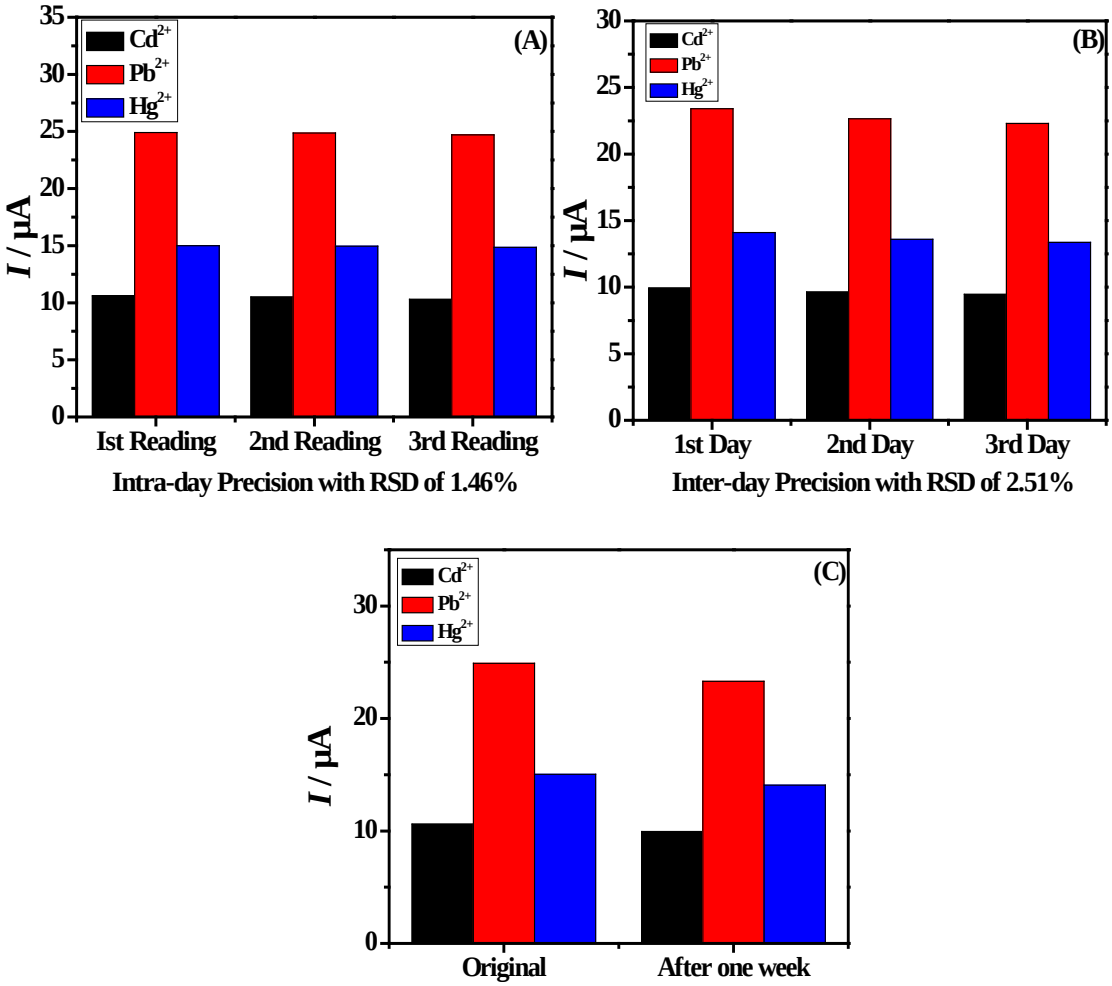

Fig. 3.18. *Evaluation of reproducibility and stability of sensor's current responses, as shown in (A) intra day current response, (B) inter day current response, (C) current responses after time of one week.*

3.2.7 Analysis of metal ions in drinking water samples using BPTC/GCE

Hg^{2+}, Pb^{2+}, and Cd^{2+} were analyzed in drinking-water samples using the developed sensor, with a focus on recovery rate analysis to evaluate practical performance of BPTC/GCE. The sample preparation involved concentrating a 50 milliliters of drinking water to 10 milliliters, followed by mixing a portion of the condensed water with BRB (pH 4) without any additional treatment. Next, various standard concentrations of Hg^{2+}, Cd^{2+}, and Pb^{2+} were spiked in the same condensed water sample and analyzed using the modified electrode

and optimized procedure developed in this experiment. The obtained findings presented in Table 3.5 demonstrate the potential practical utility of the BPTC/GCE for analyzing real drinking water samples.

Table 3.5. *Detection of* Hg^{2+}, Pb^{2+}, and Cd^{2+}, *simultaneously, in drinking water samples using the developed BPTC/GCE.*

Samples	Target Metal ions	Concentrations (μM)	Spiked Amount	% Recovery	%RSD
Drinking water sample 1	Hg^{2+}	2.50	2.49	99.6	0.28
	Cd^{2+}	2.50	2.48	99.2	0.57
	Pb^{2+}	2.50	2.49	99.6	0.28
Drinking water sample 2	Hg^{2+}	1.20	1.19	99.0	0.71
	Cd^{2+}	1.20	1.19	99.2	0.59
	Pb^{2+}	1.20	1.19	98.9	0.77

3.3 Sensor 3: $FeCoSe_2$ nanorods modified GCE for isoniazid detection

There is an increasing demand for the development of electrochemical devices with higher sensitivity, and portability for pharmaceutical analysis. New electrode materials with exceptional properties are explored for the electroanalysis of drugs. One such material that has gained attention is bimetallic cobalt-iron diselenide ($FeCoSe_2$) nanorods. $FeCoSe_2$ nanorods possess distinct characteristics, including high-surface-area, outstanding conductivity, and strong affinity towards isoniazid, which render them as a likely electrode material, for the creation of sensitive and selective electrochemical sensor. Moreover, nanorods can serve as effective electrode modifier to enhance the electrochemical performances of sensing platforms. This is because they can improve electron transfer kinetics and increase the surface-area of the electrode, leading to higher sensitivity and selectivity of the sensor. Overall, the development of $FeCoSe_2$ nanorods as an electrode modifier represents a significant step forward in the field of electrochemical sensing for

pharmaceutical analysis, with potential applications in drug screening, disease diagnosis, and personalized medicine The synthesis and characterization of $FeCoSe_2$ nanorods were carried out and this materials was used as an electrode modifier for the purpose of selectively detecting isoniazid, a commonly used anti-tuberculosis medication.

.

3.3.1 Structural and morphological characterization of $FeCoSe_2$

3.3.1.1. XRD analysis for characterization of nanorods

The X-ray diffraction pattern displayed in Fig. 3.19 offers a clear indication of the crystallinity of the synthesized $FeCoSe_2$ as manifested by the sharp and intense peaks. These diffraction signals exhibit various hkl planes and their identification through the Powder Diffraction Standard Database (JCPDS # 21-0432) reveals critical information regarding the crystal structure and orientation of the synthesized material.

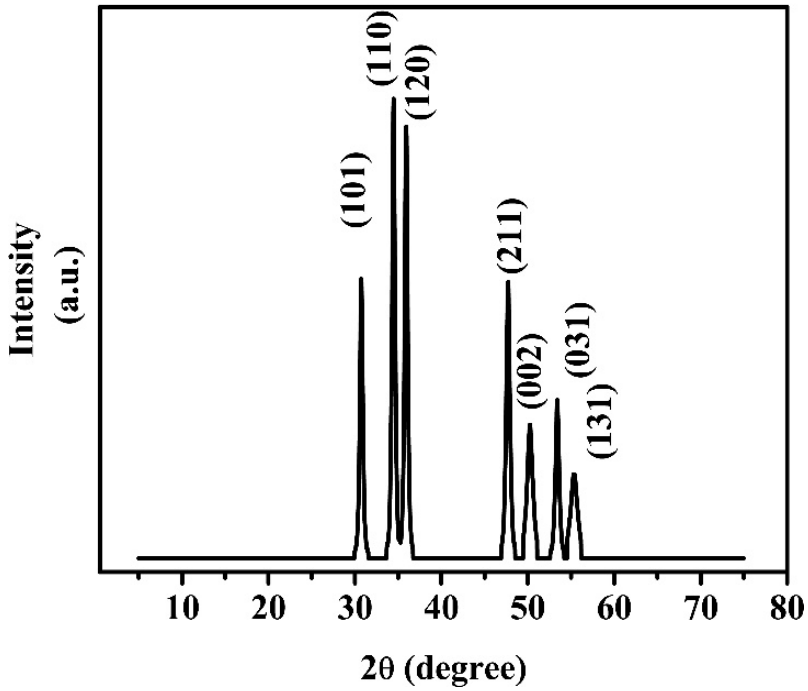

Fig. 3.19. *XRD pattern of the synthesized $FeCoSe_2$.*

3.3.1.2 Surface analysis and pore size distribution of $FeCoSe_2$

The surface properties of the $FeCoSe_2$ nanorods were analyzed using N_2 adsorption-desorption isotherms. The isotherms showed a mesoporous nature based on IUPAC classification, with H3 hysteresis loop observed between 0.4 -0.8 $\frac{P}{Po}$ (here p is relative pressure, and p_o is saturation pressure of N_2). As shown in Fig. 3.20, the $FeCoSe_2$ nano-catalyst exhibited a BET surface-area of 93.14 m^2g^{-1}. The conductivity of the material was affected by both its surface morphology and internal porous structure. The pore size distribution curve was determined from the desorption isotherm, using Barret-Joyner-Halenda (BJH) method. A unimodal distribution of pores with a pore size of 5.5 nm was obtained from the narrow scattering of pores. This suggests that the $FeCoSe_2$ nanocomposite has a well-defined porous structure along with uniform pores distribution.

The selective electrochemical sensing of isoniazid over the electrode surface modified with the synthesized $FeCoSe_2$ nanocomposite catalyst was credited to its higher BET surface-area and mesoporous nature, providing more active sites for the target analyte. The efficient mass transport properties of the mesoporous structure could also enhance the electroanalytical response of proposed sensor. The surface-area and pore size distribution analysis provide insights into the surface properties of the $FeCoSe_2$ nanocomposite that are crucial for designing highly efficient and selective electrochemical sensors.

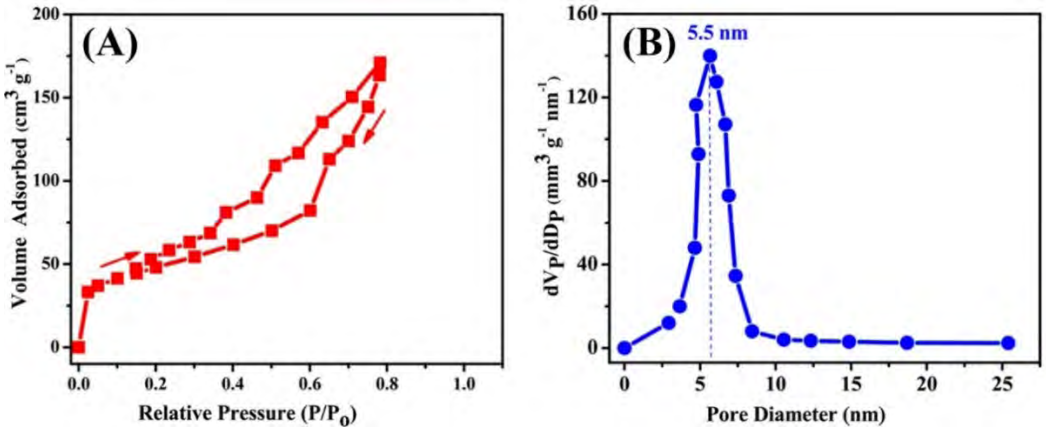

Fig. 3.20. *The surface properties of the $FeCoSe_2$ nanorods analyzed using two methods: (A) N_2 adsorption/desorption isotherm, (B) pore size distribution curve obtained using BJH method.*

3.3.1.3 Morphology of $FeCoSe_2$ nanorods

The $FeCoSe_2$ nanorods synthesized in this study were analyzed using SEM as shown in Fig. 3.21(A-C). The images reveal that the nanorods have diameters ranging from 40 to 90 nm and exhibit a uniform distribution without agglomeration, making them suitable for electrochemical applications. The optimal dispersion of metals in the synthesized $FeCoSe_2$ nanorods led to enhanced catalytic activity for the electrochemical sensing of isoniazid, as discussed in the follow up sections. The TEM image in Fig. 3.21(D) shows the presence of uniformly shaped rod structures with an average diameter of 40 nm in the synthesized material. These findings demonstrate the successful synthesis of $FeCoSe_2$ nanorods and suggest their potential for electrochemical applications.

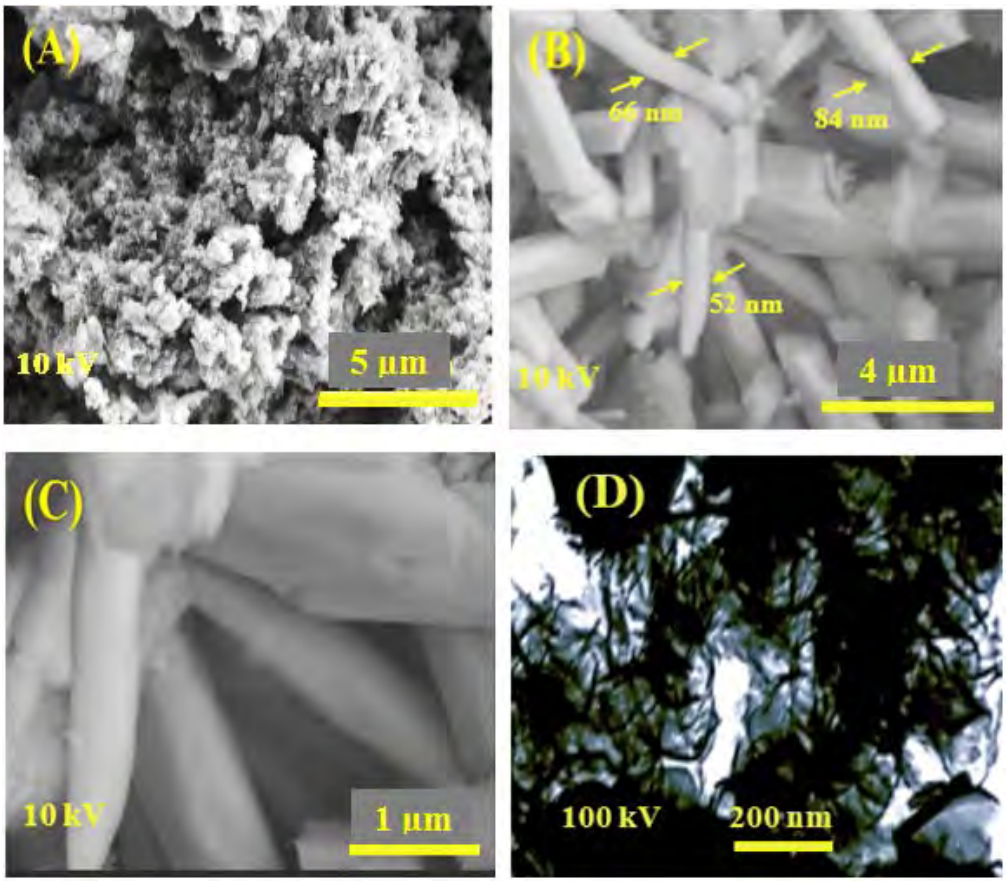

Fig. 3.21 *(A-C) Displays SEM micrographs of $FeCoSe_2$ nanorods at different magnifications and (D) a TEM image.*

3.3.1.4 EDX Analysis

The EDX mapping provides information about the spatial distribution of the elements, which can help confirm the homogeneity and uniformity of the synthesized material. Overall, the EDX analysis and mapping play a crucial role in characterizing the synthesized material and understanding its properties for potential applications. The surface of the prepared catalyst was investigated by performing EDX analysis on randomly selected points as presented in the Fig. 3.22. The EDX study provided information about the elemental composition and weight percentage of each element present in the sample.

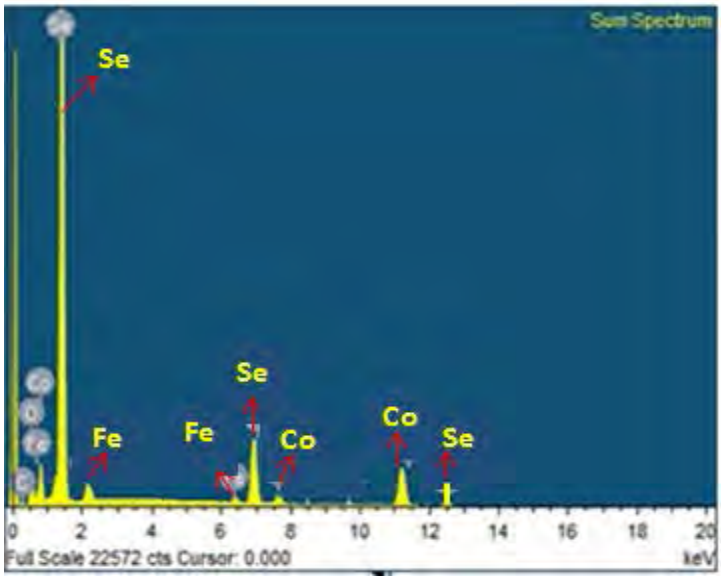

Fig. 3.22. *EDX profile of $FeCoSe_2$ nanocomposite.*

The EDX analysis of the $FeCoSe_2$ sample in Fig. 3.23(A) reveals distinct peaks corresponding to Co, Fe, and Se elements. The resulting weight percentages are 19.26%, 1.21%, and 59.91% for Co, Fe, and Se respectively. The EDX mapping results as shown in Fig. 3.23(B-E) show uniform distribution of Fe, Co, and Se elements throughout the sample, indicating a homogenous dispersion of the metal alloy NPs. These findings highlight the successful synthesis of $FeCoSe_2$ nanorods with a uniform composition, which is essential for their effective use in various electrochemical applications.

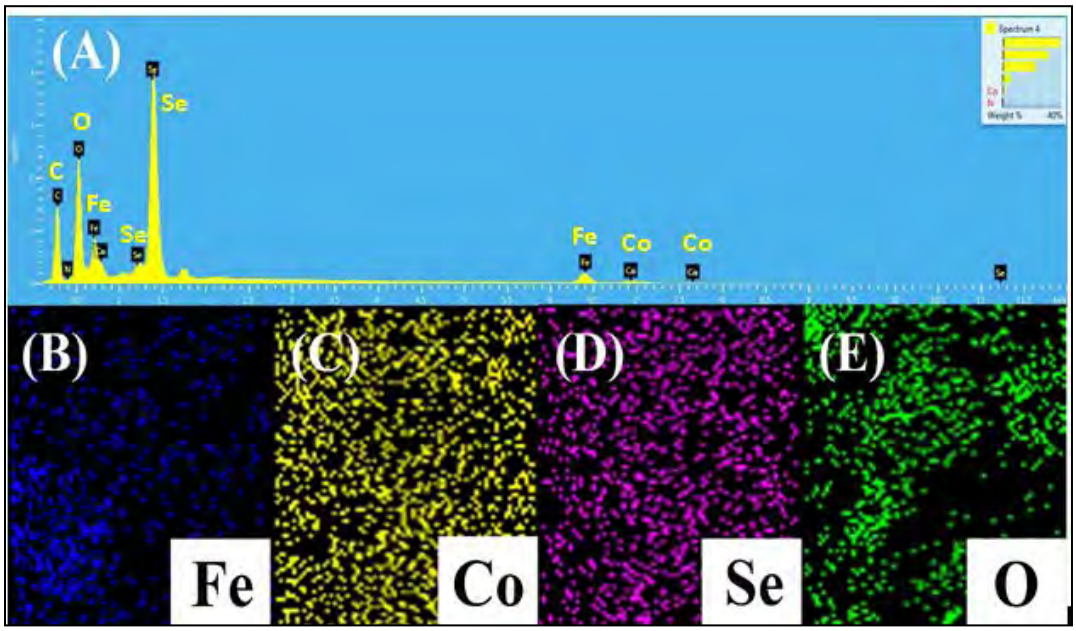

Fig. 3.23. *(A) EDX profile for chemical composition and (B-E) EDX mapping for elemental distribution of the prepared $FeCoSe_2$ nanocomposite.*

3.3.1.5 TPR analysis

The reduction behavior of the catalysts and their potential catalytic applications were probed through TPR analysis. Fig. 3.24 displays the TPR profiles of the prepared nanocomposite. The reduction of cobalt oxide generally occurs in two steps, as described by equation 3.2 and 3.3 [230,231]:

$$Co_3O_4 + H_2 \rightarrow 3CoO + H_2O \qquad \text{(Eq. 3.2)}$$

$$3CoO + 3H_2 \rightarrow 3Co^0 + 3H_2O \qquad \text{(Eq. 3.3)}$$

The TPR analysis of the $FeCoSe_2$ nanocomposite showed a different reduction pattern compared to the monometallic Co catalyst. The Co_3O_4 in the monometallic Co sample underwent a three-step reduction process at temperatures ranging from 150-800 ^oC, while the $CoSe_2$ catalyst underwent an easier reduction process than Co. The addition of Fe to $FeCoSe_2$ lowered the temperature required for Co_3O_4 reduction, causing the reduction peaks to shift towards lower temperatures. This suggests that the combination of Co, Fe,

and Se in the nanocomposite could enhance its catalytic efficiency as demonstrated in the electrochemical sensing of INZ.

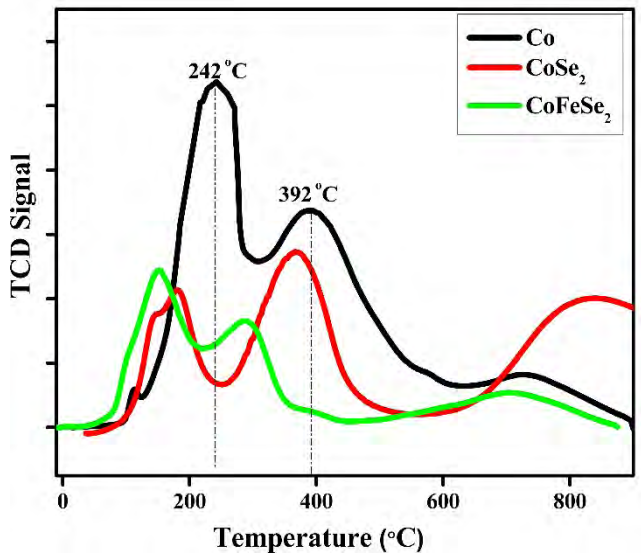

Fig. 3.24. *TPR profiles of the synthesized nanocatalysts.*

3.3.1.6 Electrochemical investigation of $FeCoSe_2$/GCE by cyclic voltammetry

Cyclic voltammetry was performed using a 5 mM solution of potassium ferrocyanide to study the electrochemical characteristics of $FeCoSe_2$/GCE. The CV results obtained at $FeCoSe_2$/GCE presented in Fig. 3.25 reveal sharp peaks with a small potential difference between anodic and cathodic signals and a substantial increase in the peak currents for oxidation/reduction indicate faster electron transfer process. These results suggest the potential of $FeCoSe_2$/GCE for use in electroanalytical applications [232].The active-surface-area of the electrodes was determined using the Randles Sevcik equation. The modified-GCE was found to have higher active surface-area as compared to the bare-GCE. The larger active-surface-area possesses more active-sites leading to enhanced electrochemical activity.

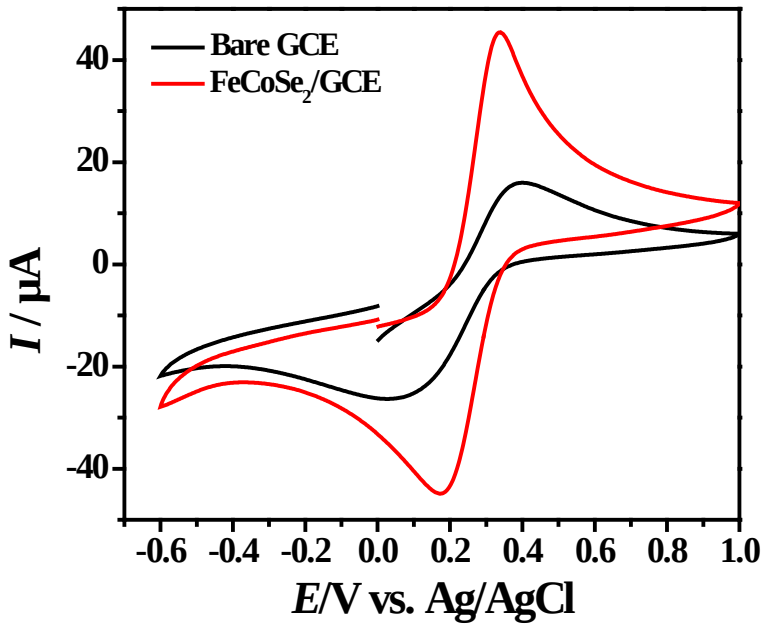

Fig. 3.25. *CVs of bare and $FeCoSe_2$/GCE in 5 mM $K_3[Fe(CN)_6]$ at under optimized conditions.*

3.3.2 Testing the performance of $FeCoSe_2$/GCE for INZ oxidation

The electrooxidation behavior of isoniazid (INZ) was examined in BRB of pH 7 using SWASV technique. Voltammograms indicated the presence of an oxidation signal for INZ at a potential of 0.45 V. A couple of factors such as outstanding conductivity along with larger active surface-area The $FeCoSe_2$ nanorods could account for the increased current responses for the electro-oxidation of INZ at $FeCoSe_2$/GCE in comparison to bare-GCE. These properties enable efficient transfer of electrons between the electrode surface and the INZ molecules, resulting in a higher current response. Moreover, the larger active-surface-area of the $FeCoSe_2$ nanorods provides more interaction sites for INZ molecules to attach to the electrode surface, resulting in intense signals as required for more reliable quantitative analysis. Fig. 3.26(B) depicts the mechanism of electro-oxidation of the INZ on $FeCoSe_2$/GCE [233].

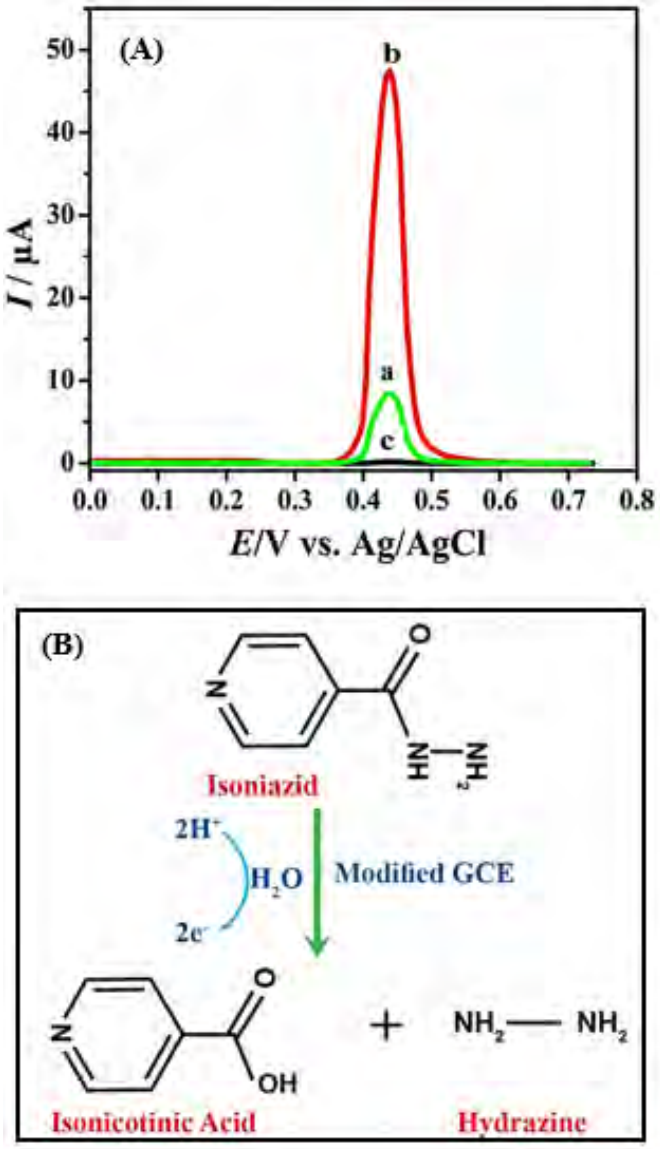

Fig. 3.26. *(A) SWASV measurements conducted (a.) bare-GCE in solution of INZ (25 µM), (b.) $FeCoSe_2$/GCE in solution of INZ (25 µM), and (c) $FeCoSe_2$/GCE in blank sample (solvent +BRB of pH 7) under optimal parameters, and (B) The process of electrochemical oxidation of isoniazid investigated. Using $FeCoSe_2$/GCE.*

3.3.3 Optimization of experimental parameters

The electrochemical detection of INZ using $FeCoSe_2$/GCE exhibited an incremental increase in peak heights with a gradual increase in the pH of the solution from pH 4 - pH 7. Fig. 3.27(A) demonstrates that the peak current for the oxidation of INZ gradually increased with the rise in the solution's pH. However, as the pH of the solution further increases beyond 7, the peak current values start to fall. This might be due to the formation of hydroxide ions, which can interact with the electroactive species, leading to a decrease in the electrochemical activity of the $FeCoSe_2$/GCE electrode. The experiments showed pH 7 as the most favorable condition for the best INZ sensing of the sensor. The shift of the peak potential value toward more negative direction as the pH increases suggested that the transfer of electrons taking place at the surface of electrode are coupled with protons transfer. By analyzing the slope value derived from the plot of Ep versus pH illustrated in Fig. 3.27(B), it can be deduced that the isoniazid INZ process is a type of electron transfer process that is coupled with protons.

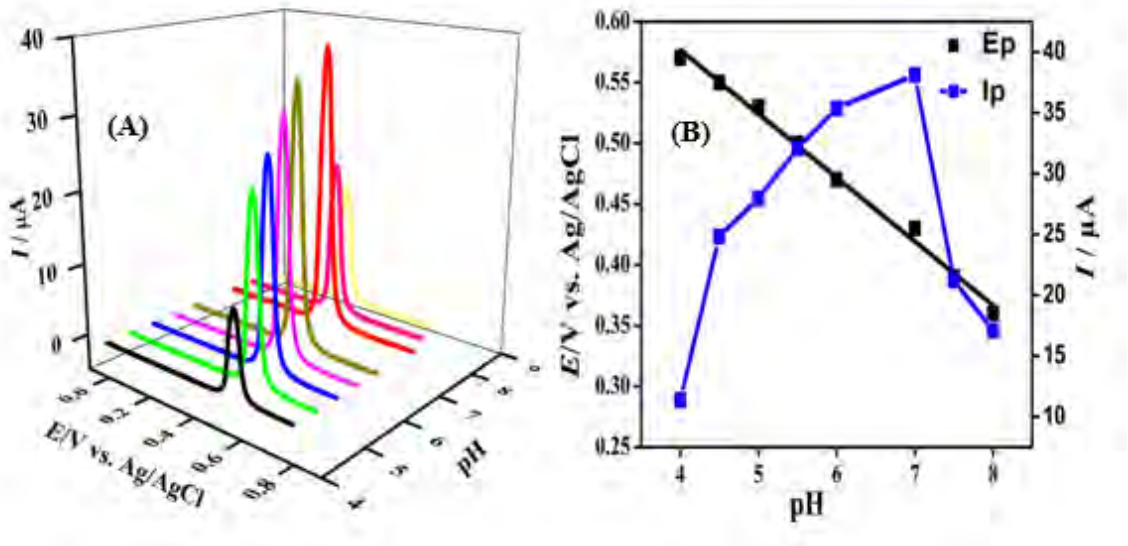

Fig. 3.27. *(A) SWASV of 16µM INZ at pH 4-8 using $FeCoSe_2$/GCE, (B) E_p and I_p plotted against pH to analyze electrochemical behavior.*

SWASV was used to examine the effect of various accumulation potentials on current responses related to the oxidation of INZ as displayed in the Fig. 3.28(A). Voltammograms show that the current increases gradually in the positive potential direction, reaching its highest value at 0.0 V with respect to Ag/AgCl reference electrode. However, beyond this potential, the current decreased rapidly. Consequently, the potential of 0.0 V was recognized as the most optimal accumulation potential INZ detection.

The impact of different accumulation-times on the Ip was also analyzed and is showed in the Fig. 3.28(B). The findings indicated enhancement in the Ip value with the increase in accumulation time, with the most intense signal at 90 seconds. The peak height then started to decrease upon further increase in accumulation time. Consequently, an accumulation time of 90 seconds was set as the optimal value for subsequent electroanalytical experiments.

The reason for the gradual increase in the Ip in the positive potential direction can be related to the higher concentration of INZ at the electrode surface, possible due to prolonging accumulation process. However, beyond the optimal potential, the oxidation of INZ might be hampered due to electrode fouling or competition with other electroactive species. The rise in the peak current values with the accumulation time can be attributed to the higher deposition of INZ on the surface of the electrode. However, beyond the optimal accumulation time, the peak current value may decrease due to the saturation of the electrode surface or the initiation of unwanted side reactions. The reasons for selecting these values were based on the fact that the optimal accumulation potential and time contribute significantly to the electrochemical performance of the sensor. The accumulation potential aids in the effective adsorption of INZ on the electrode surface, while A longer accumulation time allows for the analyte to accumulate on the surface of electrode, leading to higher sensitivity.

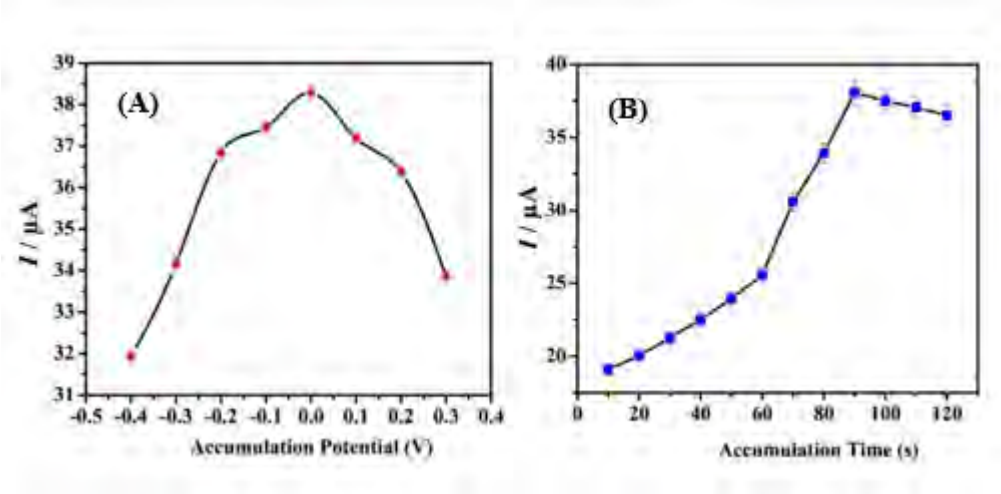

Fig. 3.28 *(A) the influence of accumulation potential (accumulation time constant at 90 seconds, (B) The effect of different accumulation times (constant accumulation potential of 0.0 V), on the oxidation peak current of INZ (18µM) at $FeCoSe_2$/GCE.*

Based upon the SWAS voltammograms presented in Fig. 3.29(A) , a calibration curve was plotted between peak current against INZ concentrations in the range between 0.03 and 1 µM. The linear correlation observed among the INZ concentrations and oxidation peak current values in the calibration curve suggests that the $FeCoSe_2$/GCE electrode is a suitable platform for detecting low concentrations of INZ. By applying equation 3.4 and 3.5, the LOD and LOQ of INZ were determined. The equations utilized the slope value of the current vs. concentration plot (represented by "m") and the standard deviation of the peak current of the blank solution indicated as "s" [234].

$$\text{LOD} = \frac{3s}{m} \qquad \text{(Eq. 3.4)}$$

$$\text{LOQ} = \frac{10s}{m} \qquad \text{(Eq. 3.5)}$$

In Fig. 3.29(B), the relationship between the concentrations of INZ and the peak current response at the $FeCoSe_2$/GCE is presented, revealing a linear correlation between the two

variables. Using this correlation, the LOD and LOQ for INZ were quantified to be 1.24×10^{-10} M and 4.14×10^{-10} M. The parameters achieved from the calibration curves are also provided in Table 3.6.

Table 3.6. *The following table presents the important parameters and regression data acquired from the calibration curves:*

Parameters	Measured Values
Measured potential (mV)	433
Linear range (μM)	0.03-1
Correlation coefficient (R^2)	0.998
LOD (M)	1.24×10^{-10}
LOQ (M)	4.14×10^{-10}

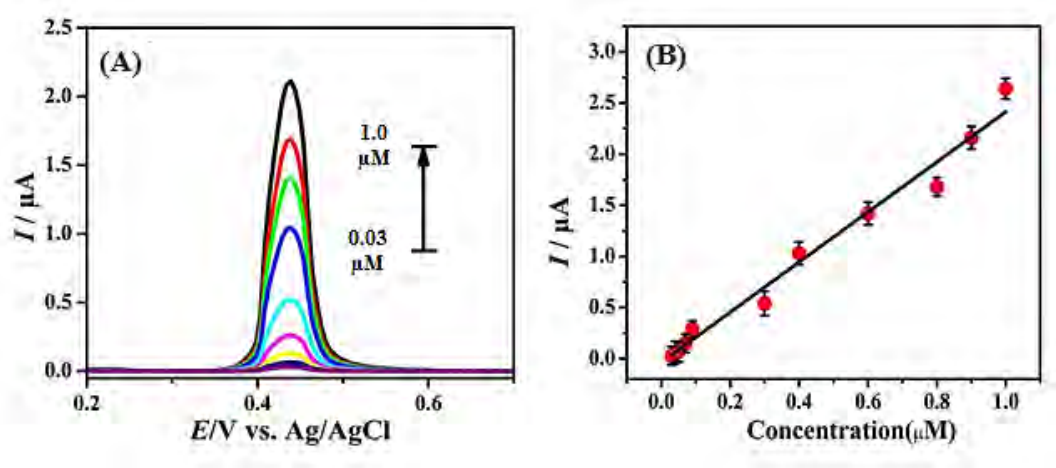

Fig. 3.29. *(A) SWAS voltammograms of INZ at $FeCoSe_2$/GCE in BRB solution (pH 7) under optimized conditions, over the concentration range of 0.03-1 μM. (B) The plot of oxidation current values (I_{pa}) versus INZ concentrations shown in the calibration curve.*

3.3.4 Precision and reliability assessment of $FeCoSe_2$/GCE for the detection of isoniazid

In order to verify the credibility of the proposed method, the precision of the $FeCoSe_2$/GCE was assessed. The intra-day precision was evaluated by conducting three measurements within a single day, and computing the %RSD, which was found to be 2.22%. Additionally, the inter-day precision was assessed by conducting three measurements on different days, resulting in a %RSD of 0.56%. In addition, the %RSD for isoniazid detection was within the acceptable range of less than 5%, as shown in Fig. 3.30. These results demonstrate the high precision of the $FeCoSe_2$/GCE and indicate its suitability for the accurate and reliable detection of INZ.

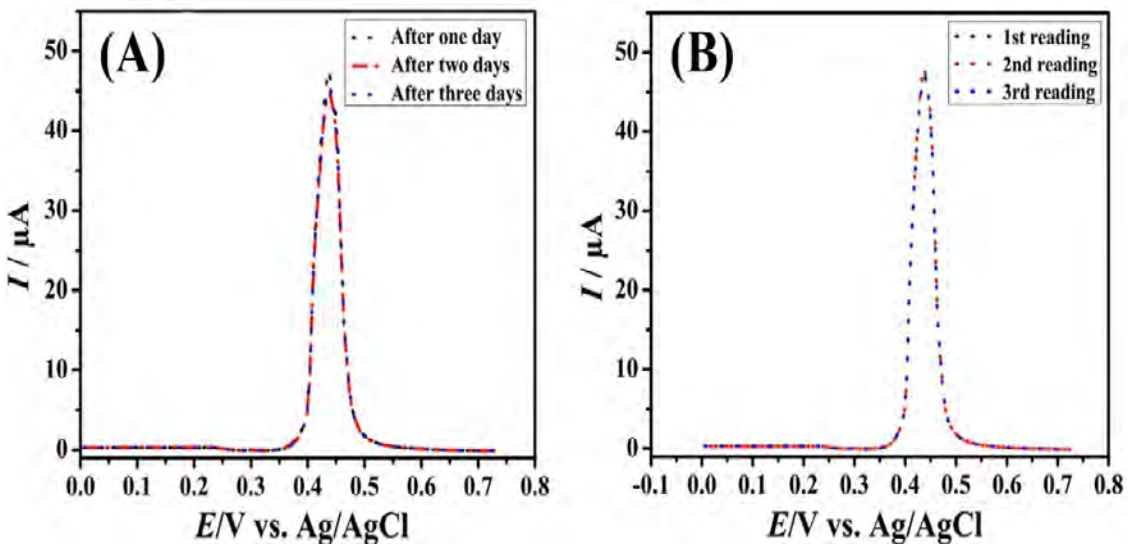

Fig. 3.30. *Results showed that the developed sensor showed good stability and reproducibility along with (A) an intra-day precision of 2.22% and, (B) inter-day precision of 0.56%.*

3.3.5 Interference Study

Fig. 3.31 demonstrates the effectiveness of the proposed method by conducting interference experiments to evaluate the impact of common interferences that may be present in biological samples. The results indicate that there was minimal interference in the anodic peak current response of INZ even at excess of 500-folds of the Ca^{2+}, NH^{4+}, Mg^{2+}, glucose, and excess of 200-folds of uric acid and ascorbic acid, with an RSD of only 1.59%. This indicates that the $FeCoSe_2$/GCE has excellent anti-jamming properties. Furthermore, the outcomes suggest that the suggested method has the potential to be an efficient and reliable approach for accurately detecting INZ in complex biological samples due to its remarkable sensitivity, and selectivity. Table 3.8 is presented to demonstrate the superiority of the proposed method in comparison to previously reported modified electrodes for the INZ detection.

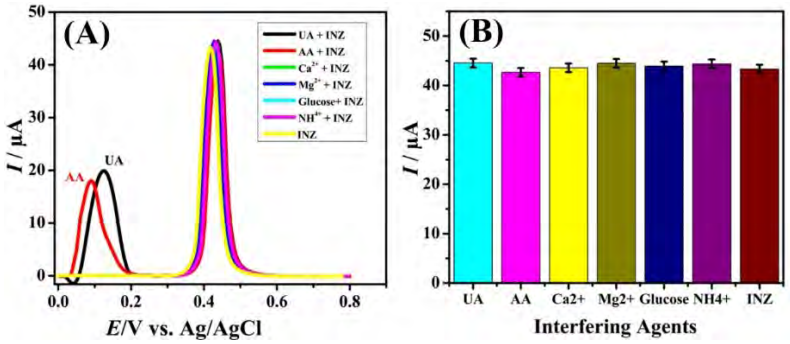

Fig. 3.31. *(A) Interference measurements of 25 µM INZ solution at $FeCoSe_2$/GCE in BRB (pH 7) with various co-existing species using SWASV and (B) Bar graph comparing the impact of interfering species on INZ detection.*

The validity of prosed sensor for real sample analysis was also investigated by detection of INZ in pharmaceutical formulation. The concentration of INZ in the pharmaceutical formulations was determined from the calibration curves. The quantified sample values are found to be in close agreement with the claimed amounts as summarized in Table 3.7. Thus the proposed method is found promising for the direct determination of INZ from pharmaceutical samples.

Table 3.7. *Real sample analysis in Pharmaceutical Formulation*

Samples	Labeled Claim (mg)	Amount Found (mg)	%RSD (n=3)
Tablets Solonex	50	49.90	0.21
	100	99.30	0.34
	300	299.80	0.25

Table 3.8. *Compare our proposed modified GCE's analytical parameters for detecting isoniazid with previously reported methods, highlighting its superior performance.*

Electrodes Used	Techniques Used	Linear range(µM)	LOD	Ref.
Ag-P(MMA-co-AMPS)ESP	AMP	0.05 – 150	10 nM	[235]
GO-PAG-GCE	DPV	20 – 1400	2.59 µM	[236]
Cu-GO-GCE	AMP	0.1 – 500	23.4 nM	[237]
SPCE-PH-electrode	DPV	0.5 – 110	17 µM	[238]
MWCPE	DPV	1 – 1000	0.5 µM	[239]
PdNPs-CILE	CV	5 – 100	0.47 µM	[240]
ERGO-GCE	LSV	2 – 70	0.17 µM	[241]
RGO–Au/GCE	DPV	0.1 – 1000	0.01 µM	[242]
CoTRP(dcbpy)$_2$]-Ni-GO	BIA	100 – 1000	3.5 µM	[243]
$FeCoSe_2$/GCE	SWASV	0.03 – 1	0.12 nM	This work

3.3.6 Real Sample Analysis of $FeCoSe_2$/GCE for Isoniazid Detection

To assess the real-world utility of $FeCoSe_2$/GCE, SWASV technique was employed to measure the presence of the drug INZ in physiological fluids, specifically human serum

and urine samples. By using standard addition methods, INZ was spiked to biological fluid samples to investigate the drug's metabolic behavior. Prior to analysis, samples were diluted 15 times with pH 7 BRB to ensure accuracy. Each sample was examined three times (n=3) to verify reproducibility. The reliability of $FeCoSe_2$/GCE in detecting INZ in biological fluids was confirmed by the low value of RSD of 2.5%, and 3.4% for the urine and human serum samples, correspondingly. These values were obtained during the recovery analysis of spiked INZ samples using $FeCoSe_2$/GCE. The results of the sample analyses are presented in Table 3.9. The aim of the study is to detect the drug INZ in physiological fluids and understand its behavior in biological systems. The drugs detection in the biological fluids is very essential step in pharmacokinetic studies, which involves the investigation of the absorption, distribution, metabolism, and excretion of drugs in the body. Accurate detection of drugs in biological fluids is essential for determining the appropriate dosage and frequency of drug administration, identifying potential drug interactions, and assessing the risk of side effects.

Table 3.9. *$FeCoSe_2$/GCE Application for INZ Detection in Biological Samples*

Samples	Analyte	INZ added (µM)	INZ Found (µM)	Recovery (%)	%RSD (n=3)
Urine	INZ.	5.00	4.95	98.82	2.51
Human serum	INZ.	2.00	1.95	98.01	3.40

3.4 Sensor 4: Co-Pd@Al_2O_3/GCE for venlafaxine detection

Modification of electrodes with nanoparticles is a promising approach to enhance the electrochemical sensing of transducer. As a result, it is becoming increasingly popular in various electroanalytical sensing applications. Nanoparticles modification of electrode surface is advantageous for electrocatalytic role. Hence, with this consideration, enhancement in the electrochemical detection signal of venlafaxine was tried by modifying GCE with the synthesized bimetallic Co-Pd@Al_2O_3 NPs. The designed platform was used

for detecting venlafaxine in human serum samples. The sensor showed superior venlafaxine detection performance as demonstrated by the experimental results discussed in onward sections.

3.4.1 Structural and morphological characterization

The AAS analysis of Co-Pd@Al_2O_3 revealed matching concentrations of metals with the theoretical metal loadings of the catalyst. Fig. 3.32(A) presents the results of EDX analysis conducted to confirm the elemental composition of the prepared catalyst. The EDX analysis showed that the composition of the catalyst contained Co, Pd, O, and Al in concentrations of 13.34 wt%, 4.74 wt%, 47.97 wt%, and 33.95 wt%, respectively. These results are consistent with the concentrations obtained from AAS analysis.

SEM analysis was conducted to study the surface morphology of the Co-Pd@Al_2O_3. The results shown in Fig. 3.32(B) demonstrate the presence of spherical Co-Pd alloy nanoparticles that are evenly distributed on the surface of alumina. The sizes of the nanoparticles are in the range from 45-85 nm. EDX mapping shown in Fig. 3.32(C) further supports the even distribution of the metal nanoparticles over the alumina support.

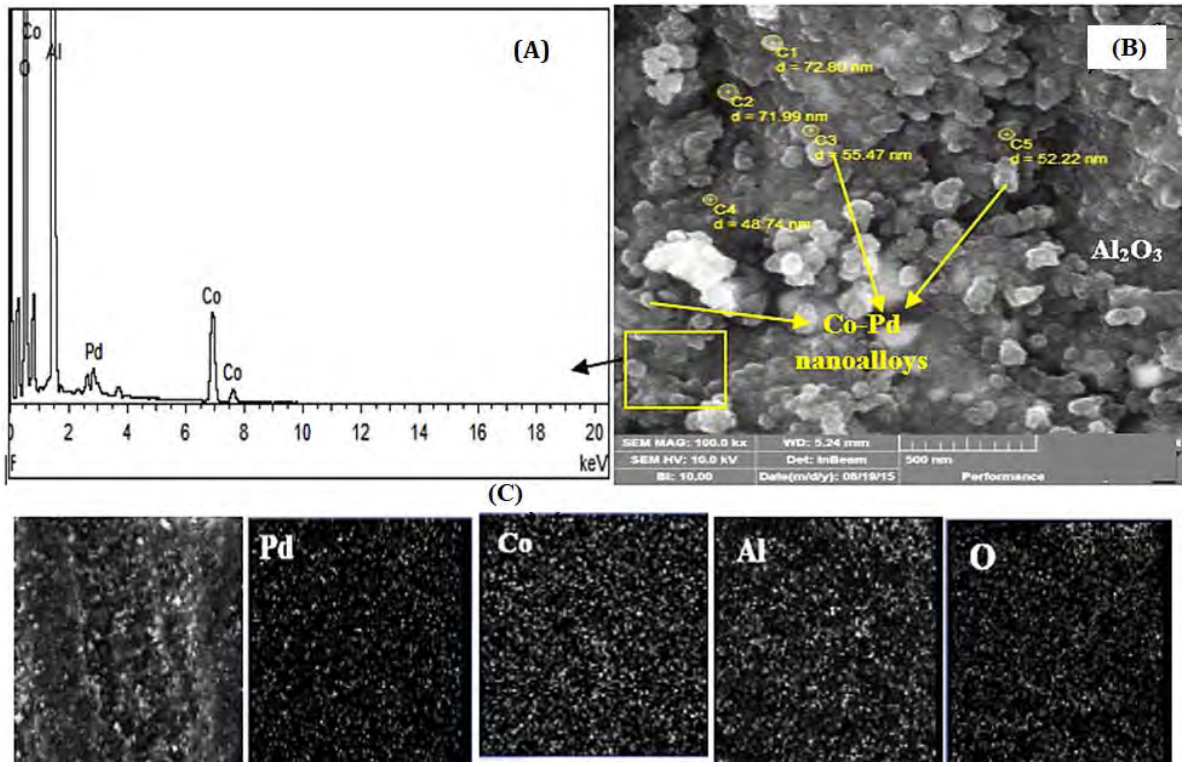

Fig. 3.32. *The synthesized Co-Pd@Al_2O_3, with (A) EDX spectrum, (B) SEM micrograph, and (C) EDX elemental mapping.*

The crystalline properties of the bimetallic catalyst were analyzed using XRD analysis. The XRD pattern in Fig. 3.33 reveals prominent peaks at 37.3°, 45.7°, and 67.1°, which correspond to the (311), (400), and (440) hkl respectively, providing information about the crystalline properties of the bimetallic catalyst. These values correspond to the standard pattern of Al_2O_3 (ICDD card no. 00-001-1303), which exhibits a cubic crystal structure, thus confirming the crystalline nature of the synthesized bimetallic catalyst. In addition, the XRD analysis revealed two broad peaks at 32.9° and 59.6° corresponding to the standard pattern of Co (JCPDS:15-0806) with hkl values of (210) and (411), respectively, that confirms the presence of Co in the bimetallic catalyst. Furthermore, the XRD analysis also revealed small peaks at 39.2° and 55.7°, which match the reference card for Pd metal (JCPDS: 46-1043) with hkl planes of (111) and (200, indicating the presence of Pd in the bimetallic catalyst. Using the Debye-Scherrer formula, which relates the peak broadening in radians to crystal size, X-ray wavelength, and angle of diffraction, the average size of the Co-Pd alloy nanoparticles in the bimetallic catalyst was estimated to be

18 nm. The broad diffraction peaks observed in the XRD pattern of the bimetallic catalyst indicate that the size of the nanoparticles is relatively small. The small average crystallite size of 18 nm observed in the XRD pattern also suggests that the Co-Pd@Al_2O_3 catalyst consists of nanoscale particles. This nanoscale nature is desirable for many applications, as it often results in improved in higher surface area, increased reactivity and enhanced catalytic performance. However, the ideal crystallite size depends on the specific application and the properties desired for the material. Nanoparticles offer a higher surface area-to-volume ratio, which facilitates a more efficient interaction between the electrode and analyte, leading to improved detection efficiency and sensitivity. In fact the use of 18 nm Co-Pd@Al_2O_3 nanoparticles for electrode modification led to successful detection of venlafaxine.

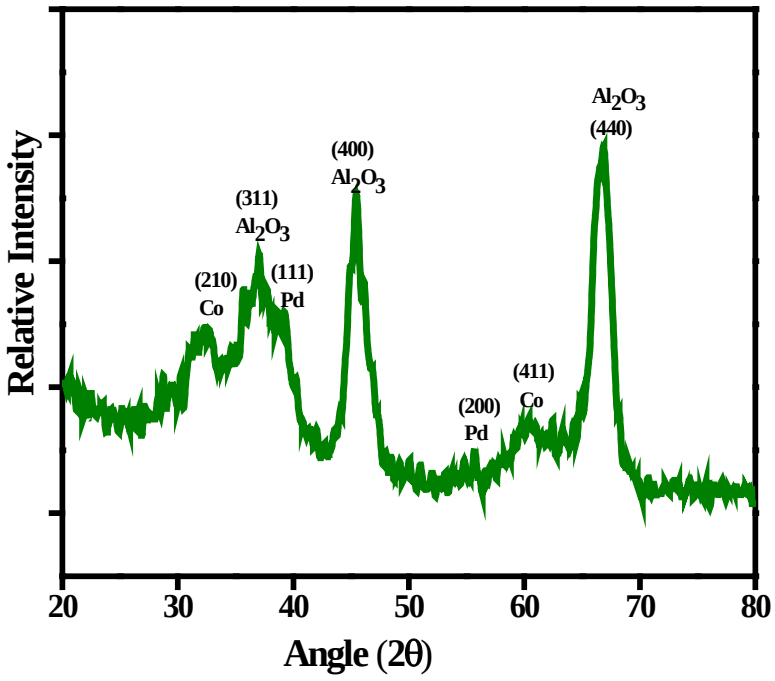

Fig. 3.33. *The X-ray diffraction (XRD) pattern of the bimetallic Co-Pd@Al_2O_3 nanoalloy catalyst.*

The analysis of surface area of the Co-Pd@Al_2O_3 catalyst is important as it directly affects the number of active sites that are available for catalytic reactions. The BET surface area analysis was carried out to determine the active sites available for catalytic reactions of the Co-Pd@Al_2O_3. The obtained BET surface area of 112 m^2/g is lower than that of pure Al_2O_3 (205 m^2 /g). The decrease in surface area can be attributed to the filling of pores with metal particles and the sintering process, which causes the metal particles on the surface of the alumina support to fuse together as shown in Fig. 3.34(B). The surface area analysis can also provide information about the mesoporous nature of the catalyst, which is important for electrode modification. Overall, the surface area analysis of the Co-Pd@Al_2O_3 catalyst can provide important information about its porosity, surface activity, and mesoporous structure, which are all important factors for electrode modification and catalytic performance [244]. The Co-Pd@Al_2O_3 catalyst displayed a type IV hysteresis loop in the adsorption-desorption isotherms as depicted in Fig. 3.34(A), which indicates the presence of mesopores and suggests that the catalyst has a relatively narrow pore size distribution. This is consistent with the TEM analysis which showed the presence of well-dispersed spherical nanoparticles of 45 to 85 nm in size. The presence of mesopores in the catalyst structure allows for greater surface area and pore volume, promoting the diffusion of reactants and products, and ultimately leading to enhanced catalytic activity.

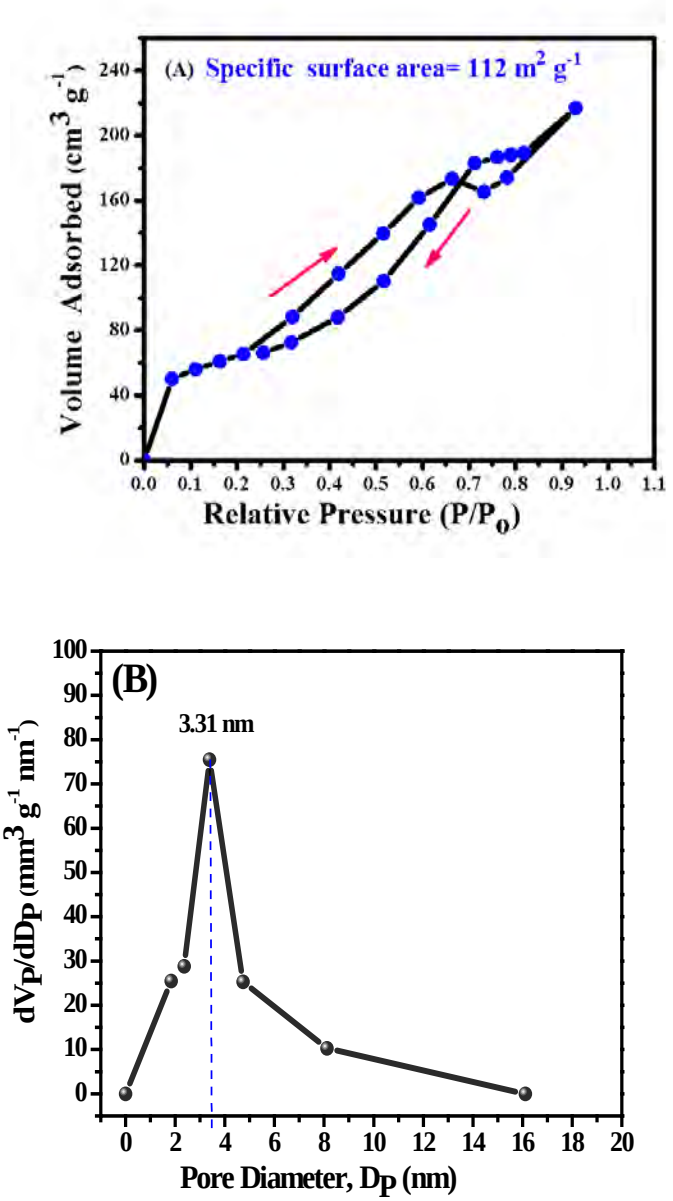

Fig. 3.34. *(A) The N_2 adsorption-desorption isotherm of the Co-Pd@Al_2O_3 catalyst, (B) The corresponding pore size distribution of the Co-Pd@Al_2O_3 catalyst.*

The study aimed to investigate the physical and chemical properties of the Co-Pd@Al_2O_3 catalyst, including its surface area, crystal structure, metal loading, and reducibility, in order to probe its potential for use as electrode modifier in electrochemical analysis of VEN. The reduction behavior of metal alloy nanoparticles in bimetallic systems

was investigated through the TPR profile of Co-Pd@Al_2O_3. As shown in Fig. 3.35, the introduction of Pd metal to the Co-Al_2O_3 monometallic catalyst shifted the reduction peaks to a lower temperature range, suggesting improvement in reducibility and catalytic activity. The combination of Pd and Co metals in bimetallic systems leads to improved metal dispersion and smaller particle size, which are envisioned to contribute to enhanced catalytic activity.

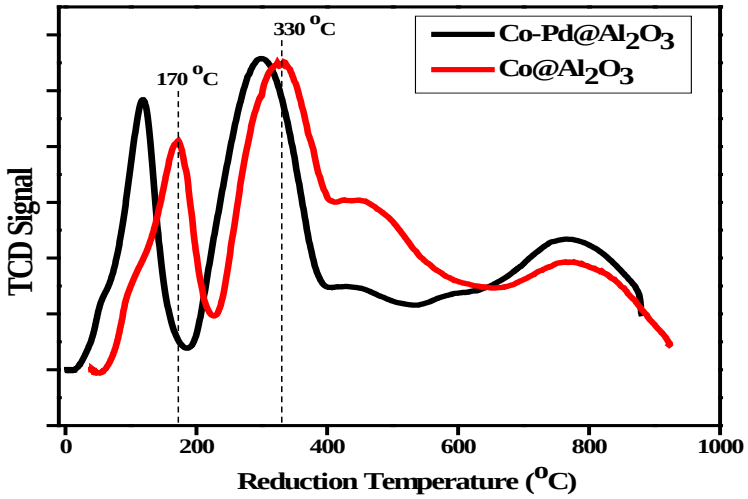

***Fig. 3.35**. The TPR (Temperature Programmed Reduction) profiles of the prepared catalysts.*

3.4.2 Charge transport behavior of GCE modified with Co-Pd@Al_2O_3

Electrochemical impedance spectroscopy was employed to assess the electron transfer efficiency of the GCE modified with Co-Pd@Al_2O_3. A solution of potassium ferricyanide with a concentration of 5.0 mM in a 1.0 M potassium chloride solution was used for the EIS analysis. The EIS results are illustrated in Fig. 3.36, where the Nyquist plots are presented with the Randles circuit as inset. The impedance spectrum was characterized by the electrolyte resistance, charge transfer resistance and the Warburg impedance. At high frequency, diameter of the semicircular portion of the impedance spectrum indicates charge transfer process at the electrode-electrolyte interface. On the other hand, diffusional processes can be associated at a lower frequency with the linear part. EIS data revealed that the R_{ct} values for the unmodified-GCE and Co-Pd@Al_2O_3/GCE are 6.41 kΩ and 3.33 kΩ,

respectively. The results indicate that the Co-Pd@Al_2O_3/ GCE exhibits enhanced charge transfer efficiency as compared to the unmodified-GCE [245,246].

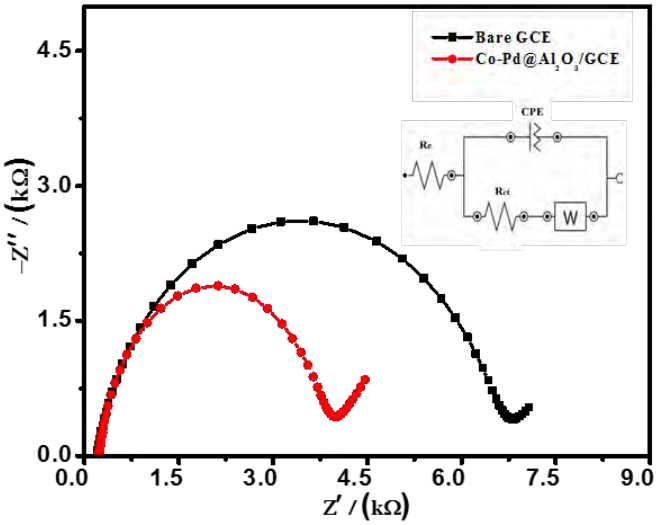

Fig. 3.36. *Nyquist plots compared between bare GCE and Co-Pd@Al_2O_3/GCE using potassium ferricyanide (5 mM) and 1.0 M KCl as the redox probe.*

CV was conducted using 1.0 M KCl containing 5.0 mM $K_3[Fe(CN)_6]$ to investigate the electron transfer process of the redox probe through Co-Pd@Al_2O_3/GCE. The resulting cyclic voltammograms showed a reversible redox behavior, with Co-Pd@Al_2O_3/GCE displaying faster electron transfer compared than bare-GCE. The Randles-Sevcik equation confirmed greater surface area and conductivity of Co-Pd@Al_2O_3/GCE, resulting in a 2-fold increase in electrochemical active surface area and current intensity of the signals of the redox probe (0.02 cm^2 for bare-GCE and 0.04 cm^2 for Co-Pd@Al_2O_3/ GCE).

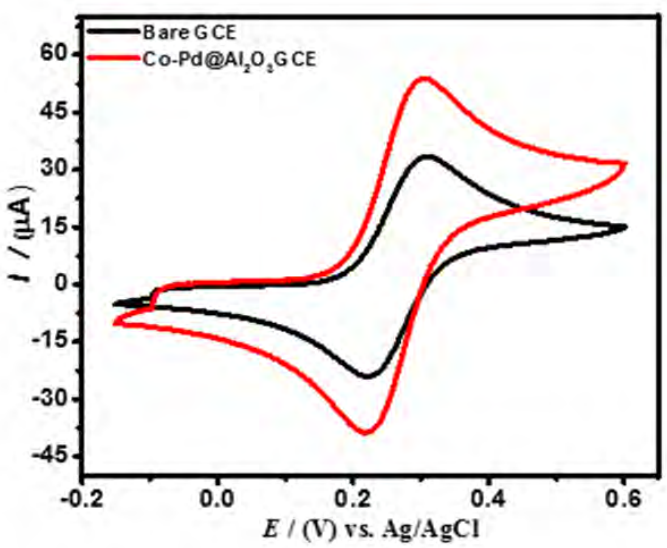

Fig. 3.37*. The electrochemical response of bare-GCE and Co-Pd@Al_2O_3/GCE probed using CV in a solution of $K_3[Fe(CN)_6]$ (5 mM) and KCl (0.1 M).*

3.4.3 SWASV for analyzing VEN via Co-Pd@Al_2O_3/GCE

Fig. 3.38 shows the results of SWASV performed of the electro-oxidation behavior of VEN. The Co-Pd@Al_2O_3/GCE demonstrated a notably higher current response compared to bare GCE for the electro-oxidation of VEN. The intense peak observed at Co-Pd@Al_2O_3/GCE can be attributed to its superior conductivity and electrocatalytic activity towards oxidation of VEN. These findings indicate that Co-Pd@Al_2O_3/GCE is an efficient platform for the voltammetric determination of VEN.

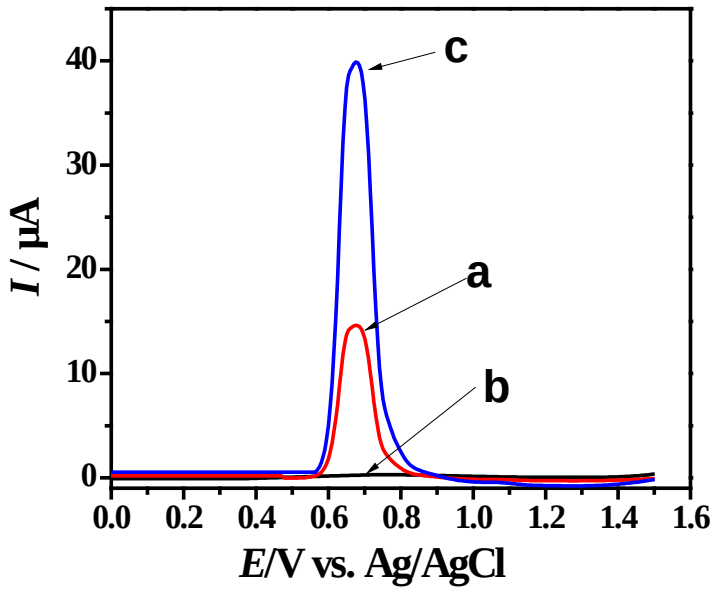

Fig. 3.38. *SWASV analysis of VEN was performed in three scenarios: (a) 2 µM VEN at bare-GCE, (b) Co-Pd@Al_2O_3/GCE in blank solution, and (c) Co-Pd@Al_2O_3/GCE in 2 µM VEN with pH 7 BRB solution. The SWASV measurements were conducted at a scan rate of 50 mV/s, with a deposition potential of –0.5 V, and a deposition time of 60 seconds.*

3.4.4. Optimization of the experimental parameters

3.4.4.1. Impact of electrolyte and pH on the signal of analyte

The electro-oxidation response of VEN was probed in a number of electrolyte solutions such as BRB, acetate, and phosphate buffer solutions. Results showed that BRB is more suitable as much enhanced current response and distinct electrooxidation peaks of VEN appeared in this medium. Furthermore, The impact of pH on the VEN oxidation current response using Co-Pd@Al_2O_3/GCE was examined across a pH range of 6-11. The best current response was observed at pH 7 as obvious from observation of Fig. 3.39(A).

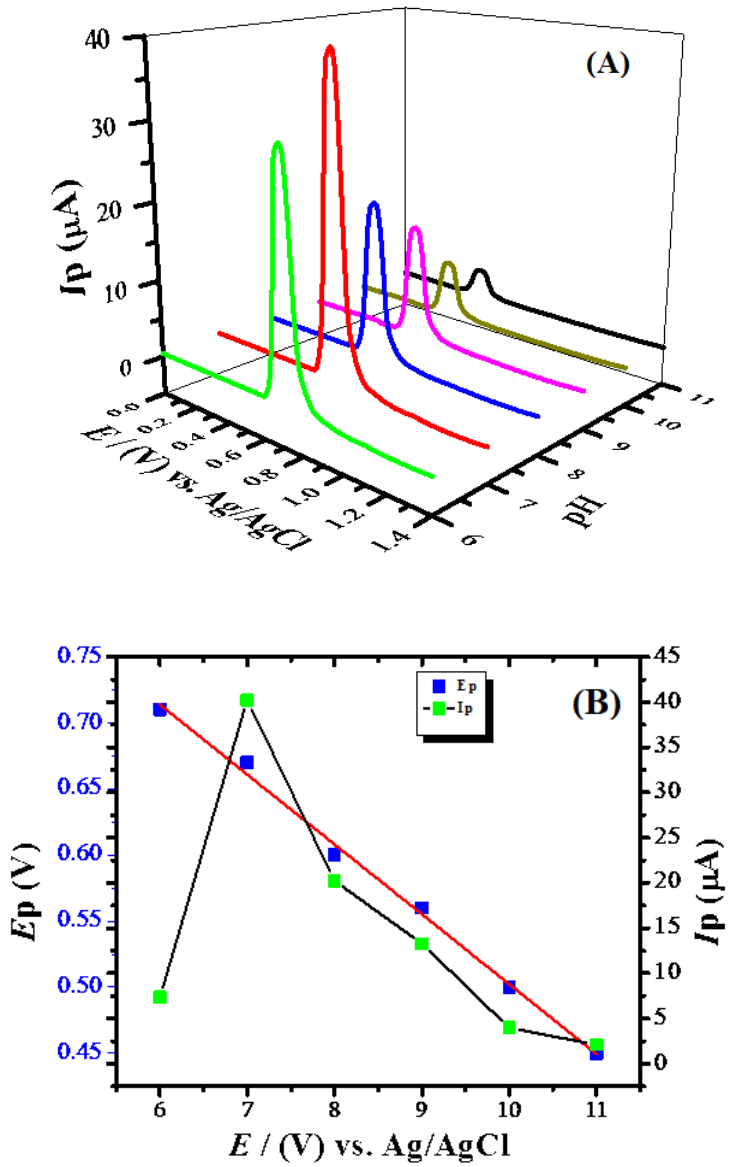

Fig. 3.39. *(A) Square Wave Voltammograms of a 2 µM VEN solution under varying pH conditions keeping all other optimum conditions (B) The Linear plot among the peak-potential and pH of the medium.*

Fig. 3.39(B) illustrates that as the pH increases, the peak potential shifts towards a more negative value. The observed shift in the optimal pH for the oxidation signal of VEN using Co-Pd@ Al_2O_3/GCE can be explained by considering the protonation state of acidic and basic functional groups during the VEN oxidation process. The oxidation process of

VEN involves two protons and two electrons as obvious from the Nernstian slope of the linear relationship of peak potential and pH as shown in Fig. 3.39(C). Using the half peak width value for electrons involvement and Ep / mV = E^0 – (59m/n) pH, it was estimated that two protons are involved along with the transfer of two electrons [247]. These findings helped in proposing oxidation mechanism of VEN as shown in Scheme 3

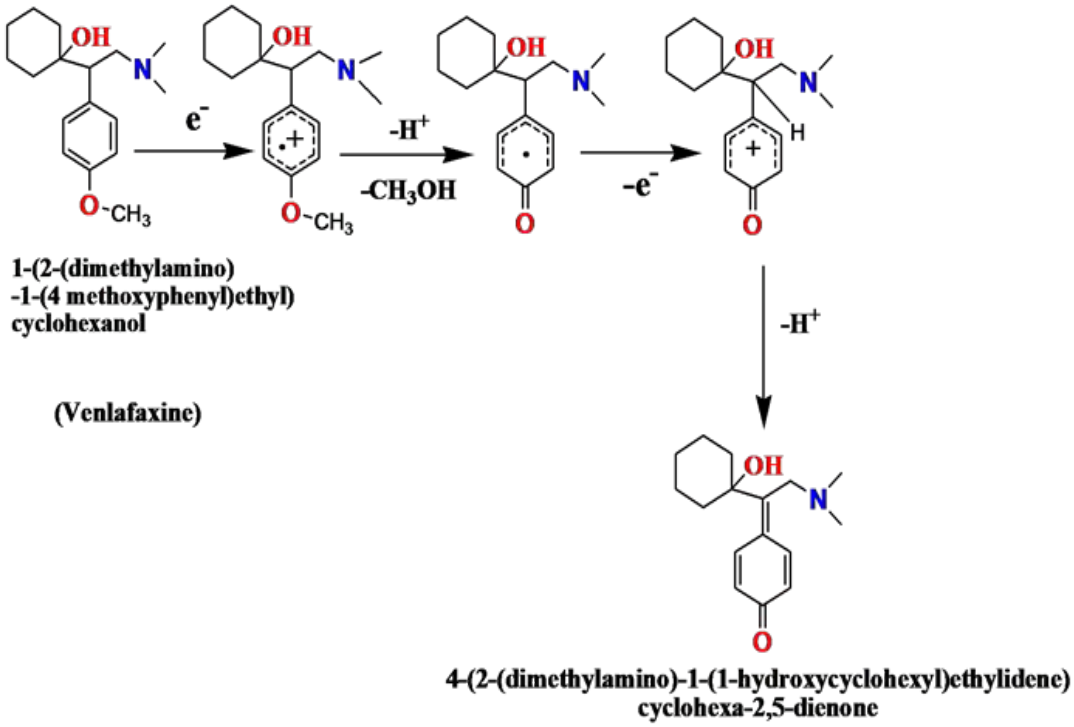

Scheme 3. *A possible mechanism proposed for electro- oxidation of VEN using Co-Pd@Al_2O_3/GCE.*

3.4.4.2 Effect of deposition potential and time on analyte analysis

In order to study the adsorption mechanism of VEN on the electrode surface, the impact of various deposition potentials and deposition times were probed using SWASV at an initial concentration of 2 µM VEN. The findings indicated that the highest peak current was achieved at deposition potential and deposition time of –0.5 V and 60 s as depicted in Fig. 3.40. Consequently, all further electroanalytical experiments of VEN were conducted under these optimized conditions.

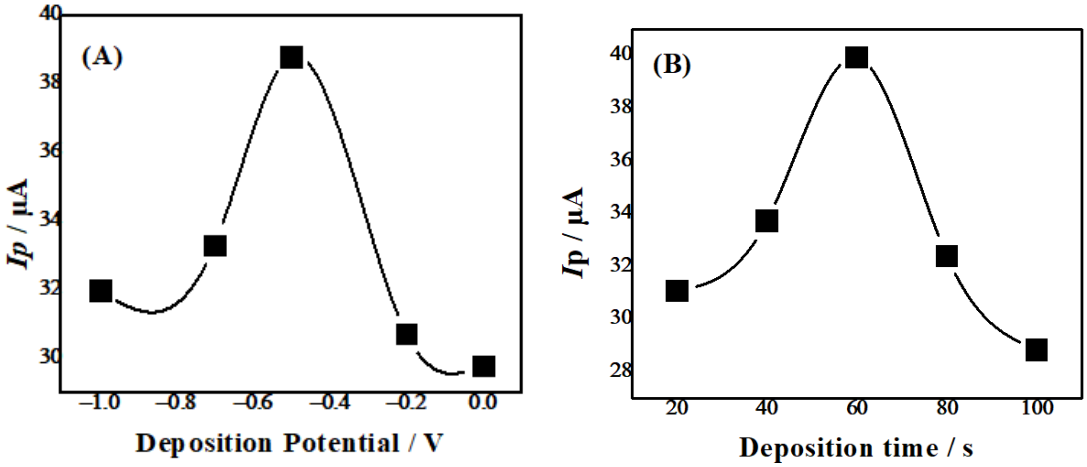

Fig. 3.40*. (A) Deposition potential's influence on VEN oxidation 2 µM INZ with constant deposition time (60 s) using SWASV. (B) Impact of accumulation time on oxidation of INZ (2 µM) at Co-Pd@Al_2O_3/GCE with fixed accumulation potential (–0.5 V) using SWASV.*

3.4.5. Application of Co-Pd@Al_2O_3/GCE for VEN analysis

The electrochemical detection of VEN at various concentrations was carried out at Co-Pd@ Al_2O_3/GCE using SWASV. Fig. 3.41 displays the voltammograms acquired for various VEN concentrations. The calibration curve of VEN in 0.5 µM-1.95 nM concentration range shown in the inset of Fig. 3.41 was used to determine the LOD. The current values (n = 11) of the blank solution at the peak position of VEN were used to compute the standard deviation [248]. Based on the analysis, the LOD was found to be 1.86 pM..

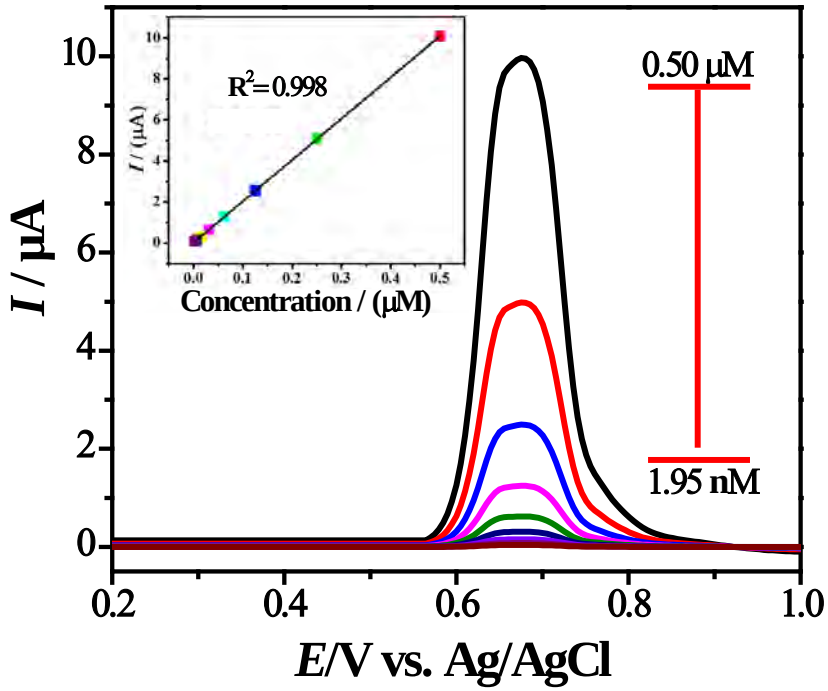

Fig. 3.41. *SWASV of VEN at Pd@Al_2O_3/GCE showed linear response in the concentration range of 1.95 nM - 0.5 µM. The inset graph illustrates a direct correlation between concentration of VEN and peak current (I_{pa}), using optimum parameters (BRB solution of pH 7the scan rate of 50 mV/s, accumulation potential and time of –0.5 V, 60 s respectively)*

Table 3.10 compares the VEN detection performance of Co-Pd@ Al_2O_3/GCE with other reported modified electrodes. The results suggest that Co-Pd@ Al_2O_3/GCE is more sensitive which could be attributed to its unique design and improved material properties compared to the other electrodes reported in literature. Therefore, the proposed sensor is a suitable platform for detecting VEN.

***Table 3.10**. Comparison of VEN detection by Co-Pd@Al_2O_3/GCE with reported sensors.*

Electrodes Used	Linear Range (µM)	LOD (µM)	Ref.
NAF-CNT-GCE	0.04 - 62.2	0.012	[249]
Mercury-film-microelectrode	1.3 - 24.3	0.69	[250]
Fe_3O_4@CNC-Cu-GSPE	0.05 – 600	0.01	[251]
La^{3+}/Co_3O_4-nanocubes-SPE	1 – 500	0.5	[252]
MWCNT-RTIL-GCE	2 – 2000	1.69	[253]
Eu^{3+} doped NiO-CPE	0.04 – 300	0.01	[254]
Gd_2O_3-SPE	5 – 900	0.21	[139]
Co-Pd@Al_2O_3/GCE	1.95 nM - 0.5 µM	1.86 pM	This work

3.4.6 Testing reproducibility, repeatability and stability of Co-Pd@Al_2O_3/GCE

The Co-Pd@ Al_2O_3/GCE was examined for its repeatability, reproducibility and stability. Five consecutive measurements were conducted on this electrode and the resulting %RSD values less than 1% demonstrated its repeatability. Moreover, four separately fabricated electrodes were employed to detect 0.5 µM VEN, and matching of the peak heights with %RSD below 5% indicated acceptable reproducibility. To evaluate the stability of the electrode, it was used to detect VEN after 3, 6, and 9 days, and the RSD with less than 5%, demonstrated stability up to this much time. Thus, the reliability and stability of Co-Pd@ Al_2O_3/GCE point to its promising applicability for voltammetric determination of VEN.

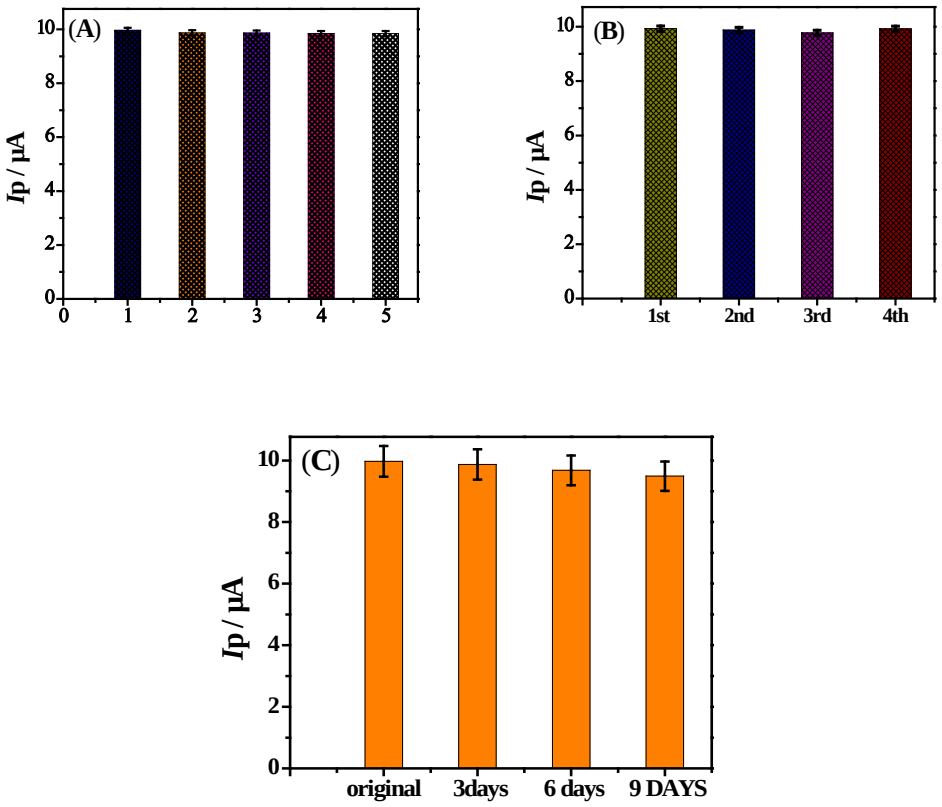

Fig. 3.42. *Current responses for evaluating, (A) Repeatability, (B) Fabrication reproducibility, and (C) Stability of the* Co-Pd@ Al_2O_3/GCE.

3.4.7 Interference effects on the performance of Co-Pd@Al_2O_3/GCE

To assess the selectivity of Co-Pd@Al_2O_3/ GCE for the detection of VEN in the presence of potential interfering substances typically found in human plasma and pharmaceutical samples, various interfering species were tested. Interference study showed high selectivity of Co-Pd@Al_2O_3/GCE for VEN detection. A 100-fold excess of common interfering substances including citric acid, ascorbic acid, glucose, uric acid, and sucrose, did not significantly affect the oxidation peak current of 0.5 µM VEN under optimized conditions. The maximum concentration of each interfering substance that resulted in a %RSD of less than 5% was defined as the tolerance limit. These results indicate the excellent interference tolerance of the proposed electrode. Moreover, the Co-Pd@Al_2O_3/GCE electrode exhibited high selectivity for determination of VEN in biological fluids, with excellent recoveries ranging from 95-99%.

For the assessment of the practical application of the designed sensor, it was subjected to VEN detection in serum samples. The proposed method entails determining the VEN concentration in a solution by spiking a known amount of VEN into a biological fluid sample, followed by measuring the percentage of VEN recovered through a direct calibration approach. The obtained percentage recovery results of VEN in biological fluid samples using the Co-Pd@Al_2O_3/GCE under optimized conditions are presented in Table 3.11. Recovery results suggest practical applicability of the designed platform for VEN detection in biological fluids.

Table 3.11. *Selectivity of Co-Pd@Al_2O_3/GCE for VEN determination in solution containing common coexisting species.*

Interferents	VEN : Interfering Species	%Recovery ± RSD[a]
Citric Acid	1: 50	98.7% ± 0.45
	1: 100	99.0% ± 0.57
Glucose	1: 50	98.1% ± 0.39
	1: 100	98.3% ± 0.35
Ascorbic Acid	1: 50	97.1% ± 0.48
	1: 100	98.0% ± 0.43
Sucrose	1: 50	97.9% ± 0.46
	1: 100	98.1% ± 0.43
Uric Acid	1: 50	98.2% ± 0.49
	1: 100	98.7% ± 0.45

a : average of three readings

Table 3.12. *Evaluation of VEN recovery in serum samples using Co-Pd@Al_2O_3/GCE.*

Samples	No VEN Added	Amount Added (µM)	Amount Found (µM)	%Recovery ± RSD
1. Sample	-	0.50	0.49	98.0 ± 0.48
2. Sample	-	0.25	0.25	98.4 ± 0.49

Conclusions and outlook

Electrode modifier were prepared, characterized and applied for four different types of electrochemical sensing platforms that detected the target analytes in water and biological samples. BTC/GCE and BPTC/GCE sensors were found suitable for the simultaneous trace level detection of heavy metal ions. While $FeCoSe_2$/GCE and Co-Pd@Al_2O_3 were found sensitive and selective for the detection of isoniazid (INZ) and venlafaxine (VEN) drugs respectively. The synthesized electrode modifiers were structurally and morphologically characterized by SEM, TEM, EDX and XRD analysis. Electrochemical characterization of the designed sensing platforms was performed by EIS, CV and SWASV, which confirmed effective charge transport, enhancement in electrode active surface area and electrocatalytic role of the recognition layer that imparted high sensitivity characteristics through host guest complexation. Results of electrochemical investigations showed that the selected modifiers serve as effective electro-catalysts, leading to enhanced current response as evidenced by the intense signals of multiple HM ions and targeted drugs. For getting further amplified electroanalytical signals, conditions such as scan rate, pH, deposition time, amount of the electrode modifier, accumulation potential and supporting electrolyte were optimized. Under optimized conditions the effective coordination of the recognition layer with the targeted analytes led to much better detection limits. The prepared sensing platforms were found to work even in the presence of various interfering agents. The designed sensors exhibited good repeatability and long-term stability with negligible current variations. Moreover, the sensors showed practical applicability as validated by good percentage recoveries of the real sample analysis.

The BTC/GCE sensor demonstrated well defined and well resolved signals in the stripping SWASV step of the electroreduced metal ions such as Zn^{2+}, Pb^{2+}, As^{3+} and Hg^{2+}. The modified electrode showed improved performance for the targeted metal ions in comparison to unmodified glassy carbon electrode owing to increased surface area and greater conductivity. The voltammograms obtained at the BTC/GCE displayed promising repeatability, sensitivity, selectivity, anti-interference ability and reproducibility. Interestingly the LODs in picomolar range, (the LOD for Zn^{2+}, Pb^{2+}, As^{3+}, and Hg^{2+} calculated are 14.6 pM, 28.8 pM, 71.9 pM and 66.3 pM) of the selected metal ions detected through BTC/GCE are better than their life-threatening levels set by the WHO.

For the second sensor, BPTC was synthesized and used as a recognition layer of the electrochemical scaffold for capturing the signals of Hg^{2+}, Pb^{2+} and Cd^{2+}. The modified-GCE demonstrated good conductivity, sensitivity and selectivity due to its ability of host-guest complexation and consequent preconcentration of the target metal ions at the electrode/electrolyte interface, thus resulting in intense peak currents. The experimental conditions were optimized to obtain linear calibration curves as required for the evaluation of the detection limits. The LODs for Hg^{2+}, Pb^{2+} and Cd^{2+}, were determined to be 25.7 pM, 15.5 pM, and 37.1 pM respectively. BPTC modified GCE demonstrated the qualities of easy fabrication, fast responsiveness and multianalyte sensing without signals overlapping. The optimized procedure and sensor's, effectiveness were further validated by successfully detecting HM ions in two distinct drinking water samples. The obtained results showcased the potential of BPTC/GCE sensor as a reliable and efficient tool for HM ion detection in real water samples.

In the third study, bimetallic cobalt-iron diselenide ($FeCoSe_2$) nanorods were synthesized and characterized by a variety of techniques including SEM, TEM, XRD, TRP and EDX. Their catalytic role was examined by subjecting $FeCoSe_2$/GCE for the electrooxidation of an antituberculosis drug, isoniazid (INZ). The voltammetric signal of INZ at the GCE was six times enhanced by $FeCoSe_2$. Electrochemical results in a wide pH range revealed pH dependent electrooxidation of INZ involving two electrons transfer accompanied with two protons transfer as validated by the half peak width of voltammetric signals and the plot of peak potential as a function of pH of the solution. The $FeCoSe_2$/GCE exhibited wide linearity range for INZ detection and strong resilience towards interfering species. The LOD obtained for INZ detect is calculated to be 0.12 nM. The superior performance of the sensor is attributable to the good electrical conductivity, greater surface area, and impressive catalytic properties of $FeCoSe_2$ nanorods. The developed sensor was also found promising for the detection of INZ in human serum and urine samples.

The fourth sensor was prepared by immobilizing Co-Pd@Al_2O_3 over the surface of carbon based transducer for the sensing of a strong antidepressant, venlafaxine (VEN). Co-Pd@Al_2O_3 was synthesized and characterized structurally and morphologically. EIS, CV and SWASV revealed the electrocatalytic role of Co-Pd@Al_2O_3 for facilitating VEN

electrooxidation. The modified electrode found practically applicable for VEN detection in water and biological fluids. The limit of detection with a value of 1.86 pM revealed much higher sensitivity of Co-Pd@Al_2O_3/GCE for venlafaxine. The voltammograms at the designed nanosensor were found to be reproducible, thus making it suitable for regular electroanalysis and monitoring of venlafaxine.

It can be concluded that electrochemical sensors have great potential and scope for use in environmental and medical fields. Their application horizon can be extended to the investigation of electronic transport in biological molecules and monitoring of metabolites in water, human serum, and urine as required in clinical diagnostics for getting insights into the mechanism of drugs action and their final fate. For the stability of the sensors, the modifiers must remain anchored with the electrode surface and should not leach into the analytes solution. For good sensitivity of the sensor, the modifier should possess host guest complexation ability, for which it must have analyte binding sites or moieties. Electrochemical sensors offer advantages of cost cut off, ease of fabrication and handling, rapid responsiveness and multianalyte detection as signals of different species appear at different potentials. The results of investigations carried out on the designed nanosensors highlight the importance of optimizing experimental conditions such as pH, deposition time, and supporting electrolyte to achieve optimal sensor performance. In summary, the findings of these investigations demonstrate the potential of electrochemical sensors to detect a broad range of analytes in real-world samples with remarkable sensitivity and specificity.

References:

[1] Karimi-Maleh, H., Karimi, F., Alizadeh, M., & Sanati, A. L. (2019). Electrochemical sensors, a bright future in the fabrication of portable kits in analytical systems. *The Chemical Record*, *20*(7), 682–692. https://doi.org/10.1002/tcr.201900092

[2] Namieśnik, J. (2000). Trends in environmental analytics and monitoring. *Critical Reviews in A nalytical C hemistry*, *30*(2-3), 221-269. https://doi.org/10.1080/10408340091164243

[3] Kaya, H. K., Çağlayan, T., & Kuralay, F. (2022). Functionalized nanomaterial-based electrochemical sensors for point-of-care devices. In *Functionalized N anomaterial-Based E lectrochemical Se nsors* (pp. 309-335). Woodhead Publishing. https://doi.org/10.1016/B978-0-12-823788-5.00021-1

[4] Wang, J. (2008). Electrochemical glucose biosensors. *Chemical reviews*, *108*(2), 814-825. https://doi.org/10.1021/cr068123a

[5] Banitaba, S. N., & Ehrmann, A. (2021). Application of electrospun nanofibers for fabrication of versatile and highly efficient electrochemical devices: A review. *Polymers*, *13*(11), 1741.https://doi.org/10.3390/polym13111741

[6] Privett, B. J., Shin, J. H., & Schoenfisch, M. H. (2008). Electrochemical sensors. *Analytical chemistry*, *80*(12), 4499-4517. https://doi.org/10.1021/ac8007219

[7] Bratov, A., Abramova, N., & Ipatov, A. (2010). Recent trends in potentiometric sensor arrays—A review. *Analytica c himica a cta*, *678*(2), 149-159. https://doi.org/10.1016/j.aca.2010.08.035

[8] Pushpanjali, P. A., Manjunatha, J. G., & Hareesha, N. (2021). An overview of recent developments of carbon-based sensors for the analysis of drug molecules. *Journal of Electrochemical Sc ience and Engineering*, *11*(3), 161-177. https://doi.org/10.5599/jese.999

[9] de Lacy Costello, B. P. J., Evans, P., & Ratcliffe, N. M. (1996). Preparation of polypyrrole composites and the effect of volatile amines on their electrical properties. The Analyst, 121(6), 793. Vanamo, U. (2015). Solid-state reference and ion-selective electrodes: towards portable potentiometric sensing. https://urn.fi/URN:ISBN:978-952-12-3190-2

[10] Brandt, I. S., de Araujo, C. I. L., Stenger, V., Delatorre, R. G., & Pasa, A. A. (2008). Electrical characterization of Cu/Cu_2O electrodeposited contacts. *ECS Transactions*, *14*(1), 413. https://doi.org/10.1149/1.2956056

[11] Vyskočil, V., & Barek, J. (2009). Mercury electrodes–possibilities and limitations in environmental electroanalysis. *Critical Reviews in Analytical Chemistry*, *39*(3), 173-188. https://doi.org/10.1080/10408340903011820

[12] Mele, G., Del Sole, R., & Lü, X. (2021). Applications of TiO_2 in sensor devices. In *Titanium Dioxide (Tio₂) and Its Applications* (pp. 527-581). Elsevier. https://doi.org/10.1016/B978-0-12-819960-2.00004-3

[13] Corb, I., Manea, F., Radovan, C., Pop, A., Burtica, G., Malchev, P., ... & Schoonman, J. (2007). Carbon-based composite electrodes: preparation, characterization and application in electroanalysis. Sensors, 7(11), 2626-2635.https://doi.org/10.3390/s7112626

[14] Edwards, G. A., Bergren, A. J., & Porter, M. D. (2007). Chemically modified electrodes. In *Handbook of e lectrochemistry* (pp. 295-327). Elsevier..https://doi.org/10.1016/B978-044451958-0.50021-5

[15] Vashist, S. K., Zheng, D., Al-Rubeaan, K., Luong, J. H., & Sheu, F. S. (2011). Advances in carbon nanotube based electrochemical sensors for bioanalytical applications. *Biotechnology adv ances*, *29*(2), 169-188. https://doi.org/10.1016/j.biotechadv.2010.10.002

[16] Nisar, A., Shah, A., Zahid, A., Iftikhar, F. J., Hassan, A., Shah, A. H., ... & Kraatz, H. B. (2018). Sensitive and selective detection of multiple metal ions using amino acids modified glassy carbon electrodes. *Journal of t he E lectrochemical Soc iety*, *165*(3), B67.https://doi.org/10.1149/2.0151803jes

[17] Ali, H., Khan, E., & Ilahi, I. (2019). Environmental chemistry and ecotoxicology of hazardous heavy metals: environmental persistence, toxicity, and bioaccumulation. *Journal of chemistry, 2019*. https://doi.org/10.1155/2019/6730305

[18] Waheed, A., & Ullah, N. (2018). Nanomaterials-based electrochemical detection of heavy metals in water: current status, challenges and future direction. *Trends i n Analytical Chemistry, 105,* 37–51. https://doi.org/10.1016/j.trac.2018.04.012

[19] Fay, R. M., & Mumtaz, M. M. (1996). Development of a priority list of chemical mixtures occurring at 1188 hazardous waste sites, using the HazDat database. *Food and c hemical t oxicology*, *34*(11-12), 1163-1165.https://doi.org/10.1016/S0278-6915(97)00090-2

[20] Spiegel, H., 2002. Trace element accumulation in selected bioindicators exposed to emissions along the industrial facilities of Danube Lowland. *Turkish Journal of Chemistry, 26(6),* pp.815-824.https://journals.tubitak.gov.tr/cgi/viewcontent.cgi?article=2841&context=chem

[21] Rahman, Z., & Singh, V. P. (2019). The relative impact of toxic heavy metals (THMs)(arsenic (As), cadmium (Cd), chromium (Cr)(VI), mercury (Hg), and lead (Pb)) on the total environment: an overview. *Environmental m onitoring and assessment*, *191*, 1-21. https://doi.org/10.1007/s10661-019-7528-7

[22] Malik, D. S., & Maurya, P. K. (2015b). Heavy metal concentration in water, sediment, and tissues of fish species (Heteropneustis fossilisandPuntius ticto) from Kali River, India. *Toxicological & E nvironmental C hemistry, 96,* 2014(8), 1–12. https://doi.org/10.1080/02772248.2015.1015296

[23] Okereafor, U., Makhatha, M., Mekuto, L., Uche-Okereafor, N., Sebola, T., & Mavumengwana, V. (2020). Toxic metal implications on agricultural soils, plants, animals, aquatic life and human health. *I nternational j ournal of e nvironmental research and public health, 17(7), 2204.* https://doi.org/10.3390/ijerph17072204

[24] Javed, M., & Usmani, N. (2016). Accumulation of heavy metals and human health risk assessment via the consumption of freshwater fish Mastacembelus armatus inhabiting, thermal power plant effluent loaded canal. *SpringerPlus, 5(1)* https://doi.org/10.1186/s40064-016-2471-3

[25] Siraj, M. S., Khisroon, M., Khan, A., Zaidi, F., Ullah, A., & Rahman, G. (2018). Bio-monitoring of tissue accumulation and genotoxic effect of heavy metals in cyprinus carpio from River Kabul Khyber Pakhtunkhwa Pakistan. *Bulletin of E nvironmental Contamination and Toxicology, 100(3),* 344–349. https://doi.org/10.1007/s00128-017-2265-5

[26] Shah, A., Sultan, S., Zahid, A., Aftab, S., Nisar, J., Nayab, S., Qureshi, R., Khan, G. M., Hussain, H., & Özkan, S. (2017). Highly sensitive and selective electrochemical

sensor for the trace level detection of mercury and cadmium. *Electrochimica Acta, 258,* 1397-1403. https://doi.org/10.1016/j.electacta.2017.12.002

[27] Bukola, D., Zaid, A., Olalekan, E. I., & Falilu, A. (2015). Consequences of anthropogenic activities on fish and the aquatic environment. *Poultry, Fisheries & Wildlife Sciences*, *3*(2), 1-12. https://doi.org/10.4172/2375-446X.1000138

[28] Sabiha-Javied, Mehmood, T., Chaudhry, M. A., Tufail, M., & Irfan, N. (2009). Heavy metal pollution from phosphate rock used for the production of fertilizer in Pakistan. *Microchemical Jo urnal, 91(1),* 94–99. https://doi.org/10.1016/j.microc.2008.08.009

[29] Grzebisz, W. (2011). Magnesium–food and human health. *Journal of Elementology*, *16*(2). https://doi.org/ 10.5601/jelem.2011.16.2.13

[30] Toor, G. S., Haggard, B. E., & Donoghue, A. M. (2007). Water extractable trace elements in poultry litters and granulated products. *The Journal of Applied Poultry Research, 16(3),* 351–360. https://doi.org/10.1093/japr/16.3.351

[31] Azeez, J. O., Adekunle, I., Atiku, O. S., Akande, K., & Jamiu-Azeez, S. (2009). Effect of nine years of animal waste deposition on profile distribution of heavy metals in Abeokuta, south-western Nigeria and its implication for environmental quality. *Waste M anagement, 29(9),* 2582–2586. https://doi.org/10.1016/j.wasman.2009.05.013

[32] Rashid, A., Schutte, B. J., Ulery, A., Deyholos, M. K., Sanogo, S., Lehnhoff, E. A., & Beck, L. (2023). Heavy Metal Contamination in Agricultural Soil: Environmental Pollutants Affecting Crop Health. *Agronomy*, *13*(6), 1521. https://doi.org/10.3390/agronomy13061521

[33] Tian, H., Lu, L., Hao, J., Gao, J. R., Cheng, K. W. E., Liu, K., Qiu, P., & Zhu, C. G. (2013). A review of key hazardous trace elements in chinese coals: abundance, occurrence, behavior during coal combustion and their environmental impacts. *Energy & Fuels, 27(2),* 601–614. https://doi.org/10.1021/ef3017305

[34] Roberts, T. L. (2014). Cadmium and phosphorous fertilizers: the issues and the science. *Procedia en gineering*, *83*, 52-59. https://doi.org/10.1016/j.proeng.2014.09.012

[35] Sharma, R. K., & Agrawal, M. (2005). Biological effects of heavy metals: an overview. *Journal of E nvironmental B iology, 26 (2 Suppl),* 301–313. https://pubmed.ncbi.nlm.nih.gov/16334259/

[36] Ullah, I., Zhao, L., Hai, Y., Fahim, M., Alwayli, D., Wang, X., & Li, H. (2021). Metal elements and pesticides as risk factors for Parkinson's disease-A review. *Toxicology Reports*, *8*, 607-616. https://doi.org/10.1016/j.toxrep.2021.03.009

[37] Hayat, M. T., Nauman, M., Nazir, N., Ali, S., & Bangash, N. (2019). Environmental hazards of cadmium: past, present, and future. In *Cadmium toxicity and tolerance in plants* (pp. 163-183). Academic Press. https://doi.org/10.1016/B978-0-12-814864-8.00007-3

[38] Chen, J., Zhang, B., Zhang, S., Zeng, J., Chen, P., Liu, W., & Wang, X. (2021). A complete atmospheric emission inventory of F, As, Se, Cd, Sb, Hg, Pb, and U from coal-fired power plants in Anhui Province, eastern China. *Environmental Geochemistry and H ealth*, *43*, 1817-1837.https://doi.org/10.1007/s10653-020-00753-6

[39] Dargahi, A., Hasani, K., Mokhtari, S. A., Vosoughi, M., Moradi, M., & Vaziri, Y. (2021). Highly effective degradation of 2, 4-Dichlorophenoxyacetic acid herbicide in a three-dimensional sono-electro-Fenton (3D/SEF) system using powder activated carbon (PAC)/Fe_3O_4 as magnetic particle electrode. *Journal of environmental chemical engineering*, *9*(5), 105889. https://doi.org/10.1016/j.jece.2021.105889

[40] Ščančar, J., Milačič, R., Stražar, M., Burica, O., & Bukovec, P. (2001). Environmentally safe sewage sludge disposal: The impact of liming on the behaviour of Cd, Cr, Cu, Fe, Mn, Ni, Pb, and Zn. *Journal of environmental monitoring*, *3*(2), 226-231.https://doi.org/10.1039/B008948F

[41] Campbell, P. G., & Gailer, J. (2016). Effects of non-essential metal releases on the Environment and human health. *Metal Su stainability: G lobal Challenges, Consequences, and Prospects*, 221-252. https://doi.org/10.1002/9781119009115.ch10

[42] Zoroddu, M. A., Aaseth, J., Crisponi, G., Medici, S., Peana, M., & Nurchi, V. M. (2019). The essential metals for humans: a brief overview. *Journal of i norganic biochemistry*, *195*, 120-129. https://doi.org/10.1016/j.jinorgbio.2019.03.013

[43] Jarup, L. (2003). Hazards of heavy metal contamination. *British Medical Bulletin, 68(1),* 167–182. https://doi.org/10.1093/bmb/ldg032

[44] Appenroth, Klaus-J. (2009). Definition of “Heavy metals” and their role in biological systems. *Soil Biology,* 19–29. https://doi.org/10.1007/978-3-642-02436-8_2

[45] Nowrouzi, M., Mansouri, B., Nabizadeh, S. M., & Pourkhabbaz, A. (2014). Analysis of heavy metals concentration in water and sediment in the Hara biosphere reserve, southern Iran. *Toxicology and I ndustrial H ealth, 30(1),* 64–72. https://doi.org/10.1177/0748233712451767

[46] Jaishankar, M., Tseten, T., Anbalagan, N., Mathew, B. B., & Beeregowda, K. N. (2014b). Toxicity, mechanism and health effects of some heavy metals. *Interdisciplinary Toxicology, 7(2),* 60–72. https://doi.org/10.2478/intox-2014-0009

[47] Flora, G., Gupta, D., & Tiwari, A. (2012). Toxicity of lead: a review with recent updates. *Interdisciplinary T oxicology, 5(2),* 47–58. https://doi.org/10.2478/v10102-012-0009-2

[48] Bowers, T. S., Beck, B. D., & Karam, H. S. (1994). Assessing the relationship between environmental lead concentrations and adult blood lead levels. *Risk Analysis, 14(2),* 183–189. https://doi.org/10.1111/j.1539-6924.1994.tb00043.x

[49] Hughes, M. (2002). Arsenic toxicity and potential mechanisms of action. *Toxicology L etters, 133(1),* 1–16. https://doi.org/10.1016/s0378-4274(02)00084-x

[50] Stohs, S. J., & Bagchi, D. (1995b). Oxidative mechanisms in the toxicity of metal ions. *Free R adical B iology and M edicine, 18(2),* 321–336. https://doi.org/10.1016/0891-5849(94)00159-h

[51] Tchounwou, P. B., Ayensu, W. K., Ninashvili, N., & Sutton, D. J. (2003). Review: Environmental exposure to mercury and its toxicopathologic implications for public health. *Environmental Toxicology, 18(3),* 149–175. https://doi.org/10.1002/tox.10116

[52] Siddiqi, Z. M. (2018). Transport and fate of mercury (Hg) in the environment: need for continuous monitoring. *Handbook of Environmental Materials Management,* 1–20. https://doi.org/10.1007/978-3-319-58538-3_56-1

[53] Toxicological Profile for Chromium. (2002). In CRC Press eBooks. https://doi.org/10.1201/9781420061888_ch63

[54] Flora, S. J. (2015). Arsenic: chemistry, occurrence, and exposure. In *Handbook of arsenic t oxicology* (pp. 1-49). Academic Press. https://doi.org/10.1016/B978-0-12-418688-0.00001-0

[55] Levy, D., Barbarick, K. A., Siemer, E., & Sommers, L. E. (1992). Distribution and partitioning of trace metals in contaminated soils near leadville, colorado. *Journal of Environmental Q uality, 21(2),* 185–195. https://doi.org/10.2134/jeq1992.00472425002100020006x

[56] Wuana, R. A., & Okieimen, F. E. (2011). Heavy metals in contaminated soils: a review of sources, chemistry, risks and best available strategies for remediation. *International Sc holarly R esearch N otices E cology, 2011* , 1–20. https://doi.org/10.5402/2011/402647

[57] Hughes, M. N., & Poole, R. K. (1991). Metal speciation and microbial growth--the hard (and soft) facts. *Journal of G eneral M icrobiology, 137(4),* 725–734. https://doi.org/10.1099/00221287-137-4-725

[58] Sintorini, M. M., Widyatmoko, H., Sinaga, E., & Aliyah, N. (2021). Effect of pH on metal mobility in the soil. *IOP C onference Se ries: E arth and E nvironmental science, 737(1),* 012071. https://doi.org/10.1088/1755-1315/737/1/012071

[59] Li, Q., Wang, Y., Li, Y., Li, L., Mingdeng, T., Lai, D. Y., Chen, L., & Ai, S. (2022). Speciation of heavy metals in soils and their immobilization at micro-scale interfaces among diverse soil components. *Science of t he Total E nvironment, 825,* 153862. https://doi.org/10.1016/j.scitotenv.2022.153862

[60] Balasoiu, C. F., Zagury, G. J., & Deschênes, L. (2001). Partitioning and speciation of chromium, copper, and arsenic in CCA-contaminated soils: influence of soil composition. *Science o f the T otal E nvironment, 280(1–3),* 239–255. https://doi.org/10.1016/s0048-9697(01)00833-6

[61] Kapahi, M., & Sachdeva, S. (2019). Bioremediation options for heavy metal pollution. *Journal of H ealth and P ollution, 9(24),* 191203. https://doi.org/10.5696/2156-9614-9.24.191203

[62] Sandrin, T. R., & Hoffman, D. W. (2007). Bioremediation of organic and metal co-contaminated environments: effects of metal toxicity, speciation, and bioavailability on

biodegradation. *Environmental B ioremediation T echnologies*, 1–34. https://doi.org/10.1007/978-3-540-34793-4_1

[63] Guzzi, G., Ronchi, A., & Pigatto, P. D. (2021). Toxic effects of mercury in humans and mammals. *Chemosphere, 263,* 127990. https://doi.org/10.1016/j.chemosphere.2020.127990

[64] Chilingar, N. H. S. S. G. V. (2000). Influence of porosity and direction of flow on tortuosity in unconsolidated porous media. *Energy Sour ces, 22(3),* 207–213. https://doi.org/10.1080/00908310050013992

[65] Genchi, G., Sinicropi, M. S., Lauria, G., Carocci, A., & Catalano, A. (2020). The effects of cadmium toxicity. *International Journal of E nvironmental R esearch and public health, 17(11),* 3782. https://doi.org/10.3390/ijerph17113782

[66] Kokab, T., Shah, A., Iftikhar, F. J., Nisar, J., Akhter, M. S., & Khan, S. B. (2019). Amino acid-fabricated glassy carbon electrode for efficient simultaneous sensing of zinc(II), cadmium(II), copper(II), and mercury(II) ions. *ACS O mega, 4(26),* 22057–22068. https://doi.org/10.1021/acsomega.9b03189

[67] De Oliveira, E. S., Caixeta, E. S., Santos, V. C., & Pereira, B. B. (2021). Arsenic exposure from groundwater: environmental contamination, human health effects, and sustainable solutions. *Journal of Toxicology and Environmental Health-part B-critical reviews, 24(3),* 119–135. https://doi.org/10.1080/10937404.2021.1898504

[68] Tripathi, R. D., Srivastava, S., Mishra, S., Singh, N., Tuli, R., Gupta, D. K., & Maathuis, F. J. M. (2007). Arsenic hazards: strategies for tolerance and remediation by plants. *Trends i n B iotechnology, 25(4),* 158–165. https://doi.org/10.1016/j.tibtech.2007.02.003

[69] Rajasekar, A., Selvi, A., Theertagiri, J., Ananthaselvam, A., Kumar, K. A., Madhavan, J., & Rahman, P. K. S. M. (2019). Integrated remediation processes toward heavy metal removal/recovery from various environments-a review. *Frontiers i n Environmental Science, 7,* 66. https://doi.org/10.3389/fenvs.2019.00066

[70] Rahaman, M. S., Rahman, M. M., Mise, N., Sikder, M. T., Ichihara, G., Uddin, M. K., Kurasaki, M., & Ichihara, S. (2021). Environmental arsenic exposure and its contribution to human diseases, toxicity mechanism and management. *Environmental Pollution, 289,* 117940. https://doi.org/10.1016/j.envpol.2021.117940

[71] Santra, S. C., Samal, A. C., Bhattacharya, P., Banerjee, S., Biswas, A., & Majumdar, J. (2013). Arsenic in foodchain and community health risk: a study in gangetic west bengal. *Procedia Environmental Sc iences, 1 8,* 2–13. https://doi.org/10.1016/j.proenv.2013.04.002

[72] Tchounwou, P.B., Yedjou, C.G., Patlolla, A.K. and Sutton, D.J., 2012. Heavy metal toxicity and the environment. *Molecular, C linical and E nvironmental T oxicology: Volume 3: e nvironmental t oxicology,* 133-164.https://doi.org/10.1007/978-3-7643-8340-4_6

[73] Đukić-ćosić, D., Baralić, K., Javorac, D., Buha, A., & Bulat, Z. (2020). An overview of molecular mechanisms in cadmium toxicity. *Current O pinion i n Toxicology, 19,* 56–62. https://doi.org/10.1016/j.cotox.2019.12.002

[74] Jain, J., & Gauba, P. (2017). Heavy metal toxicity-implications on metabolism and health. *International J ournal of P harma and B io Sc iences, 8(4),* 452-460. https://doi.org/10.22376/ijpbs.2017.8.4.b452-460

[75] Stohs, S. J., & Bagchi, D. (1995c). Oxidative mechanisms in the toxicity of metal ions. *Free R adical B iology and M edicine, 18(2),* 321–336. https://doi.org/10.1016/0891-5849(94)00159-h

[76] Waheed, A., & Ullah, N. (2018). Nanomaterials-based electrochemical detection of heavy metals in water: Current status, challenges and future direction. *Trends i n Analytical Chemistry, 105,* 37–51. https://doi.org/10.1016/j.trac.2018.04.012

[77] Samantaray, D., Mohapatra, S. and Mishra, B.B. (2014). Microbial bioremediation of industrial effluents. In *Microbial B iodegradation and B ioremediation* , 325-339. Elsevier. https://doi.org/10.1016/b978-0-12-800021-2.00014-5

[78] Wang, S., Wu, W., Liu, F., Liao, R., & Hu, Y. (2017). Accumulation of heavy metals in soil-crop systems: a review for wheat and corn. *Environmental Science and Pollution R esearch, 24(18),* 15209–15225. https://doi.org/10.1007/s11356-017-8909-5

[79] Liang, S., Gao, N., Li, Z., Shen, S., & Li, J. (2016). Investigation of correlativity between heavy metals concentration in indigenous plants and combined pollution soils. *Chemistry and E cology, 32(9),* 872–883. https://doi.org/10.1080/02757540.2016.1203909

[80] Moiseenko, T. I., & Gashkina, N. A. (2020). Distribution and bioaccumulation of heavy metals (Hg, Cd and Pb) in fish: influence of the aquatic environment and climate. *Environmental R esearch L etters, 15(11),* 115013. https://doi.org/10.1088/1748-9326/abbf7c

[81] Gall, J. E., Boyd, R. W., & Rajakaruna, N. (2015b). Transfer of heavy metals through terrestrial food webs: a review. *Environmental M onitoring and Assessment, 187,* 1-21. https://doi.org/10.1007/s10661-015-4436-3

[82] Saha, R., Nandi, R., & Saha, B. (2011). Sources and toxicity of hexavalent chromium. *Journal of C oordination C hemistry*, *64*(10), 1782-1806. https://doi.org/10.1080/00958972.2011.583646

[83] De Flora, S. (2000). Threshold mechanisms and site specificity in chromium (VI) carcinogenesis. *Carcinogenesis*, *21*(4), 533-541. https://doi.org/10.1093/carcin/21.4.533

[84] Cieślak-Golonka, M. (1996). Toxic and mutagenic effects of chromium (VI). A review. *Polyhedron*, *15*(21), 3667-3689. https://doi.org/10.1016/0277-5387(96)00141-6

[85] Wang, Y., Su, H., Gu, Y., Song, X., & Zhao, J. (2017). Carcinogenicity of chromium and chemoprevention: a brief update. *OncoTargets and therapy*, 4065-4079. https://doi.org/10.2147/OTT.S139262

[86] Sharma, P., Singh, S. P., Parakh, S. K., & Tong, Y. W. (2022). Health hazards of hexavalent chromium (Cr (VI)) and its microbial reduction. *Bioengineered*, *13*(3), 4923-4938. https://doi.org/10.1016/j.taap.2019.114636

[87] Pavesi, T., & Moreira, J. C. (2020). Mechanisms and individuality in chromium toxicity in humans. *Journal of appl ied t oxicology*, *40*(9), 1183-1197. https://doi.org/10.1002/jat.3965

[88] Zhitkovich, A. (2011). Chromium in drinking water: sources, metabolism, and cancer risks. *Chemical r esearch i n t oxicology*, *24*(10), 1617-1629. https://doi.org/10.1021/tx200251t

[89] Standeven, A. M., & Wetterhahn, K. E. (1991). Is there a role for reactive oxygen species in the mechanism of chromium (VI) carcinogenesis?. *Chemical research in toxicology*, *4*(6), 616-625. https://doi.org/10.1021/tx00024a003

[90] Narayani, M., & Shetty, K. V. (2013). Chromium-resistant bacteria and their environmental condition for hexavalent chromium removal: a review. *Critical Reviews in E nvironmental Sc ience and T echnology*, *43*(9), 955-1009.https://doi.org/10.1080/10643389.2011.627022

[91] Ali, H., & Khan, E. (2019). Trophic transfer, bioaccumulation, and biomagnification of non-essential hazardous heavy metals and metalloids in food chains/webs—Concepts and implications for wildlife and human health. *Human and Ecological R isk A ssessment, 25(6),* 1353–1376. https://doi.org/10.1080/10807039.2018.1469398

[92] Xiao, R., Wang, S., Li, R., Wang, J. J., & Zhang, Z. (2017). Soil heavy metal contamination and health risks associated with artisanal gold mining in Tongguan, Shaanxi, China. *Ecotoxicology and e nvironmental s afety*, *141*, 17-24. https://doi.org/10.1016/j.ecoenv.2017.03.002

[93] Gall, J. E., Boyd, R. S., & Rajakaruna, N. (2015). Transfer of heavy metals through terrestrial food webs: a review. *Environmental m onitoring and as sessment*, *187*, 1-21.https://doi.org/10.1007/s10661-015-4436-3

[94] Emami, M. H., Saberi, F., Mohammadzadeh, S., Fahim, A., Abdolvand, M., Dehkordi, S. A. E., ... & Maghool, F. (2023). A review of heavy metals accumulation in red meat and meat products in the Middle East. Journal of Food Protection, 100048. https://doi.org/10.1016/j.jfp.2023.100048

[95] Gumpu, M. B., Sethuraman, S., Krishnan, U. M., & Rayappan, J. B. B. (2015). A review on detection of heavy metal ions in water – An electrochemical approach. *Sensors and A ctuators B -Chemical, 213,* 515–533. https://doi.org/10.1016/j.snb.2015.02.122

[96] Azam, I., Afsheen, S., Zia, A., Javed, M., Saeed, R., Sarwar, M. K., & Munir, B. (2015). Evaluating insects as bioindicators of heavy metal contamination and accumulation near industrial area of Gujrat, Pakistan. *BioMed r esearch international*, *2015*. https://doi.org/10.1155/2015/942751

[97] Chowdhury, S., Dubey, V. K., Choudhury, S., Das, A., Jeengar, D., Sujatha, B., ... & Kumar, V. (2023). Insects as bioindicator: A hidden gem for environmental

monitoring. *Frontiers i n E nvironmental Sc ience*, *11*, 273. https://doi.org/10.3389/fenvs.2023.1146052

[98] Ahmed, A. S., Sultana, S., Habib, A., Ullah, H., Musa, N., Hossain, M. B., ... & Sarker, M. S. I. (2019). Bioaccumulation of heavy metals in some commercially important fishes from a tropical river estuary suggests higher potential health risk in children than adults. *Plos one* , *14*(10), e0219336. https://doi.org/10.1371/journal.pone.0219336

[99] Ilyas, M., Ahmad, W., Khan, H., Yousaf, S., Yasir, M., & Khan, A. (2019). Environmental and health impacts of industrial wastewater effluents in Pakistan: a review. *Reviews on E nvironmental H ealth, 34(2),* 171–186. https://doi.org/10.1515/reveh-2018-0078

[100] Authman, M. M., Zaki, M. S., Khallaf, E. A., & Abbas, H. H. (2015). Use of fish as bio-indicator of the effects of heavy metals pollution. *Journal of A quaculture Research & Development*, *6*(4), 1-13. http://dx.doi.org/10.4172/2155-9546.1000328

[101] Dobrovoljc, K., Falnoga, I., Žnidarič, M. T., Mazej, D., Ščančar, J., & Bulog, B. (2012). Cd, Cu, Zn, Se, and metallothioneins in two amphibians, Necturus maculosus (Amphibia, Caudata) and Bufo bufo (Amphibia, Anura). *Biological t race element research*, *150*, 178-194. https://doi.org/10.1007/s12011-012-9461-2

[102] Hui, C. A. (2004). Geophagy and potential contaminant exposure for terrestrial vertebrates. *Reviews of e nvironmental c ontamination an d t oxicology*, 115-134. https://doi.org/10.1007/978-1-4419-9100-3_5

[103] Ashraf, S. (2022). Exposure and effects of toxic trace metals in birds OF PAKISTAN. *Pakistan Journal of Science*, *74*(4). https://doi.org/10.57041/pjs.v74i4.762

[104] Cotín Martínez, J. (2012). Birds as bioindicators of pollution in aquatic and terrestrial environments. http://hdl.handle.net/2445/35946

[105] Walcarius, A., Minteer, S. D., Wang, J., Lin, Y., & Merkoci, A. (2013). Nanomaterials for bio-functionalized electrodes: recent trends. *Journal of M aterials Chemistry B*, *1*(38), 4878-4908. https://doi.org/10.1039/C3TB20881H

[106] Vareda, J. P., Valente, A. J., & Durães, L. (2019). Assessment of heavy metal pollution from anthropogenic activities and remediation strategies: A review. *Journal*

of e nvironmental m anagement, *246*, 101-118. https://doi.org/10.1016/j.jenvman.2019.05.126

[107] Radu, T., & Diamond, D. (2009). Comparison of soil pollution concentrations determined using AAS and portable XRF techniques. *Journal of Hazardous Materials, 171(1–3),* 1168–1171. https://doi.org/10.1016/j.jhazmat.2009.06.062

[108] Cabrera-Vique, C., Teissedre, P., Cabanis, M., & Cabanis, J. C. (1997). Determination and levels of chromium in french wine and grapes by graphite furnace atomic absorption spectrometry. *Journal of A gricultural and Food Che mistry, 45(5),* 1808–1811. https://doi.org/10.1021/jf960691b

[109] Arienzo, M., & Capasso, R. (2000). Analysis of metal cations and inorganic anions in olive oil mill waste waters by atomic absorption spectroscopy and ion chromatography. Detection of metals bound mainly to the organic polymeric fraction. Journal of agricultural and food chemistry, 48(4), 1405-1410. https://doi.org/10.1021/jf990588x

[110] Das, A. K., & Chakraborty, R. (1997). Electrothermal atomic absorption spectrometry in the study of metal ion speciation. *Fresenius' j ournal of analytical chemistry*, *357*, 1-17. https://doi.org/10.1007/s002160050102

[111] Gajek, M., Pawlaczyk, A., & Szynkowska-Jozwik, M. I. (2021). Multi-elemental analysis of wine samples in relation to their type, origin, and grape variety. *Molecules*, *26*(1), 214. https://doi.org/10.3390/molecules26010214

[112] Ammann, A. A. (2007). Inductively coupled plasma mass spectrometry (ICP MS): a versatile tool. *Journal of m ass s pectrometry*, *42*(4), 419-427. https://doi.org/10.1002/jms.1206

[113] Griboff, J., Wunderlin, D. A., & Monferran, M. V. (2017). Metals, As and Se determination by inductively coupled plasma-mass spectrometry (ICP-MS) in edible fish collected from three eutrophic reservoirs. Their consumption represents a risk for human health?. *Microchemical J ournal*, *130*, 236-244. https://doi.org/10.1016/j.microc.2016.09.013

[114] Hutton, L. A., O'Neil, G. W., Read, T. L., Ayres, Z. J., Newton, M. E., & Macpherson, J. V. (2014). Electrochemical X-ray fluorescence spectroscopy for trace heavy metal analysis: enhancing X-ray fluorescence detection capabilities by four

orders of magnitude. *Analytical C hemistry, 86(9),* 4566–4572. https://doi.org/10.1021/ac500608d

[115] O'Neil, G. W., Newton, M. E., & Macpherson, J. V. (2015). Direct identification and analysis of heavy metals in solution (Hg, Cu, Pb, Zn, Ni) by use of in situ electrochemical x-ray fluorescence. Analytical Chemistry, 87(9), 4933–4940. https://doi.org/10.1021/acs.analchem.5b00597

[116] Shi, D., Wu, W., & Li, X. (2021). Multiplexed detection of aqueous Cd^{2+}, Pb^{2+} and Cu^{2+} ions at mercury-on-graphene film modified electrode by DPASV. *Sensing and Bio-Sensing Research*, *34*, 100464. https://doi.org/10.1016/j.sbsr.2021.100464

[117] Kumar, K. S., Devendiran, M., Kumar, P. S., & Narayanan, S. S. (2021). Quercetin-rGO based mercury-free electrode for the determination of toxic Cd (II) and Pb (II) ions using DPASV technique. *Environmental R esearch, 20 2,* 111707. https://doi.org/10.1016/j.envres.2021.111707

[118] Munir, A., Shah, A., Nisar, J., Ashiq, M. N., Akhter, M. S., & Shah, A. (2019). Selective and simultaneous detection of Zn^{2+}, Cd^{2+}, Pb^{2+}, Cu^{2+}, Hg^{2+} and Sr^{2+} using surfactant modified electrochemical sensors. *Electrochimica A cta, 32 3,* 134592. https://doi.org/10.1016/j.electacta.2019.134592

[119] Malik, L. A., Bashir, A., Qureashi, A., & Pandith, A. H. (2019). Detection and removal of heavy metal ions: a review. *Environmental C hemistry L etters, 17(4),* 1495–1521. https://doi.org/10.1007/s10311-019-00891-z

[120] Cui, L., Wu, J., & Ju, H. (2015). Electrochemical sensing of heavy metal ions with inorganic, organic and bio-materials. *Biosensors and B ioelectronics, 63 ,* 276–286. https://doi.org/10.1016/j.bios.2014.07.052

[121] Jurado, A., Vàzquez-Suñé, E., Carrera, J., López De Alda, M., Pujades, E., & Barceló, D. (2012). Emerging organic contaminants in groundwater in Spain: A review of sources, recent occurrence and fate in a European context. *Science of The Total Environment*, *440*, 82–94. https://doi.org/10.1016/j.scitotenv.2012.08.029

[122] Shaw, L., Phung, C., & Grace, M. (2015). Pharmaceuticals and personal care products alter growth and function in lentic biofilms. *Environmental Che mistry*, *12*(3), 301. https://doi.org/10.1071/en14141

[123] Chitravathi, S., & Munichandraiah, N. (2016). Voltammetric determination of paracetamol, tramadol and caffeine using poly(Nile blue) modified glassy carbon

electrode. *Journal of E lectroanalytical Ch emistry*, *764*, 93–103. https://doi.org/10.1016/j.jelechem.2016.01.021

[124] Alahi, M. E. E., & Mukhopadhyay, S. C. (2018). Detection methods of nitrate in water: A review. *Sensors and A ctuators A : P hysical*, *280*, 210–221. https://doi.org/10.1016/j.sna.2018.07.026

[125] Hammi, S., el Ataouna, K., Bouti, K., Elbouazzi, O., Laine, M., & Bourkadi, J. E. (2016). Importance of therapeutic drug monitoring in the treatment of active tuberculosis - a retrospective study of 4 cases. *International Journal of Medicine and Surgery*, *3*(1), 10–13. https://doi.org/10.15342/ijms.v3i1.92

[126] Rosa, J., Machado, T. C., da Silva, A. K., Kuminek, G., Bortolluzzi, A. J., Caon, T., & Cardoso, S. G. (2019). Isoniazid-Resveratrol Cocrystal: A novel alternative for topical treatment of cutaneous tuberculosis. *Crystal G rowth & D esign*, *19*(9), 5029–5036. https://doi.org/10.1021/acs.cgd.9b00313

[127] Azad, U. P., & Ganesan, V. (2012). Efficient electrocatalytic oxidation and selective determination of isoniazid by $Fe(tmphen)_3^{2+}$ -exchanged nafion®-modified electrode. *Journal o f S olid S tate Electrochemistry*, *16*(9), 2907–2911. https://doi.org/10.1007/s10008-012-1724-5

[128] Mahmoud, B. G., Khairy, M., Rashwan, F. A., & Banks, C. E. (2017). Simultaneous voltammetric determination of acetaminophen and isoniazid (hepatotoxicity-related drugs) utilizing bismuth oxide nanorod modified screen-printed electrochemical sensing platforms. *Analytical Chemistry*, *89*(3), 2170–2178. https://doi.org/10.1021/acs.analchem.6b05130

[129] Tan, S. M., Sofer, Z., Luxa, J., & Pumera, M. (2016). Aromatic-exfoliated transition metal dichalcogenides: implications for inherent electrochemistry and hydrogen evolution. *ACS Catalysis*, *6*(7), 4594–4607. https://doi.org/10.1021/acscatal.6b00761

[130] Gilic, M., Petrovic, M., Cirkovic, J., Paunovic, N., Savic-Sevic, S., Nikitovic, Z., Romcevic, M., Yahia, I., & Romcevic, N. (2017). Low-temperature photoluminescence of $CuSe_2$ nano-objects in selenium thin films. *Processing and Application of Ceramics*, *11*(2), 127–135. https://doi.org/10.2298/pac1702127g

[131] Ding, C. H., Tang, J. J., Chen, S., Liu, Z. Q., & Li, N. (2017). $Co_{0.85}Se$/multi-walled carbon nanotube composite as alternative cathode catalyst for microbial fuel cells. *Journal*

of Nanos cience and Nano technology, *17*(2), 1438–1442. https://doi.org/10.1166/jnn.2017.12697

[132] Dutta, A. K., Maji, S. K., Mondal, A., Karmakar, B., Biswas, P., & Adhikary, B. (2012). Iron selenide thin film: Peroxidase-like behavior, glucose detection and amperometric sensing of hydrogen peroxide. *Sensors and A ctuators B: Ch emical*, *173*, 724–731. https://doi.org/10.1016/j.snb.2012.07.070

[133] Theerthagiri, J., Sudha, R., Premnath, K., Arunachalam, P., Madhavan, J., & Al-Mayouf, A. M. (2017). Growth of iron diselenide nanorods on graphene oxide nanosheets as advanced electrocatalyst for hydrogen evolution reaction. *International J ournal of hydrogen Energy*, *42*(18), 13020–13030. https://doi.org/10.1016/j.ijhydene.2017.04.042

[134] Singh, A. K., & Xu, Q. (2013). Synergistic catalysis over bimetallic alloy nanoparticles. *Chemcatchem*, *5*(3), 652–676. https://doi.org/10.1002/cctc.201200591

[135] Møller, L. R., & Østergaard, J. R. (2009). Treatment with venlafaxine in six cases of children with narcolepsy and with cataplexy and hypnagogic hallucinations. *Journal of Child and A dolescent P sychopharmacology*, *19*(2), 197–201. https://doi.org/10.1089/cap.2008.036

[136] Baranwal, J., Barse, B., Gatto, G., Broncova, G., & Kumar, A. (2022). Electrochemical sensors and their applications: A review. *Chemosensors*, *10*(9), 363. https://doi.org/10.3390/chemosensors10090363

[137] G., S., N., U., R., N., P., K., G., V., & B., C. (2020). A review on properties, applications and toxicities of metal nanoparticles. *International Journal of A pplied Pharmaceutics*, 58–63. https://doi.org/10.22159/ijap.2020v12i5.38747

[138] Qian, L., Durairaj, S., Prins, S., & Chen, A. (2021). Nanomaterial-based electrochemical sensors and biosensors for the detection of pharmaceutical compounds. *Biosensors and Bioelectronics*, *175*, 112836. https://doi.org/10.1016/j.bios.2020.112836

[139] Beitollahi, H., Jahani, S., Tajik, S., Ganjali, M. R., Faridbod, F., & Alizadeh, T. (2019). Voltammetric determination of venlafaxine as an antidepressant drug employing Gd2O3 nanoparticles graphite screen printed electrode. *Journal of Rare Earths*, *37*(3), 322–328. https://doi.org/10.1016/j.jre.2018.09.001

[140] Zainal, Z., Lee, C. Y., Hussein, M. Z., Kassim, A., & Yusof, N. A. (2007). Electrochemical-assisted photodegradation of mixed dye and textile effluents using TiO_2

thin films. *Journal of H azardous Materials*, *146*(1–2), 73–80. https://doi.org/10.1016/j.jhazmat.2006.11.055

[141] Wang, J., Xu, D., Kawde, A. N., & Polsky, R. (2001). Metal nanoparticle-based electrochemical stripping potentiometric detection of dna hybridization. *Analytical Chemistry*, *73*(22), 5576–5581. https://doi.org/10.1021/ac0107148

[142] Shah, A., Nosheen, E., Munir, S., Badshah, A., Qureshi, R., Rehman, Z. U., Muhammad, N., & Hussain, H. (2013). Characterization and DNA binding studies of unexplored imidazolidines by electronic absorption spectroscopy and cyclic voltammetry. *Journal of P hotochemistry and Photobiology B : B iology*, *120*, 90–97. https://doi.org/10.1016/j.jphotobiol.2012.12.015

[143] Holze, R. (2003). Buchbesprechung: Broadening electrochemical horizons Von Alan M. Bond. *Angewandte Chemie*, *115*(26), 3041. https://doi.org/10.1002/ange.200390540

[144] Safavi, A., Maleki, N., & Tajabadi, F. (2007). Highly stable electrochemical oxidation of phenolic compounds at carbon ionic liquidelectrode. *The An alyst*, *132*(1), 54–58. https://doi.org/10.1039/b612672c

[145] Jerkiewicz, G. (2022). Applicability of platinum as a counter-electrode material in electrocatalysis research. *ACS C atalysis*, *12*(4), 2661-2670.https://doi.org/10.1021/acscatal.1c06040

[146] Tian, M., Cousins, C., Beauchemin, D., Furuya, Y., Ohma, A., & Jerkiewicz, G. (2016). Influence of the working and counter electrode surface area ratios on the dissolution of platinum under electrochemical conditions. *ACS Catalysis*, *6*(8), 5108-5116. https://doi.org/10.1021/acscatal.6b00200

[147] Ghernaout, D., & Ghernaout, B. (2011b). On the controversial effect of sodium sulphate as supporting electrolyte on electrocoagulation process: A Review. *Desalination and Water Treatment*, *27*(1–3), 243–254. https://doi.org/10.5004/dwt.2011.1983

[148] Ghalkhani, M., Fernandes, I. P., Oliveira, S. C. B., Shahrokhian, S., & Oliveira–Brett, A. M. (2011). Anodic behavior of clioquinol at a glassy carbon electrode. *Bioelectrochemistry*, *80*(2), 175-181. https://doi.org/10.1016/j.bioelechem.2010.10.001

[149] Michael, A. M., Mahmoud, A. M., & Fahmy, N. M. (2023). Determination of Clomipramine using eco-friendly solid-contact ionophore-doped potentiometric sensor. *BMC chemistry*, *17*(1), 1-9. https://doi.org/10.1186/s13065-023-00938-x

[150] Ahmadpour, S., Tashkhourian, J., & Hemmateenejad, B. (2020). A chemometric investigation on the influence of the nature and concentration of supporting electrolyte on charging currents in electrochemistry. *Journal of Electroanalytical Chemistry*, *871*, 114296. https://doi.org/10.1016/j.jelechem.2020.114296

[151] Creager, S. (2007). Solvents and supporting electrolytes. In *Handbook of electrochemistry* (pp. 57-72). Elsevier. https://doi.org/10.1016/B978-044451958-0.50004-5

[152] Liu, L., Liu, L., Wang, Y., & Ye, B. C. (2019). A novel electrochemical sensor based on bimetallic metal–organic framework-derived porous carbon for detection of uric acid. *Talanta*, *199*, 478-484. https://doi.org/10.1016/j.talanta.2019.03.008

[153] Baghayeri, M., Amiri, A., Fayazi, M., Nodehi, M., & Esmaeelnia, A. (2021). Electrochemical detection of bisphenol a on a MWCNTs/$CuFe_2O_4$ nanocomposite modified glassy carbon electrode. *Materials Chemistry and Physics*, *261*, 124247. https://doi.org/10.1039/C9TB01020C

[154] Niu, X., Li, X., Chen, W., Li, X., Weng, W., Yin, C., ... & Li, G. (2018). Three-dimensional reduced graphene oxide aerogel modified electrode for the sensitive quercetin sensing and its application. *Materials Science and Engineering: C*, *89*, 230-236. https://doi.org/10.1016/j.msec.2018.04.015

[155] Pizarro, J., Segura, R., Tapia, D., Navarro, F., Fuenzalida, F., & Aguirre, M. J. (2020). Inexpensive and green electrochemical sensor for the determination of Cd (II) and Pb (II) by square wave anodic stripping voltammetry in bivalve mollusks. *Food chemistry*, *321*, 126682. https://doi.org/10.1016/j.foodchem.2020.126682

[156] Anastasiadou, Z. D., Jannakoudakis, P. D., & Girousi, S. T. (2010). Square wave anodic stripping voltammetry determination of eco-toxic metals in samples of biological and environmental importance. *Central European Journal of Chemistry*, *8*, 999-1008. https://doi.org/10.2478/s11532-010-0091-2

[157] Rahm, C. E., Gupta, P., Gupta, V. K., Huseinov, A., Griesmer, B., & Alvarez, N. T. (2022). Impact of physical and chemical parameters on square wave anodic stripping voltammetry for trace Pb^{2+} detection in water. *Analyst*, *147*(15), 3542-3557. https://doi.org/10.1039/D2AN00724J

[158] Kurbanoglu, S., & Ozkan, S. A. (2018). Electrochemical carbon based nanosensors: A promising tool in pharmaceutical and biomedical analysis. *Journal of pharmaceutical and biomedical analysis*, *147*, 439-457. https://doi.org/10.1016/B978-0-12-813691-1.00006-3

[159] Bakirhan, N. K., Uslu, B., & Ozkan, S. A. (2017). Sensitive and selective assay of antimicrobials on nanostructured materials by electrochemical techniques. In *Nanostructures for Antimicrobial Therapy* (pp. 55-83). Elsevier. https://doi.org/10.1016/B978-0-323-46152-8.00003-2

[160] Delmo, N., Mostafiz, B., Ross, A. E., Suni, J., & Peltola, E. (2023). Developing an electrochemical sensor for the in vivo measurements of dopamine. *Sensors & Diagnostics*, *2*(3), 559-581. https://doi.org/10.1039/D2SD00230B

[161] Rajeshwar, K. I. J. G., Ibanez, J. G., & Swain, G. M. (1994). Electrochemistry and the environment. *Journal of applied electrochemistry*, *24*(11), 1077-1091. https://doi.org/10.1007/BF00241305

[162] Koç, Y., MORALI, U., Erol, S., & AVCI, H. (2021). Investigation of electrochemical behavior of potassium ferricyanide/ferrocyanide redox probes on screen printed carbon electrode through cyclic voltammetry and electrochemical impedance spectroscopy. *Turkish Journal of Chemistry*, *45*(6), 1895-1915. https://doi.org/10.3906/kim-2105-55

[163] Sýs, M., Khaled, E., Metelka, R., & Vytřas, K. (2017). Electrochemical characterisation of novel screen-printed carbon paste electrodes for voltammetric measurements. *Journal of the Serbian Chemical Society, volume 82, issue: 7-8*. https://doi.org/10.2298/JSC170207048S

[164] Perenlei, G., Tee, T. W., Yusof, N. A., & Kheng, G. J. (2011). Voltammetric detection of potassium ferricyanide mediated by multi-walled carbon nanotube/titanium dioxide composite modified glassy carbon electrode. *International Journal of Electrochemical Science*, *6*(2), 520-531.https://doi.org/10.1016/S1452-3981(23)15013-9

[165] Rejithamol, R., Krishnan, R. G., & Beena, S. (2021). Disposable pencil graphite electrode decorated with a thin film of electro-polymerized 2, 3, 4, 6, 7, 8, 9, 10-octahydropyrimido [1, 2-a] azepine for simultaneous voltammetric analysis of

dopamine, serotonin and tryptophan. *Materials Chemistry and Physics*, *258*, 123857. https://doi.org/10.1016/j.matchemphys.2020.123857

[166] Buledi, J. A., Ameen, S., Khand, N. H., Solangi, A. R., Taqvi, I. H., Agheem, M. H., & Wajdan, Z. (2020). CuO nanostructures based electrochemical sensor for simultaneous determination of hydroquinone and ascorbic acid. *Electroanalysis*, *32*(7), 1600-1607. https://doi.org/10.1002/elan.202000083

[167] Batchelor-McAuley, C., Kätelhön, E., Barnes, E. O., Compton, R. G., Laborda, E., & Molina, A. (2015). Recent advances in voltammetry. *ChemistryOpen*, *4*(3), 224-260. https://doi.org/10.1002/open.201500042

[168] Johnson, D. C. (1982). Analytical electrochemistry: theory and instrumentation of dynamic techniques. *Analytical Chemistry*, *54*(5), 9-19. https://doi.org/10.1021/ac00242a002

[169] Zouraris, D. (2021). Electrochemical study of redox enzymes and their utilization on modified electrodes. http://dx.doi.org/10.26240/heal.ntua.20463

[170] Ciszkowska, M., & Stojek, Z. (1999). Voltammetry in solutions of low ionic strength. Electrochemical and analytical aspects. *Journal of Electroanalytical Chemistry*, *466*(2), 129-143. https://doi.org/10.1016/S0022-0728(99)00141-2

[171] Berry, B. W., Martínez-Rivera, M. C., & Tommos, C. (2012). Reversible voltammograms and a Pourbaix diagram for a protein tyrosine radical. *Proceedings of the National Academy of Sciences*, *109*(25), 9739-9743. https://doi.org/10.1073/pnas.1112057109

[172] Mirkin, M. V., & Bard, A. J. (1992). Simple analysis of quasi-reversible steady-state voltammograms. *Analytical Chemistry*, *64*(19), 2293-2302. https://doi.org/10.1021/ac00043a020

[173] Marichev, V. A. (2008). Reversibility of platinum voltammograms in aqueous electrolytes and ionic product of water. *Electrochimica acta*, *53*(27), 7952-7960. https://doi.org/10.1073/pnas.1112057109

[174] Arzaee, N. A., Mohamad Noh, M. F., Halim, A. A., Faizal Abdul Rahim, M. A., Haziqah Mohd Ita, N. S., Mohamed, N. A., Farhana Mohd Nasir, S. N., Ismail, A. F., & Mat Teridi, M. A. (2021). Cyclic voltammetry - A promising approach towards

improving photoelectrochemical activity of hematite. *Journal of Alloys and Compounds*, *852*, 156757. https://doi.org/10.1016/j.jallcom.2020.156757

[175] Lim, A. C., Jadhav, H. S., & Seo, J. G. (2018). Electron transport shuttle mechanism *via* an Fe–N–C bond derived from a conjugated microporous polymer for a supercapacitor. *Dalton Transactions*, *47*(3), 852–858. https://doi.org/10.1039/c7dt04094f

[176] Henstridge, M. C., Wang, Y., Limon-Petersen, J. G., Laborda, E., & Compton, R. G. (2011). An experimental comparison of the Marcus–Hush and Butler–Volmer descriptions of electrode kinetics applied to cyclic voltammetry. The one electron reductions of europium (III) and 2-methyl-2-nitropropane studied at a mercury microhemisphere electrode. *Chemical Physics Letters*, *517*(1–3), 29–35. https://doi.org/10.1016/j.cplett.2011.10.004

[177] Saeed, U., Fatima, B., Hussain, D., Ashiq, R., Naeem Ashiq, M., & Najam-ul-Haq, M. (2022). CoTe nanorods based electrochemical sensor for quantitative detection of albumin from chronic kidney disease patients. *Journal of Electroanalytical Chemistry*, *906*, 115999. https://doi.org/10.1016/j.jelechem.2021.115999

[178] Elgrishi, N., Rountree, K. J., McCarthy, B. D., Rountree, E. S., Eisenhart, T. T., & Dempsey, J. L. (2017). A Practical beginner's guide to cyclic voltammetry. *Journal of Chemical Education*, *95*(2), 197–206. https://doi.org/10.1021/acs.jchemed.7b00361

[179] Izquierdo, J., & Kranz, C. (2016). Electrochemical techniques for investigating redox active macromolecules. *European Polymer Journal*, *83*, 428-449. https://doi.org/10.1016/j.eurpolymj.2016.05.016

[180] Amine, A., & Mohammadi, H. (2018). Amperometry. *Reference Module in Chemistry, Molecular Sciences and Chemical Engineering*. https://doi.org/10.1016/b978-0-12-409547-2.14204-0

[181] Gonon, F. G., Navarre, F., & Buda, M. J. (1984). In vivo monitoring of dopamine release in the rat brain with differential normal pulse voltammetry. *Analytical chemistry*, *56*(3), 573-575. https://doi.org/10.1021/ac00267a060

[182] Jakubowska, M., & Kubiak, W. W. (2008). Signal processing in normal pulse voltammetry by means of dedicated mother wavelet. *Electroanalysis: An International*

Journal Devoted to Fundamental and Practical Aspects of Electroanalysis, *20*(2), 185-193. https://doi.org/10.1002/elan.200704037

[183] Rusling, J. F., & Nassar, A. E. F. (1994). Electron transfer rates in electroactive films from normal pulse voltammetry. Myoglobin-surfactant films. *langmuir*, *10*(8), 2800-2806. https://doi.org/10.1021/la00020a049

[184] Lovrić, M., & Osteryoung, J. (1982). Theory of differential normal pulse voltammetry. *Electrochimica A cta*, *27*(7), 963-968. https://doi.org/10.1016/0013-4686(82)80220-X

[185] Lovric, M., O'Dea, J. J., & Osteryoung, J. (1983). Faradaic response in derivative and differential normal pulse voltammetry. *Analytical C hemistry*, *55*(4), 704-708. https://doi.org/10.1021/ac00255a028

[186] Brumleve, T. R., & Osteryoung, J. (1981). Theory of differential normal pulse voltammetry in the alternating pulse mode for totally irreversible electrode reactions. *Analytical Chemistry*, *53*(7), 988-991. https://doi.org/10.1021/ac00230a015

[187] Osteryoung, J. G., & Schreiner, M. M. (1988). Recent advances in pulse voltammetry. *CRC C ritical R eviews in A nalytical C hemistry*, *19*(sup1), S1-S27. https://doi.org/10.1080/15476510.1988.10401465

[188] Sharif, M. O. (2017). *Towards i dentifying disinfectants and qua ntifying disinfectant le vels in w ater* (Doctoral dissertation). https://doi.org/10.13140/RG.2.2.24985.31842

[189] Chen, A., & Shah, B. (2013). Electrochemical sensing and biosensing based on square wave voltammetry. *Analytical M ethods*, *5*(9), 2158-2173. https://doi.org/10.1039/C3AY40155C

[190] Santos, F. D. S., da Silva, L. V., Campos, P. V. S., de Medeiros Strunkis, C., Ribeiro, C. M. G., & Salles, M. O. (2022). Recent advances of electrochemical techniques in food, energy, environment, and forensic applications. *ECS Se nsors Plus*, *1*(1), 013603. https://doi.org/10.1149/2754-2726/ac5cdf

[191] Robles, I., Godínez, L. A., Manríquez, J., Rodríguez, F., Rodríguez, A., & Bustos, E. (2014). Electrochemical detection of mercury removal from polluted bentonite and

quartz using different removing agents. In *Environmental R isk A ssessment of Soi l Contamination*. IntechOpen. https://doi.org/10.5772/57446

[192] Wygant, B. R., & Lambert, T. N. (2022). Thin film electrodes for anodic stripping voltammetry: a mini-review. *Frontiers in C hemistry*, *9*, 809535. https://doi.org/10.3389/fchem.2021.809535

[193] Xia, Y., Li, J., Zhu, G., & Yi, Y. (2022). Innovative strategy based on novel Ti3C2Tx MXenes nanoribbons/carbon nanotubes hybrids for anodic stripping voltammetry sensing of mercury ion. *Sensors and A ctuators B : C hemical*, *355*, 131247. https://doi.org/10.1016/j.snb.2021.131247

[194] March, G., Nguyen, T. D., & Piro, B. (2015). Modified electrodes used for electrochemical detection of metal ions in environmental analysis. *Biosensors*, *5*(2), 241-275.https://doi.org/10.3390/bios5020241

[195] Lisdat, F., & Schäfer, D. (2008). The use of electrochemical impedance spectroscopy for biosensing. *Analytical and bi oanalytical chemistry*, *391*, 1555-1567. https://doi.org/10.1007/s00216-008-1970-7

[196] Zhou, S. F., Wang, J. J., Gan, L., Han, X. J., Fan, H. L., Mei, L. Y., Huang, J., & Liu, Y. Q. (2017). Individual and simultaneous electrochemical detection toward heavy metal ions based on L-cysteine modified mesoporous $MnFe_2O_4$ nanocrystal clusters. *Journal of A lloys and C ompounds*, *721*, 492–500. https://doi.org/10.1016/j.jallcom.2017.05.321

[197] Gergin, İ., Gökçeören, A. T., & Sarac, A. S. (2015). Synthesis and electrochemical investigation of polyindole based fiber as sensor electrode by EIS method. *Fibers and Polymers*, *16*, 1468-1477. https://doi.org/10.1007/s12221-015-5144-x

[198] Xing, Y., Zhang, C., Chen, X., Zhao, H., & Guo, Z. (2021). Highly sensitive detection of salvianic acid a drug by a novel electrochemical sensor based on HKUST-1 loaded on three-dimensional graphene-MWCNT composite. *Journal of Pharmaceutical and B iomedical A nalysis*, *206*, 114389.https://doi.org/10.1016/j.jpba.2021.114389

[199] Baghayeri, M., Amiri, A., Maleki, B., Alizadeh, Z., & Reiser, O. (2018). A simple approach for simultaneous detection of cadmium(II) and lead(II) based on glutathione

coated magnetic nanoparticles as a highly selective electrochemical probe. *Sensors and Actuators B: Chemical*, *273*, 1442–1450. https://doi.org/10.1016/j.snb.2018.07.063

[200] *MyCourses: kirja*. (n.d.).

https://mycourses.aalto.fi/mod/book/tool/print/index.php?id=388663

[201] Inkson, B. J. (2016). Scanning electron microscopy (SEM) and transmission electron microscopy (TEM) for materials characterization. In *Materials characterization us ing nonde structive e valuation (NDE) methods* (pp. 17-43). Woodhead publishing. https://doi.org/10.1016/B978-0-08-100040-3.00002-X

[202] Zhou, W., Apkarian, R., Wang, Z. L., & Joy, D. (2007). Fundamentals of scanning electron microscopy (SEM). *Scanning Microscopy for Nanotechnology: Techniques and A pplications*, 1-40. https://link.springer.com/chapter/10.1007/978-0-387-39620-0_1

[203] Vos, K., Vandenberghe, N., & Elsen, J. (2014). Surface textural analysis of quartz grains by scanning electron microscopy (SEM): From sample preparation to environmental interpretation. *Earth-Science R eviews*, *128*, 93-104. https://doi.org/10.1016/j.earscirev.2013.10.013

[204] Tang, C. Y., & Yang, Z. (2017). Transmission electron microscopy (TEM). In *Membrane characterization* (pp. 145-159). Elsevier. https://doi.org/10.1016/B978-0-444-63776-5.00008-5

[205] Asadi Asadabad, M., & Jafari Eskandari, M. (2015). Transmission electron microscopy as best technique for characterization in nanotechnology. *Synthesis and Reactivity in Inorganic, Metal-Organic, and Nano-Metal Chemistry*, *45*(3), 323-326. https://doi.org/10.1080/15533174.2013.831901

[206] Ren, L. (n.d.). Gallium-based liquid metals and their hybrids as smart electronic materials. Research Online. https://ro.uow.edu.au/theses1/520/Gumpu, M. B., Veerapandian, M., Krishnan, U. M., & Rayappan, J. B. B. (2017). Simultaneous electrochemical detection of Cd(II), Pb(II), As(III) and Hg(II) ions using ruthenium(II)-textured graphene oxide nanocomposite. *Talanta*, *162*, 574–582. https://doi.org/10.1016/j.talanta.2016.10.076

[207] Xie, Y. L., Zhao, S. Q., Ye, H. L., Yuan, J., Song, P., & Hu, S. Q. (2015). Graphene/CeO_2 hybrid materials for the simultaneous electrochemical detection of cadmium(II), lead(II), copper(II), and mercury(II). *Journal of E lectroanalytical Chemistry*, *757*, 235–242. https://doi.org/10.1016/j.jelechem.2015.09.043

[208] Zhang, B., Chen, J., Zhu, H., Yang, T., Zou, M., Zhang, M., & Du, M. (2016). Facile and green fabrication of size-controlled AuNPs/CNFs hybrids for the highly sensitive simultaneous detection of heavy metal ions. *Electrochimica Acta*, *196*, 422–430. https://doi.org/10.1016/j.electacta.2016.02.163

[209] Gao, F., Gao, N., Nishitani, A., & Tanaka, H. (2016). Rod-like hydroxyapatite and Nafion nanocomposite as an electrochemical matrix for simultaneous and sensitive detection of Hg^{2+}, Cu^{2+}, Pb^{2+} and Cd^{2+}. *Journal of Electroanalytical Chemistry*, *775*, 212–218. https://doi.org/10.1016/j.jelechem.2016.05.032

[210] Pauliukaitė, R., & Brett, C. (2005). Characterization and application of bismuth-film modified carbon film electrodes. *Electroanalysis*, *17*(15–16), 1354–1359. https://doi.org/10.1002/elan.200403282

[211] Wei, Y., Yang, R., Zhang, Y. X., Wang, L., Liu, J. H., & Huang, X. J. (2011). High adsorptive γ-AlOOH(boehmite)@SiO_2/Fe_3O_4 porous magnetic microspheres for detection of toxic metal ions in drinking water. *Chemical Communications*, *47*(39), 11062. https://doi.org/10.1039/c1cc14215a

[212] Kucukkolbasi, S., Temur, O., Kara, H., & Khaskheli, A. R. (2013). Monitoring of Zn(II), Cd(II), Pb(II) and Cu(II) during refining of some vegetable oils using differential pulse anodic stripping voltammetry. *Food Analytical Methods*, *7*(4), 872–878. https://doi.org/10.1007/s12161-013-9694-5

[213] Tang, L., Wang, Y., Li, Y., Feng, H., Lu, J., & Li, J. (2009). Preparation, structure, and electrochemical properties of reduced graphene sheet films. *Advanced Functional Materials*, *19*(17), 2782–2789. https://doi.org/10.1002/adfm.200900377

[214] Locatelli, C. (1997). Anodic and cathodic stripping voltammetry in the simultaneous determination of toxic metals in environmental samples. *Electroanalysis*, *9*(13), 1014-1017. https://doi.org/10.1002/elan.1140091309

[215] Gumpu, M. B., Veerapandian, M., Krishnan, U. M., & Rayappan, J. B. B. (2017). Simultaneous electrochemical detection of Cd (II), Pb (II), As (III) and Hg (II) ions

using ruthenium (II)-textured graphene oxide nanocomposite. *Talanta,* 162, 574-582. https://doi.org/10.1016/j.talanta.2016.10.076

[216] Xie, Y. L., Zhao, S. Q., Ye, H. L., Yuan, J., Song, P., & Hu, S. Q. (2015). Graphene/CeO_2 hybrid materials for the simultaneous electrochemical detection of cadmium (II), lead (II), copper (II), and mercury (II). *Journal of Electroanalytical Chemistry*, 757, 235-242. https://doi.org/10.1016/j.jelechem.2015.09.043

[217] Gao, F., Gao, N., Nishitani, A., & Tanaka, H. (2016). Rod-like hydroxyapatite and Nafion nanocomposite as an electrochemical matrix for simultaneous and sensitive detection of Hg^{2+}, Cu^{2+}, Pb^{2+} and Cd^{2+}. *Journal of Electroanalytical Chemistry*, *775*, 212-218. https://doi.org/10.1016/j.jelechem.2016.05.032

[218] Pauliukaitė, R., & Brett, C. M. (2005). Characterization and application of bismuth-film modified carbon film electrodes. *Electroanalysis: An International Journal Devoted to Fundamental and Practical Aspects of Electroanalysis*, *17*(15-16), 1354-1359. https://doi.org/10.1002/elan.200403282

[219] Wei, Y., Yang, R., Zhang, Y. X., Wang, L., Liu, J. H., & Huang, X. J. (2011). High adsorptive γ-AlOOH (boehmite)@ SiO_2/Fe_3O_4 porous magnetic microspheres for detection of toxic metal ions in drinking water. *Chemical Communications*, *47*(39), 11062-11064. https://doi.org/10.1039/c1cc14215a

[220] Kucukkolbasi, S., Temur, O., Kara, H., & Khaskheli, A. R. (2014). Monitoring of Zn (II), Cd (II), Pb (II) and Cu (II) during refining of some vegetable oils using differential pulse anodic stripping voltammetry. *Food analytical methods*, *7*, 872-878. https://doi.org/10.1007/s12161-013-9694-5

[221] Zhang, B., Chen, J., Zhu, H., Yang, T., Zou, M., Zhang, M., & Du, M. (2016). Facile and green fabrication of size-controlled AuNPs/CNFs hybrids for the highly sensitive simultaneous detection of heavy metal ions. *Electrochimica Acta*, *196*, 422-430. https://doi.org/10.1016/j.electacta.2016.02.163

[222] Lashari, A. H., Ali, N., Mohiuddin, M., Ali, J., Ullah, S., Ujjan, S. A., ... & Rashid, W. (2022). Estimation of Water Quality Parameters of Rawal Lake and Its Associated Tributaries. *Polish Journal of Environmental Studies*, *31*(3). https://doi.org/10.15244/pjoes/139381

[223] Wei, Y., Gao, C., Meng, F. L., Li, H. H., Wang, L., Liu, J. H., & Huang, X. J. (2012). SnO2/reduced graphene oxide nanocomposite for the simultaneous electrochemical detection of cadmium (II), lead (II), copper (II), and mercury (II): an interesting favorable mutual interference. *The journal of physical chemistry C*, *116*(1), 1034-1041. https://doi.org/10.1021/jp209805c

[224] Xing, H., Xu, J., Zhu, X., Duan, X., Lu, L., Wang, W., ... & Yang, T. (2016). Highly sensitive simultaneous determination of cadmium (II), lead (II), copper (II), and mercury (II) ions on N-doped graphene modified electrode. *Journal of Electroanalytical C hemistry*, *760*, 52-58. https://doi.org/10.1016/j.jelechem.2015.11.043

[225] Ren, W., Zhang, Y., & Li, M. (2018). Sensitive determination of Zn^{2+}, Cd^{2+} and Pb^{2+} at electrochemically reduced nanoporous graphene oxide/bismuth film electrode. *Int. J. Electrochem. Sci*, *13*, 1331-1342. https://doi.org/10.20964/2018.02.44

[226] Sun, Y. F., Zhao, L. J., Jiang, T. J., Li, S. S., Yang, M., & Huang, X. J. (2016). Sensitive and selective electrochemical detection of heavy metal ions using amino-functionalized carbon microspheres. *Journal of Electroanalytical Chemistry*, *760*, 143-150. https://doi.org/10.1016/j.jelechem.2015.11.028

[227] Adarakatti, P. S., Gangaiah, V. K., Banks, C. E., & Siddaramanna, A. (2018). One-pot synthesis of Mn_3O_4/graphitic carbon nanoparticles for simultaneous nanomolar detection of Pb (II), Cd (II) and Hg (II). *Journal of materials science*, *53*, 4961-4973. https://doi.org/10.1007/s10853-017-1896-6

[228] Wu, W., Jia, M., Wang, Z., Zhang, W., Zhang, Q., Liu, G., Zhang, Z., & Li, P. (2019). Simultaneous voltammetric determination of cadmium(II), lead(II), mercury(II), zinc(II), and copper(II) using a glassy carbon electrode modified with magnetite (Fe_3O_4) nanoparticles and fluorinated multiwalled carbon nanotubes. *Microchimica Acta*, *186*(2). https://doi.org/10.1007/s00604-018-3216-5

[229] Wang, S. (2018). Simultaneously Detection of Pb^{2+} and Hg^{2+} using electrochemically reduced graphene oxide. *International Journal of Electrochemical Science*, 785–796. https://doi.org/10.20964/2018.01.84

[230] Li, X., Xu, P., Zhou, Y., Chen, Y., Jia, H., Yu, H., & Li, X. (2022). In Situ Hydrogen Temperature-Programmed Reduction Technology Based on the Integrated

Microcantilever for Metal Oxide Catalyst Analysis. *Analytical C hemistry*, *94*(47), 16502-16509. https://doi.org/10.1021/acs.analchem.2c04156

[231] Román-Martínez, M. C., Cazorla-Amorós, D., Linares-Solano, A., & De Lecea, C. S. M. (1993). TPD and TPR characterization of carbonaceous supports and Pt/C catalysts. *Carbon*, *31*(6), 895-902. https://doi.org/10.1016/0008-6223(93)90190-L

[232] Portales, M. V., Lazo Fraga, A. R., Díaz García, A. M., García-Zaldívar, O., Peláiz Barranco, A., & Aguilar Frutis, M. A. (2018). Cyclic voltammetry and impedance spectroscopy analysis for graphene-modified solid-state electrode transducers. *Journal of Solid State Electrochemistry*, *22*, 471-478. https://doi.org/10.1007/s10008-017-3776-z

[233] Li, J., Feng, H., Jiang, J., Feng, Y., Xu, Z., & Qian, D. (2015). One-pot in situ synthesis of a $CoFe_2O_4$ nanoparticle-reduced graphene oxide nanocomposite with high performance for levodopa sensing. *Rsc A dvances*, *5*(121), 99669-99677. https://doi.org/10.1039/C5RA15379D

[234] Ahmad, K., Mohammad, A., Ansari, S. N., & Mobin, S. M. (2018). Construction of graphene oxide sheets based modified glassy carbon electrode (GO/GCE) for the highly sensitive detection of nitrobenzene. *Materials Research Express*, *5*(7), 075601. https://doi.org/10.1088/2053-1591/aacd98

[235] Rastogi, P. K., Ganesan, V., & Azad, U. P. (2016). Electrochemical determination of nanomolar levels of isoniazid in pharmaceutical formulation using silver nanoparticles decorated copolymer. *Electrochimica A cta*, *188*, 818–824. https://doi.org/10.1016/j.electacta.2015.12.058

[236] Devadas, B., Cheemalapati, S., Chen, S. M., Ali, M. A., & Al-Hemaid, F. M. A. (2014). Highly sensing graphene oxide/poly-arginine-modified electrode for the simultaneous electrochemical determination of buspirone, isoniazid and pyrazinamide drugs. *Ionics*, *21*(2), 547–555. https://doi.org/10.1007/s11581-014-1179-z

[237] S.T. Balamurugan, T. (2017). High sensitive electrochemical quantification of isoniazid in biofluids using copper particles decorated graphene oxide nano composite. *International J ournal of E lectrochemical Sc ience*, 9150–9160. https://doi.org/10.20964/2017.10.44

[238] Bergamini, M. F., Santos, D. P., & Zanoni, M. V. B. (2010). Determination of isoniazid in human urine using screen-printed carbon electrode modified with poly-l-histidine. *Bioelectrochemistry*, *77*(2), 133–138. https://doi.org/10.1016/j.bioelechem.2009.07.010

[239] Shahrokhian, S., & Amiri, M. (2006). Multi-walled carbon nanotube paste electrode for selective voltammetric detection of isoniazid. *Microchimica Acta*, *157*(3–4), 149–158. https://doi.org/10.1007/s00604-006-0665-z

[240] Absalan, G., Akhond, M., Soleimani, M., & Ershadifar, H. (2016). Efficient electrocatalytic oxidation and determination of isoniazid on carbon ionic liquid electrode modified with electrodeposited palladium nanoparticles. *Journal of Electroanalytical Chemistry*, *761*, 1–7. https://doi.org/10.1016/j.jelechem.2015.11.041

[241] Cheemalapati, S., Palanisamy, S., & Chen, S. M. (2013). Electrochemical determination of isoniazid at electrochemically reduced graphene oxide modified electrode. *International J ournal of E lectrochemical Sc ience*, *8*(3), 3953-3962. https://doi.org/10.1016/S1452-3981(23)14444-0

[242] Guo, Z., Wang, Z. Y., Wang, H. H., Huang, G. Q., & Li, M. M. (2015b). Electrochemical sensor for Isoniazid based on the glassy carbon electrode modified with reduced graphene oxide–Au nanomaterials. *Materials Science and Engineering: C*, *57*, 197–204. https://doi.org/10.1016/j.msec.2015.07.045

[243] Aguirre-Araque, J. S., Gonçalves, J. M., Nakamura, M., Rossini, P. O., Angnes, L., Araki, K., & Toma, H. E. (2019). GO composite encompassing a tetraruthenated cobalt porphyrin-Ni coordination polymer and its behavior as isoniazid BIA sensor. *Electrochimica Acta*, *300*, 113–122. https://doi.org/10.1016/j.electacta.2019.01.097

[244] Naik, B., Prasad, V. S., & Ghosh, N. N. (2009). Development of a simple aqueous solution based chemical method for synthesis of mesoporous γ-alumina powders with disordered pore structure. *Journal of P orous M aterials*, *17*(1), 115–121. https://doi.org/10.1007/s10934-009-9271-x

[245] Rudaz, S., Stella, C., Balant-Gorgia, A. E., Fanali, S., & Veuthey, J. L. (2000). Simultaneous stereoselective analysis of venlafaxine and O-desmethylvenlafaxine enantiomers in clinical samples by capillary electrophoresis using charged

cyclodextrins. *Journal of Pharmaceutical and Biomedical Analysis*, *23*(1), 107–115. https://doi.org/10.1016/s0731-7085(00)00280-6

[246] Vaze, V. D., & Srivastava, A. K. (2007). Electrochemical behavior of folic acid at calixarene based chemically modified electrodes and its determination by adsorptive stripping voltammetry. *Electrochimica Acta*, *53*(4), 1713–1721. https://doi.org/10.1016/j.electacta.2007.08.017

[247] Yan, H., Xiao, H., Xie, Q., Liu, J., Sun, L., Zhou, Y., ... & Yao, S. (2015). Simultaneous electroanalysis of isoniazid and uric acid at poly (sulfosalicylic acid)/electroreduced carboxylated graphene modified glassy carbon electrode. *Sensors and Actuators B: Chemical*, *207*, 167-176. https://doi.org/10.1016/j.snb.2014.10.002

[248] Tajik, S., Beitollahi, H., Dourandish, Z., Zhang, K., Le, Q. V., Nguyen, T. P., ... & Shokouhimehr, M. (2020). Recent advances in the electrochemical sensing of venlafaxine: an antidepressant drug and environmental contaminant. *Sensors*, *20*(13), 3675. https://doi.org/10.3390/s20133675

[249] Sanghavi, B. J., & Srivastava, A. K. (2011). Adsorptive stripping differential pulse voltammetric determination of venlafaxine and desvenlafaxine employing Nafion–carbon nanotube composite glassy carbon electrode. *Electrochimica Acta*, *56*(11), 4188-4196. https://doi.org/10.1016/j.electacta.2011.01.097

[250] Morais, S., Ryckaert, C. P. M. C. A., & Delerue-Matos, C. (2003). Adsorptive stripping voltammetric determination of venlafaxine in urine with a mercury film microelectrode. *Analytical Letters*, *36*(11), 2515–2526. https://doi.org/10.1081/al-120024339

[251] Khalilzadeh, M. A., Tajik, S., Beitollahi, H., & Venditti, R. A. (2020). Green synthesis of magnetic nanocomposite with iron oxide deposited on cellulose nanocrystals with copper (Fe_3O_4@CNC/Cu): investigation of catalytic activity for the development of a venlafaxine electrochemical sensor. *Industrial & Engineering Chemistry Research*, *59*(10), 4219–4228. https://doi.org/10.1021/acs.iecr.9b06214

[252] Maddah, B., Cheraghveisi, M., & Najafi, M. (2019b). Developing a modified electrode based on La^{3+}/Co_3O_4Nanocubes and its usage to electrochemical detection of venlafaxine. *International Journal of Environmental Analytical Chemistry*, *100*(2), 121–133. https://doi.org/10.1080/03067319.2019.1631303

[253] Ding, L., Li, L., You, W., Gao, Z. N., & Yang, T. L. (2015). Electrocatalytic oxidation of venlafaxine at a multiwall carbon nanotubes-ionic liquid gel modified glassy carbon electrode and its electrochemical determination. *Croatica Chemica Acta*, *88*(1), 81–87. https://doi.org/10.5562/cca2420

[254] Mohammadzadeh Jahani, P., Akbari Javar, H., & Mahmoudi-Moghaddam, H. (2021b). A new electrochemical sensor based on europium-doped nio nanocomposite for detection of venlafaxine. *Measurement*, *173*, 108616. https://doi.org/10.1016/j.measurement.2020.108616